

RECTIFIED BROWNIAN MOTION IN BIOLOGY

A Thesis
Presented to
The Academic Faculty

by

William H. Mather

In Partial Fulfillment
of the Requirements for the Degree
Doctor of Philosophy in the
School of Physics

Georgia Institute of Technology
August 2007

RECTIFIED BROWNIAN MOTION IN BIOLOGY

Approved by:

Professor Ron Fox, Advisor
School of Physics
Georgia Institute of Technology

Professor Jennifer Curtis
School of Physics
Georgia Institute of Technology

Professor Toan Nguyen
School of Physics
Georgia Institute of Technology

Professor Roger Wartell
School of Biology
Georgia Institute of Technology

Professor Kurt Wiesenfeld
School of Physics
Georgia Institute of Technology

Date Approved: 20 June 2007

TABLE OF CONTENTS

LIST OF FIGURES	v
SUMMARY	x
I INTRODUCTION	1
II MATHEMATICAL BACKGROUND	5
2.1 Stochastic Processes	5
2.1.1 Reaction Networks	6
2.1.2 Langevin Equations	6
2.1.3 Fokker-Planck Equations	8
2.2 Requisite Non-equilibrium Steady State Theory	9
2.2.1 Path Integral Representations of Stochastic Systems	10
2.2.2 Steady State, Free Energy, and Irreversibility	12
2.2.3 Example: Diffusion in a Potential	15
2.2.4 Free Energy Potentials	16
III FOUNDATIONS OF RECTIFIED BROWNIAN MOTION	19
3.1 Viscosity and Thermal Noise	19
3.2 Simple Models of Rectified Brownian Motion	23
3.3 Steady State Properties of Nanoscale Biological Processes	25
3.4 Regions of Reversibility	29
3.5 Rectified Brownian Motion, Power Strokes, and Brownian Ratchets	30
IV UBIQUINONE AND ROTARY ENZYMES	35
4.1 Ubiquinone Model, Revisited	35
4.2 Simple Rotary Enzyme Model	40
4.3 Biotin Rotary Enzyme Molecular Dynamics Simulation	41
4.3.1 Simulation Details	42
4.3.2 Results	43

V	MOLECULAR MOTORS	47
5.1	Rectified Brownian Motion Model	48
VI	RECTIFIED BROWNIAN MOTION MODEL FOR KINESIN	56
6.1	Structural and Chemical Functional Elements	57
6.1.1	Neck Linkers and the Coiled-Coil Neck	58
6.1.2	Neck Linker Zippering	60
6.1.3	Weak Binding	61
6.1.4	T-gate	62
6.2	Bias Amplification Mechanism Revisited	62
6.3	Detailed Biasing Mechanism	64
6.4	Waiting Mechanism	66
6.5	Concluding Comments on the Kinesin Model	68
VII	CONCLUSION	73
APPENDIX A	FOUNDATIONS OF RBM	75
APPENDIX B	RBM KINESIN MODEL	82
REFERENCES	91

LIST OF FIGURES

1	<p>A model for the ubiquinone shuttle [20]. The ubiquinone molecule in this simplified model functions as an intermediate carrier of protons and electrons between donor and acceptor molecules on opposite sides of a lipid membrane bilayer. Oxidized (UQ) and reduced (UQH_2) forms of ubiquinone are interconverted via redox reactions between donor molecules (oxidized form D_O, reduced form D_R) and acceptor molecules (oxidized form A_O, reduced form A_R). Redox reactions are assumed to occur at a reactive site of small width δ around the membrane boundaries. Ubiquinone undergoes free diffusion in a coordinate x between the two boundaries at locations $x = 0$ and $x = L$, and this diffusion is rectified by non-equilibrium redox reactions that drive the flow of electrons from donor to acceptor molecules on average.</p>	36
2	<p>Biocytin is constructed by a peptide linkage between the amino acid lysine and biotin. The distal ureido hydrogen (attached to nitrogen) on the reactive head can be exchanged for a carboxyl group, providing a means for a facilitated transfer of CO_2. The base of lysine connects to the remainder of the protein through peptide linkages.</p>	42
3	<p>Construction of the parameterization for biotin follows from the patching between three regions: (A) the lysine residue, (B) the peptide linkage, and (C) biotin. If (B) is assumed to locally resemble a repeating glycine polypeptide, parameterization from available sets for each region can essentially be taken from known parameter sets. Where there is an ambiguity in or a lack of a given interaction in the separate regions of a patch (this is particularly troublesome for dihedral interactions), preference is given towards maintaining regions A and C over region B.</p>	44
4	<p>A histogram for the $\tau = 200$ fs distribution of $\Delta\vec{n}(\tau) ^2$. Dots are bin counts centered horizontally on each respective interval of the histogram, while the smooth line is a best fit exponential that corresponds to $D \approx 0.8 \text{ rad}^2/\text{ns}$.</p>	46

- 5 Kinesin moves along microtubule in the plus direction by alternately attaching each head to the beta-tubulin subunits (light orange), producing a 16 nm translation for a given head and a 8 nm translation for the center of mass of the kinesin dimer. The two heads are approximately 6 nm in diameter and can together move forward against externally applied retarding forces up to 7 pN [6]. Kinesin is attached by a polypeptide neck linker (black lines) to the coiled-coil stalk, which binds cargo. This neck linker can either be free (left head, top) or bound weakly to a head in a zippered state (left head, bottom), depending on the nucleotide state of the head. Entropic and enthalpic contributions from the neck linkers and the coiled-coil provide tensions between the heads. Illustrated above is the spatial displacement step, occurring by means of strain-induced bias amplification. In the unzipped state of kinesin, the probability distribution (the unimodal curve) of the kinesin head does not favor either the forward (plus end) or backward (minus end) binding site, by symmetry. However, the small change induced by neck linker zippering is amplified by an exponential relative increase of the probability distribution near the forward binding site. This is related to the slope of the distribution near bound states, i.e. related to a force. Since a kinesin head visits the forward site more often, irreversible binding (rectification) can keep the head at the binding site to produce a forward step. Power stroke models cannot explain such a mechanism, due to the weakness of neck linker zippering. 54
- 6 An illustration of myosin V head domains bound to actin, with semi-flexible necks meeting at a common hinge and myosin head domains binding 36 nm apart at the actin pseudo-repeat length. The forward sense of motion is to the right, and the labeling of the angles corresponds to forward binding (backward binding would exchange the order of θ_1 and θ_2 in the diagram). Given these angles, the elastic free energy may be determined for a given model of the myosin necks, e.g. that of Lan and Sun used in the text [45]. Notice that this picture does not take into account the observed ability for myosin V to bind at lengths unequal to the pseudo-repeat length of actin [8, 45], but this complication does not seriously affect the argument in the text. . . . 55

- 7 A doubly-bound kinesin dimer oriented with the microtubule plus-end to the right. The N-terminal kinesin heads can bind to tubulin [33, 34, 93, 39]. The kinesin heads are connected by two neck linkers, ~ 15 amino acids (a.a.) each [71], and these neck linkers end in a coiled-coil “stalk” that can connect cargo through light chains and mediate tension, indicated by \mathbf{F} (the load force). Entropic considerations for the neck linkers suggest a thermal force, \mathbf{F}_{th} , which resists neck linker extension. A microtubule-bound head in an ATP or hydrolyzed ATP (ADP.P) state will initiate immobilization (zippering) of its neck linker onto itself through a series of hydrogen bonds, schematically indicated by hatched lines. This figure outlines structures found in Protein Data Bank file: 1IA0 [39]. 57
- 8 Key aspects of kinesin’s forward (plus-end) cycle have been elucidated through a varied multitude of experiments, including cryo-EM, x-ray structural, force bead, and others [97, 71, 7, 75, 29, 83, 14, 41]. This process is briefly reviewed, where “**T**” labels the ATP nucleotide state, “**D**” the ADP nucleotide state, “*” the no-nucleotide state, and “**P**” the phosphate after ATP hydrolysis. The free head is shaded to clarify motion between frames. Frames 1,2: the free head weakly binds to the plus-end binding site, leading to strong binding once ADP is released. ATP binding to the plus-end head is inhibited by a coordinating mechanism (labeled T-gate, ref. Section 6.1.4) that is activated by the internal strain. Frames 3–5: hydrolysis of ATP in the minus-end head leads to an intermediate ADP-phosphate state, “**D.P**,” and phosphate release alters the binding of the minus-end head into weak binding, which allows rapid release of the minus-end head from tubulin [13]. Frame 5 is to be identified with the parked state in Carter and Cross [6]. Frame 6: the free head tends not to strongly bind until ATP binds to the microtubule-bound head [28]. ATP binding initiates zippering of the microtubule-bound head’s neck linker, coinciding with a large acceleration of the rate for the free head to bind onto microtubule. This entire forward cycle consumes one ATP and moves the center of mass of the system ~ 8 nm. 69

- 9 Plots of zippered and unzipped stationary probability densities (in arbitrary units) vs. the *reduced* interval $[-d, d]$ (ref. Section 6.1.1 and Eq. 110), for the case example in Section 6.3 that ignores the effects of weak state unbinding. The use of the reduced interval, which subtracts the coiled-coil extension, hides the fact that zippering is a small change (~ 2 nm) compared to the distance travelled by one head (~ 16 nm). Zippering probabilities, e.g. Eq. 85, are not represented in these plots. As discussed in Section 6.2, the small and decreasing tails of the distribution are responsible for the generation of large biases. Apparent in these plots are the competing influences of zippering, which shifts the density towards the plus-end, and of loads, which shifts the density towards the minus end. Stall occurs when all these effects balance one another. The inclusion of weak state unbinding in the model preserves many of the features presented here. 70
- 10 Much of the biasing mechanism is assumed to occur in the parked geometry of frame 5 in Fig. 8, where the external load acting on the microtubule-bound head leads to long dwell times (ref. Section 6.4). However, the free head could have, in the time before ATP uptake, an opportunity to bind rearward during a period when forward binding is virtually excluded (due to no zippering). Thus, bias would then be $[ATP]$ dependent due to $[ATP]$ dependence of the waiting mechanism. In (a), a fast step is outlined that corrects this undesired backward stepping. Since the forward head experiences strain due to the rearward-bound head, ATP uptake is greatly inhibited in the forward head, and thus, there exists a much larger probability that the rearward head detaches first (at the expense of one ATP hydrolysis). In contrast, (b) outlines how a “real” backward step may occur once the waiting mechanism has ended, i.e. once ATP has bound to the microtubule-bound head. Notice that if the rearward head binds as in (b), the forward head is at least one chemical step ahead of the rearward head. With a few assumptions, the forward head in (b) may then be expected to release first on average. Events in (b) where instead the rearward head unbinds will alter the simple relation between binding and stepping direction, but these (potentially uncommon) events are ignored at the level of detail in this model. 71

- 11 Part (a) illustrates a rate model to minimally describe T-gate's effect on dwell times (actually, the steady-state natural lifetime). Such a simple model would doubtfully predict detailed measurements, e.g. the randomness [86]. The dashed region that contains abstract states s_1 and s_2 describes the overall ATP uptake mechanism, which includes T-gate within a Michaelis-Menton structure. The state s_3 represents the remainder of kinesin's chemical cycle. A particular form of the force dependent rate, $k(F) = 1/\tau(F)$, is taken from Eq. 87. Part (b) provides a plot of dwell times from the rate model in part (a) with parameters deduced by fitting to the model of Nishiyama et al. [56], fitting with better than visual accuracy. That the agreement with Nishiyama et al. is excellent is likely a result of the choice in Eq. 87, but this is not to state that our rate model is identical with theirs (e.g. in the manner $[ATP]$ dependence is included). Used in part (b): $\delta = 3.10$ nm, $R_0 = 193$, $\tilde{k}_+ = 5.08$ s $^{-1}$ μ M $^{-1}$, $k_- = 137$ s $^{-1}$, $k(0) = 857$ s $^{-1}$, $k_3 = 137$ s $^{-1}$, and $T = 300$ K. 72
- 12 A network diagram to describe the bias of kinesin's step, providing the rates necessary for Eq. 119. s_0 represents the reduced interval, the state where one kinesin head remains unbound. s_+ and s_- represent the plus and minus-end weak binding states, respectively. J is the steady state probability current entering the process (due to kinesin binding ATP to the microtubule-bound head), and J_+ , J_- are the exiting currents (due to strong binding transitions). The labels k_{\pm}^D are given to the rates of weak binding from a diffusing state, k_{\pm}^W to the rates of weak state unbinding (e.g. from Eq. 86), and k_{\pm}^S to the rates of strong binding. As a simplification, the strong binding rates equal a constant k^S that is independent of load. The essential irreversibility of the strong binding step corresponds to a large free energy decrease for strong binding transitions (consistent with the RBM principle). 83

SUMMARY

Nanoscale biological systems operate in the presence of overwhelming viscous drag and thermal diffusion, thus invalidating the use of macroscopically oriented thinking to explain such systems. Rectified Brownian motion (RBM), in contrast, is a distinctly nanoscale approach that thrives in thermal environments. The thesis discusses both the foundations and applications of RBM, with an emphasis on nano-biology. Results from stochastic non-equilibrium steady state theory are used to motivate a compelling definition for RBM. It follows that RBM is distinct from both the so-called power stroke and Brownian ratchet approaches to nanoscale mechanisms. Several physical examples provide a concrete foundation for these theoretical arguments. Notably, the molecular motors kinesin and myosin V are proposed to function by means of a novel RBM mechanism: strain-induced bias amplification. The conclusion is reached that RBM is a versatile and robust approach to nanoscale biology.

CHAPTER I

INTRODUCTION

Biological cells are characterized by vastly smaller length scales and weaker energy scales than found in macroscopic systems [62]. An *E. coli* bacterium, for example, measures only micrometers in diameter, while many intracellular processes are driven by the free energy of adenosine triphosphate (ATP) hydrolysis (approximately 12 – 20 $k_B T$ at physiological conditions) [85]. As a result of these small and weak scales, the hydrodynamics of cellular life resides in the extreme low Reynolds number ($\ll 1$) limit [46], and inertial effects are negligible compared to those of viscous drag. Motion is thus overdamped and described by a combination of two primary modes of motion: drift and diffusion. This thesis focuses on a distinctly diffusion-driven scheme, rectified Brownian motion (RBM), that is prevalent in subcellular biology.

Historically, a “power stroke” approach to cellular and subcellular mechanochemical mechanisms has frequently been employed, especially in the treatment of molecular motors [93].¹ Analogous to a power stroke in a macroscopic motor, a nanoscale power stroke continually expends free energy to effectively generate a force that overcomes viscous drag and other retarding forces that inhibit motion. Nanoscale enzymes that perform a power stroke require a specialized molecular structure responsible for the generation and transmission of a power stroke energy, e.g. a stiff molecular level arm connected to an enzymatic “motor” base that progressively anneals hydrogen bonds [100]. However, such an adapted structure is frequently absent, either fully or in part, in many biological mechanisms.

¹Molecular motors are mechanochemical enzymes that use chemical free energy, e.g. from ATP hydrolysis, to generate rectilinear or rotational motion. In the case of rectilinear motion, this is frequently done by interacting with a long molecular track, e.g. actin or microtubule.

A viable alternative to such a power stroke scheme is RBM, which instead harnesses naturally occurring thermal fluctuations from the fluid medium [20, 59]. Thermal diffusion spontaneously generates nanometer displacements in a time of order microseconds, such that diffusion can quickly provide significant spatial displacements in a nanoscale mechanism. This diffusion can be rectified on average by non-equilibrium boundary conditions, which are in turn established by the expenditure of free energy. The emphasis in RBM is thus how boundary effects contribute to the irreversibility and free energy expenditure in a mechanism.²

The recognition that RBM can be used as a means to drive nanoscale devices is not itself new; A. Huxley utilized RBM five decades ago in an early model to explain muscle contraction [36]. However, the relatively recent wealth of structural and kinetic information for proteins and their activity, respectively, has provided evidence that RBM may be a dominant scheme in previously power stroke-dominated realms of nano-biology. The dimeric molecular motor kinesin is one such example treated in this thesis.³ Kinesin has two “heads” that alternately step along the length of a microtubule in a “hand-over-hand” manner, such that the initially rearward head becomes mobile and binds in front of the initially forward head [103]. This mobile head is compelled to the forward position by an interaction with the other stationary head, as mediated primarily by non-rigid elements that connect the heads [76]. The lack of rigid elements suggests that a Brownian motion scheme, at least in part, governs the forward stepping of kinesin [21, 52].

Despite such progress in the realm of molecular-scale mechanisms, the argument that RBM is fundamental to nano-biology has encountered resistance. For example, some have considered RBM to be just another term for the more familiar Brownian ratchets, while others have concluded that a Brownian motion mechanism is too slow

²Indeed, RBM will be defined to be a subset of boundary driven systems as a whole [66].

³Kinesin is discussed primarily in Chapters 5 and 6. There, Figure 7 provides further structural information.

to sufficiently explain the how molecular motors can progress against experimental retarding loads of several picoNewtons [35]. This thesis attempts to address these issues from multiple angles. In particular, the foundations of RBM are laid down by physically oriented discussions of low Reynolds number dynamics and non-equilibrium steady state theory. The role of the non-equilibrium free energy profile and its connection to irreversibility will serve a key role in this endeavor. These underlying principles are illustrated by means of several physical examples that are commonly discussed in cellular biology. In this manner, RBM is argued to be a powerful, versatile, and ubiquitous tool in intracellular processes.

Of particular interest is a new RBM scheme for molecular motors: strain-induced bias amplification. Strain-induced bias amplification simultaneously explains how internal strain between two molecular motor heads can both ensure chemical coordination and sensitize the system to strongly favor forward binding over rearward binding for a mobile head [52].⁴ Bias amplification models depend critically on the role of boundary effects, in contrast to power stroke approaches, and will be demonstrated to provide an explanation to apparent experimental discrepancies in molecular motors. This is reviewed in the latter portion of this thesis, where bias amplification is applied as a unified scheme for the molecular motors kinesin and myosin V.

The thesis is outlined as follows. Chapter 2 reviews the necessary mathematical background that will be used to understand both the kinetic and thermodynamic formalism of small systems, including a brief review of Langevin equations, Fokker-Planck equations, and results that relate irreversibility to free energy expenditure. Chapter 3 utilizes these results to build a coherent picture of RBM as a widespread scheme in nanoscale biological systems. The argument is made that RBM is both a distinct and even preferable alternative to power stroke and Brownian ratchet models.

⁴Chemical coordination refers to a correlation between the respective internal states of the two heads, such that the heads are kept chemically out of phase. If the heads instead operated independently, a molecular motor would tend to rapidly detach from its track [13].

The remaining chapters explore particular applications of RBM to biological systems. Chapter 4 covers two relatively simple systems that play essential roles in fundamental metabolic processes: the ubiquinone shuttle and rotary enzymes. Simple models for ubiquinone and rotary enzymes will highlight many of the topics discussed previously. New detailed molecular dynamics (MD) simulations are also discussed for the biotin rotary enzyme, in the interest of investigating the kinetics of a non-trivial system. Chapter 5 discusses bias amplification models for the conventional variants of the molecular motors kinesin and myosin V. Chapter 6 presents a more detailed and physically motivated model for kinesin, based on the principles in Chapter 5. The ability for this model to reproduce experimental results is discussed. Chapter 7 contains concluding remarks.

CHAPTER II

MATHEMATICAL BACKGROUND

This chapter provides a background of the formalism behind the analysis of fluctuating systems, with emphasis on those found in nanoscale biological mechanisms. Section 2.1 briefly reviews time-continuous stochastic processes. Section 2.2 provides a coherent discussion of free energy and irreversibility and will be referenced frequently in this thesis.

2.1 Stochastic Processes

The dynamics of nanoscale biological mechanisms are heavily influenced by a tumultuous liquid environment. Investigation of such systems by direct simulation, e.g. by molecular dynamics, is computationally expensive or even prohibitive. Fortunately, stochastic models offer a simpler alternative that frequently reproduce the quantitative aspects of diffusive motion.¹ This stochastic approach to diffusion is typically presented in either a Langevin form or a Fokker-Planck form, each an essentially equivalent representation of the same random process. These two approaches are briefly discussed below, following a very short discussion of reaction networks (also known as master equations). A thorough review of this background material can be found in the combination of a few references [19, 23, 72].

¹Rigorous examples of classical diffusion exist [15, 27], and these may deviate from stochastic diffusion in significant ways.

2.1.1 Reaction Networks

A closed reaction network for a finite number of states represents one of the most fundamental time-continuous stochastic systems, often used in the modeling of non-equilibrium chemical reactions [32, 80].

A reaction network is a Markov process described by the rates K_{ji} for a transition from state i to state j . All transitions are here assumed to be bidirectional,² such that $K_{ji} \neq 0$ implies $K_{ij} \neq 0$. Letting p_i be the time-dependent probability to be at state i , the probability distribution of the reaction network is evolved according to the master equation

$$\begin{aligned} \frac{dp_i}{dt} &= \sum_{j|j \neq i} J_{ij} \\ J_{ij} &= K_{ij}p_j - K_{ji}p_i \end{aligned} \tag{1}$$

with J_{ij} the probability current from state i to state j .

Equivalently, the theory can be built upon stochastic trajectories. Supposing the system is at state i , a transition to some other state occurs with an exponentially distributed waiting time of rate $K_i = \sum_{j \neq i} K_{ji}$, while the probability that this transition produces some particular state j is K_{ji}/K_i . The path integral representation of a reaction network in Section 2.2.1 will demonstrate the theoretical usefulness of the trajectory picture.

2.1.2 Langevin Equations

Langevin equations are an approach to stochastic ordinary differential equations, written as an ODE with an additional noise term. In the case of a multi-dimensional system, a non-linear Langevin equation can be written [19, 72]

$$\frac{dx_i}{dt} = h_i(\vec{x}) + \sum_j g_{ij}(\vec{x})\xi_j(t) \tag{2}$$

²This is a necessary condition for any system treated with the free energy formalism in Section 2.2.

with each $\xi_i(t)$ a noise function that must be specified (each such noise is assumed to be statistically independent of the others), and the functions h_i and g_{ij} are “drift” and “noise” terms, respectively.³ The noise combination $\sum_j g_{ij}\xi_j$ represents forces from the environment that, though unknown, can be statistically characterized.

A typical example (the only case needed in this thesis) is normalized Gaussian white noise,⁴ which is characterized by the two-time correlation function

$$\begin{aligned}\langle \xi(t) \rangle &= 0 \\ \langle \xi(t_1)\xi(t_2) \rangle &= \delta(t_1 - t_2)\end{aligned}\tag{3}$$

with angular brackets representing an average over realizations of the Gaussian white noise, and $\delta(t)$ the Dirac delta function. All higher order correlation functions can be derived from Eq. 3 on the condition of Gaussian noise, where correlation functions effectively factorize [72].⁵ While Gaussian white noise is far from an ordinary function, physical systems always have a finite correlation time in their noise. In this vein, the manipulation of Gaussian white noise is often treated in physical applications as if the noise is an ordinary smooth function of time.

As an example of how Langevin equations are handled, consider simple integrated white noise ($h(x, t) = 0$ and $g(x, t) = 1$). The solution in this case is written

$$x(t) = \int_0^t dt_0 \xi(t_0) + x_0\tag{4}$$

By Eq. 3, this process has a constant average

$$\langle x(t) \rangle = \int_0^t dt_1 \langle \xi(t_1) \rangle = x_0\tag{5}$$

and a variance that increases linearly with time

$$\langle (x(t) - x_0)^2 \rangle = \int_0^t dt_1 \int_0^t dt_2 \langle \xi(t_1)\xi(t_2) \rangle = t\tag{6}$$

³The precise role of these functions can be determined by examining stochastic averages, e.g. in Eq. 7 below.

⁴Correlated (“colored”) noise is also typical. For example, the fluctuating velocity of an inertial Brownian particle can be viewed as a correlated noise that drives the positional variable.

⁵White noise that satisfies Eq. 3 may deviate from a Gaussian distribution in higher order correlation functions, but Gaussian white noise is typical in many physical stochastic processes [19].

for $t \geq 0$. All higher order moments of Gaussian white noise can be derived from a Gaussian distribution with the above average and variance.

Solutions to Eq. 2 can be solved in a similar manner, using Taylor approximations and Eq. 3 to define propagation. This physically minded approach (by Stratonovich) produces the short-time moments [19, 72]⁶

$$\begin{aligned}\langle \Delta x_i \rangle &\approx h_i \tau + \sum_{kj} \frac{1}{2} g_{kj} \frac{\partial}{\partial x_k} g_{ij} \tau \\ \langle \Delta x_i \Delta x_j \rangle &\approx \sum_k g_{ik} g_{jk} \tau\end{aligned}\tag{7}$$

with $\Delta x_i = x_i(t + \tau) - x_i(t)$ and with functions evaluated at $\vec{x}(t)$ and time t . Stochastic evolution follows from Gaussian propagators with the moments in Eq. 7. The extra term due to spatially dependent g_{ij} is a noise-induced drift, e.g. which may arise for diffusion in a thermal gradient. For simplicity, this thesis avoids spatially dependent noise and the associated noise-induced drift.

2.1.3 Fokker-Planck Equations

The Fokker-Planck equation for a diffusive stochastic process governs the evolution in time of the probability distribution [23, 72], providing an equivalent representation of the Langevin dynamics. Since the probability distribution is a natural object of study in non-equilibrium systems (consider the entropy function), Fokker-Planck equations often provide a cleaner picture of steady state thermodynamics.

The functional form of the Fokker-Planck equation can be motivated from various standpoints, but it ultimately is found to be equivalent to the probability conservation equation

$$\begin{aligned}\frac{\partial p(\vec{x}, t)}{\partial t} &= -\vec{\nabla} \cdot \vec{J}(\vec{x}, t) \\ J_i(\vec{x}, t) &= \left(V_i(\vec{x}) - \sum_j \frac{\partial}{\partial x_j} D_{ij}(\vec{x}) \right) p(\vec{x}, t)\end{aligned}\tag{8}$$

⁶An alternate (and equivalent) Ito formulation of stochastic integration can be used at the expense of treating the noise as an ordinary function.

with p the distribution, \vec{J} the probability current (which includes Fick's law), V_i the local mean drift vector, and D_{ij} a local diffusion matrix. The short-time propagator for a time τ is a Gaussian distribution with average change in position $\langle \Delta x_i \rangle \approx V_i \tau$ and covariance matrix $\langle \Delta x_i \Delta x_j \rangle \approx 2D_{ij} \tau$ [72]. Comparison of these moments to those in Eq. 7 can be used to relate the Fokker-Planck and Langevin representations of a stochastic process.

A common variant of Eq. 8 is the Smoluchowski equation for an overdamped particle with a constant diffusion matrix

$$\begin{aligned} \frac{\partial p(\vec{x}, t)}{\partial t} &= -\vec{\nabla} \cdot \vec{J}(\vec{x}, t) \\ J_i(\vec{x}, t) &= \sum_j \left(\Gamma_{ij}^{-1} F_j(\vec{x}) - D_{ij} \frac{\partial}{\partial x_j} \right) p(\vec{x}, t) \end{aligned} \quad (9)$$

where Γ_{ij} is a constant drag matrix. The relation $\sum_j \Gamma_{ij} D_{jk} = k_B T \delta_{ik}$, with δ_{ik} the Kronecker delta, is imposed as a consequence of fluctuation-dissipation relations (revisited in Section 3.1). In this form, Eq. 9 can be used to represent the diffusive fluctuations of enzymatic complexes in nanoscale biological systems.

2.2 *Requisite Non-equilibrium Steady State Theory*

Few general statements can be made concerning the thermodynamics of systems far from equilibrium. However, results in this subject continue to surface, e.g. the many fluctuation theorems that relate heat generation to irreversibility [2, 11, 12, 24, 26, 22, 47], or whole steady state thermodynamic formalisms [31, 57, 78]. This section outlines several necessary results related to non-equilibrium thermodynamics in preparation for their application to nanoscale biological systems. Results in this theory are typically demonstrated in terms of the reaction networks in Section 2.1.1, but the generalization of results to continuum systems will typically be valid.

An assumption used throughout the theory presented below is the nonexistence of truly irreversible transitions. This condition limits the general applicability of the

theory, e.g. excluding a thermodynamic treatment that explicitly includes the inertial dynamics of a Brownian particle.⁷ An appropriate overdamped limit of macromolecular dynamics should then be assumed. This limit is sensible for the naturally overdamped environment of nanoscale mechanisms, as justified in Section 3.1.

2.2.1 Path Integral Representations of Stochastic Systems

Modern non-equilibrium steady state (NESS) theory contains several theorems that are formulated in terms of stochastic trajectories.⁸ These are derived from, or at least related to, path integral representations of stochastic propagation [40, 47, 67]. A few essential results related to path integrals in stochastic systems are presented here in preparation for their thermodynamic interpretation in Section 2.2.2.

For a reaction network, the propagator $P_t(j|i)$ from state i to j in a time t is given by the corresponding matrix element of the exponentiated generating matrix \hat{W}

$$P_t(j|i) = \langle j | \exp(\hat{W}t) | i \rangle \quad (10)$$

with

$$W_{kp} = (1 - \delta_{kp}) K_{kp} - \delta_{kp} K_p \quad (11)$$

for arbitrary states k and p , and $K_p = \sum_{k|k \neq p} K_{kp}$ the escape rate from state p . As usual, the path integral approach repeatedly applies the completeness relation to achieve an expression for $P_t(j|i)$ that only requires matrix elements for the short times δt

$$\langle k | \exp(\hat{W} \delta t) | p \rangle \approx \exp(W_{kp} \delta t) + O(\delta t^2) \quad (12)$$

Defining a path as a sequence of visited states, the final form for the $P_t(j|i)$ can be expressed as a weighted summation over all possible paths \mathcal{P} that begin at state i and end at state j

$$P_t(j|i) = \sum_{\mathcal{P}|i \rightarrow j} w_t(\mathcal{P}) \quad (13)$$

⁷This failure can be attributed to the singular nature of the diffusion matrix in an inertial system.

⁸For example, the Jarzynski equality.

where $w_t(\mathcal{P})$ is the weight for the path \mathcal{P} . Supposing a given path is labeled $\mathcal{P} = \{1 \rightarrow 2 \rightarrow \dots \rightarrow n\}$, where the numbers may refer to any labeled sequence of states, $w_t(\mathcal{P})$ is defined

$$w_t(\mathcal{P}) = \int_0^\infty d\Delta t_1 \int_0^\infty d\Delta t_2 \cdots \int_0^\infty d\Delta t_n w(\mathcal{P}, \{\Delta t_i\}) \delta\left(\sum \Delta t_i - t\right) \quad (14)$$

with

$$w(\mathcal{P}, \{\Delta t_i\}) = K_{n,n-1} \cdots K_{3,2} K_{2,1} e^{-K_n \Delta t_n} \cdots e^{-K_2 \Delta t_2} e^{-K_1 \Delta t_1} \quad (15)$$

defined for the set $\{\Delta t_i\}$ of waiting times in each state of \mathcal{P} .

An important relation follows. The ratio of the path weight $w_t(\mathcal{P})$ over the weight of the reversed path $w_t(\mathcal{P}^R)$ is dependent only on the sequence of states in \mathcal{P} . Explicitly,

$$\frac{w_t(\mathcal{P})}{w_t(\mathcal{P}^R)} = \frac{K_{n,n-1} \cdots K_{3,2} K_{2,1}}{K_{1,2} K_{2,3} \cdots K_{n-1,n}} \quad (16)$$

If the path is a cycle \mathcal{C} , with first and final states identical, then

$$\frac{w_t(\mathcal{C})}{w_t(\mathcal{C}^R)} = \frac{K_{1,n} K_{n,n-1} \cdots K_{3,2} K_{2,1}}{K_{1,2} K_{2,3} \cdots K_{n-1,n} K_{n,1}} \quad (17)$$

Equations 16 and 17 will be important in Section 2.2.2, where non-equilibrium fluctuations are discussed.

There are a few complications in generalizing Equations 16 and 17 to diffusive processes, e.g. due to the infinite path length of a diffusive trajectory. One approach that preserves the result in Eq. 16 is to use a finite state approximation to the diffusive state space. Alternatively, a return to the finite time-sliced version of the path integral is possible. This latter approach utilizes the known Gaussian short-time propagators to provide the weight for a trajectory [72]. For example, consider one-dimensional diffusive motion, with diffusion constant D and local mean velocity v . An approximate ratio (taken in a logarithm that is multiplied by a thermal energy) between forward and backward propagation over a time τ is

$$k_B T \ln \left(\frac{P_\tau(x_2|x_1)}{P_\tau(x_1|x_2)} \right) \approx (x_2 - x_1) \frac{k_B T}{D} v = (x_2 - x_1) \Gamma v = (x_2 - x_1) F \quad (18)$$

with $\Gamma = k_B T/D$ the effective drag constant and $F = \Gamma v$ the effective applied force (e.g. ref. Eq. 9). Eq. 18 can then be used to form weights in the path integral formula (written for multiple dimensions and with spatially constant noise)

$$k_B T \ln \left(\frac{w_t(\mathcal{P})}{w_t(\mathcal{P}^R)} \right) = \int_{\mathcal{P}} \vec{d}x \cdot \vec{F}(x) \quad (19)$$

with the right hand side a time-discretized integral of the force along the trajectory \mathcal{P} . In the case of a locally conservative force $\vec{F} = -\vec{\nabla}U$, Eq. 19 can be integrated

$$k_B T \ln \left(\frac{w_t(\mathcal{P})}{w_t(\mathcal{P}^R)} \right) = U(x_1) - U(x_2) \quad (20)$$

Eq. 20 can be used, for instance, to derive the detailed balance condition in an equilibrium system.

2.2.2 Steady State, Free Energy, and Irreversibility

Long-time behavior of a stochastic mechanism asymptotically approaches the steady state probability distribution $p_i^{(s)}$, which can be used to build a thermodynamic theory of fluctuating non-equilibrium processes [80]. Non-equilibrium fluctuations in the overdamped systems of interest arise when $p_i^{(s)}$ breaks the detailed balance symmetry, i.e. when $J_{ji} \neq 0$ for some pair of states, thus producing a flow of probability current that can be used to perform useful tasks on average.

An equivalent (and presently more useful) picture of NESS dynamics exists in terms of stochastic trajectories [47], where non-equilibrium fluctuations arise due to an irreversibility in the system. Irreversibility is best defined in terms of the path integral representation of the NESS. The NESS probabilistic weight $P_t(\mathcal{P})$ of a path \mathcal{P} , from state i to j in a time interval t , follows from the combination of propagator and steady state weights (ref. Eq. 14)

$$P_t(\mathcal{P}) = w_t(\mathcal{P}) p_i^{(s)} \quad (21)$$

By Eq. 16, it follows that

$$\frac{P_t(\mathcal{P})}{P_t(\mathcal{P}^R)} = \frac{w_t(\mathcal{P}) p_i^{(s)}}{w_t(\mathcal{P}^R) p_j^{(s)}} \quad (22)$$

which deviates from unity only in the case that a path has a preferred direction at steady state, i.e. that the path is partially irreversible.

The kinetic relation Eq. 22 appears in other contexts. An object long used in the study NESS dynamics and thermodynamics is the affinity [32, 80]. The affinity, in its many forms, establishes a non-equilibrium measure of irreversibility in the system. A valid definition of the pairwise affinity A_{ji} for the transition from i to j is

$$A_{ji} = k_B T \ln \frac{K_{ji} p_i^s}{K_{ij} p_j^s} \quad (23)$$

which is zero only when $J_{ji} = 0$. Thus, equilibrium is equivalent to globally zero pairwise affinity. The affinity $A(\mathcal{P})$ along a path \mathcal{P} , from state i to state j , is in turn defined to be the sum of pairwise affinities along the path

$$A(\mathcal{P}) = k_B T \ln \frac{w_t(\mathcal{P}) p_i^{(s)}}{w_t(\mathcal{P}^R) p_j^{(s)}} = k_B T \ln \frac{P_t(\mathcal{P})}{P_t(\mathcal{P}^R)} \quad (24)$$

where Eq. 22 has been used. The path affinity thus measures the directional irreversibility along \mathcal{P} . The cycle affinity is defined similarly⁹

$$A(\mathcal{C}) = k_B T \ln \frac{w_t(\mathcal{C})}{w_t(\mathcal{C}^R)} = k_B T \ln \frac{P_t(\mathcal{C})}{P_t(\mathcal{C}^R)} \quad (25)$$

which has the advantage of independence from the NESS distribution (it is an intrinsic property of the cycle).

The kinetic significance of the affinity is related to its thermodynamic interpretation as the free energy expenditure for a transition, i.e.

$$A_{ji} = -\Delta\mu_{ji} \quad (26)$$

The validity of Eq. 26 can be argued from multiple standpoints, such as has been done for reaction networks and diffusive systems [24, 25, 80]. Consider the irreversible heat production rate long used in NESS theory, which is the positive quantity

$$\dot{Q}_{irr} = \frac{1}{2} \sum_{ij} A_{ji} J_{ji} \quad (27)$$

⁹Eq. 25 is related to the Watanabe formula [37, 64].

that is found from an analysis of the time dependence of the entropy $S = -\sum_i p_i \ln p_i$ [80]. If Eq. 27 is interpreted as composed of macroscopic transitions in an isothermal system, then Eq. 26 would be the free energy expenditure (negative heat production) for completing such a spontaneous macroscopic transition. Moreover, pairwise spontaneous probability current only accompanies a negative pairwise free energy. For these reasons, Eq. 26 provides a sensible non-equilibrium version of the free energy.

The relationship between the affinity and free energy may be more transparent for processes driven by a single-valued underlying energy potential function,¹⁰ i.e. those processes in some region \mathcal{R} (that is generally open to external transitions) that satisfies $K_{ji}p_i^0 = K_{ij}p_j^0$ for some distribution $p_i^0 = e^{-U_i/k_B T}$. U_i is the energy of the processes that supplies the unique equilibrium distribution in \mathcal{R} . The NESS distribution can then be written $p_i^{(s)} = e^{(\mu_i - U_i)/k_B T}$, where μ_i has the interpretation of a chemical potential. The path affinity simplifies in this case

$$\begin{aligned} A(\mathcal{P}) &= k_B T \ln \frac{p_1^{(s)} p_n^0}{p_1^0 p_n^{(s)}} = k_B T \ln e^{(\mu_1 - \mu_n)/k_B T} \\ &= \mu_1 - \mu_n = -\Delta\mu_{n1} \end{aligned} \quad (28)$$

such that

$$\frac{P_\tau(\mathcal{P})}{P_\tau(\mathcal{P}^R)} = e^{-\Delta\mu_{n1}/k_B T} \quad (29)$$

Spontaneous current along a path arises from a chemical potential gradient, as expected.

A caveat of the affinity-based free energy Eq. 26 is that it cannot generally be interpreted as a logically separable thermodynamic free energy, in that it is only defined at steady state (excepting the cases of cycles and long stochastically sampled paths, the latter of which are used in fluctuation theorems). This difficulty is related to the inability to identify a particular locus of entropy production in Eq. 27 [32]. For example, the total entropy production rate is unchanged if the pairwise affinity

¹⁰These are discussed again in Section 2.2.4.

is replaced by a new affinity

$$\tilde{A}_{ji} = A_{ji} + V_j - V_i \quad (30)$$

for some state function V_i .¹¹ For this reason, reference to the entropy production rate in a given region of state space is more precisely defined as the restricted summation in Eq. 27 over this region.

2.2.3 Example: Diffusion in a Potential

An example that is readily treated and interpreted with the formalism in Section 2.2.2 is the Fokker-Planck equation for a one-dimensional, overdamped particle in a potential $U(x)$ (ref. Section 2.1.3) [23, 31, 65]

$$\begin{aligned} \frac{\partial p(x, t)}{\partial t} &= -\frac{\partial J(x, t)}{\partial x} \\ J(x, t) &= -D \left(\frac{1}{k_B T} \frac{\partial U(x)}{\partial x} + \frac{\partial}{\partial x} \right) p(x, t) \end{aligned} \quad (31)$$

The steady state $p^{(s)}(x)$ of this problem can be solved from the condition $J(x, t) = J$, where J is the steady state current. Explicitly

$$J = -D \left(\frac{1}{k_B T} \frac{\partial U(x)}{\partial x} + \frac{\partial}{\partial x} \right) p^{(s)}(x) \quad (32)$$

A chemical potential can be introduced to simplify Eq. 32. If $\mu(x) = U(x) + k_B T \ln(p^{(s)}(x)\delta_0)$, for some constant distance δ_0 , then

$$\frac{\partial}{\partial x} e^{\mu(x)/k_B T} = -\frac{J\delta_0}{D} e^{U(x)/k_B T} \quad (33)$$

Equivalently

$$\frac{\partial \mu(x)}{\partial x} = -\frac{k_B T}{D} \frac{J}{p^{(s)}(x)} = -\Gamma v(x) \quad (34)$$

The thermodynamic force $\Pi = -\partial\mu(x)/\partial x$ in a diffusing system is thus equal to the mean drag force $\Gamma v(x)$, for ensemble velocity $v(x) = J/p^{(s)}(x)$ and drag coefficient $\Gamma = k_B T/D$.

¹¹This follows from the steady state condition $\sum_i J_{ji} = 0$.

An alternative approach to this problem is by means of the continuum expression for the affinity kernel (to be integrated along a path) [65]

$$\Pi(x) = F(x) - k_B T \frac{\partial}{\partial x} \ln p^{(s)}(x) \quad (35)$$

with $F(x) = -\partial U(x)/\partial x$. The irreversible heat production rate \dot{Q}_{irr} associated with the interval $[a, b]$ is then

$$\begin{aligned} \dot{Q}_{irr} &= \int_a^b dx \Pi(x) J(x) \\ &= -J (\mu(b) - \mu(a)) = -J \Delta\mu \geq 0 \end{aligned} \quad (36)$$

Entropy production in this case thus retains the bilinear form assumed in near-equilibrium theory, though J and $\Delta\mu$ are typically nonlinearly related to one another.

The treatment of free energy in the higher dimensional case (e.g. assuming isotropic diffusion) is entirely similar [65], with a thermodynamic force

$$\vec{\Pi}(x) = \vec{F}(x) - k_B T \vec{\nabla} \ln p^{(s)}(x) \quad (37)$$

that can be interpreted to arise from the negative ensemble velocity drag force at steady state. $\vec{\Pi}$ is integrable when the force is integrable, i.e. $\vec{F} = -\vec{\nabla}U$, such that a free energy profile satisfying $\vec{\Pi} = -\vec{\nabla}\mu$ arises

$$\mu(x) = \mu_0 + U(x) + k_B T \ln p^{(s)}(x) \quad (38)$$

The existence of $\mu(x)$ for diffusion is a useful simplification of the system energetics, as will be discussed below in Section 2.2.4, and will be taken in Section 3.5 to be generally valid for all RBM systems.

2.2.4 Free Energy Potentials

As will be discussed further in Section 3.3, a system driven by only a few sources of free energy has important restrictions imposed on its kinetics [32, 50]. The cycle free energy $\Delta\mu(\mathcal{C})$ in such systems can only be equal to integer linear combinations

of a basic set of free energies, assumed to arise from N fundamental cycles with free energies ΔG_i ($i = 1, \dots, N$). Then

$$\Delta\mu(\mathcal{C}) = \sum_i n_i \Delta G_i \quad (39)$$

for integers n_i . Eq. 39 can be viewed as a topological characterization of cycles in state space. From this condition, path free energies are similarly restricted. Suppose two paths, \mathcal{P}_1 and \mathcal{P}_2 , with shared initial and final endpoints. The application of Eq. 39 to the cycle $\mathcal{C}_{12} = \mathcal{P}_1 + \mathcal{P}_2^R$ implies

$$\Delta\mu(\mathcal{P}_1) = \Delta\mu(\mathcal{P}_2) + \sum_i n_i \Delta G_i \quad (40)$$

for the set of integers corresponding to $\Delta\mu(\mathcal{C}_{12})$.

A consequence of Equations 39 and 40 is the appearance of a NESS free energy potential $\mu(x)$ that describes irreversibility. Suppose that a region \mathcal{R} in state space satisfies $\Delta\mu(\mathcal{C}) = 0$ for all internal cycles \mathcal{C} . Then, Eq. 40 can be used to prove path independence for all internal paths between common endpoints x_f and x_i , i.e.

$$\Delta\mu(\mathcal{P}) = \mu(x_f) - \mu(x_i) \quad (41)$$

The function $\mu(x)$ provides all information concerning irreversibility for trajectories in \mathcal{R} , and thus inherits many useful properties of the affinity.¹² More generally, a multi-valued free energy potential can be constructed by the inclusion of branches that are consistent with Eq. 40, but this is a straightforward complication.

A special situation arises for systems that have tight mechanochemical coupling, i.e. systems for which completion of the mechanical portion of the device (e.g. a diffusive step) is statistically equivalent to completion of the chemical portion (e.g. the reaction cycle of ATP). More precisely, tight mechanochemical coupling implies any cycle \mathcal{C} in state space that completes n mechanical steps must satisfy $\Delta\mu(\mathcal{C}) = n\Delta G$,

¹²For example, nonzero probability current only arises in the direction of a negative free energy gradient.

with ΔG the free energy for the fundamental cycle of the device.¹³ Such a system is one with a “gate,” i.e. a transition through which all cycles with nonzero affinity must pass. $\mu(x)$ is defined for a stochastic process on either side of this gate by this condition (cycles that do not cross this gate have zero affinity). A process between two such gates similarly has a potential. Gated systems will be useful in the case of RBM, since many systems, e.g. the examples in Chapters 4 and 5, tend to be gated by one or more steps.

As a final note, the existence of a potential $\mu(x)$ in a region \mathcal{R} allows irreversibility to locally be expressed more directly in terms of short-time propagators, rather than the more fundamental individual path path weights in Eq. 56. Assume two states, x_1 and x_2 , that are contained within \mathcal{R} . If the propagators $P_\tau(x_2|x_1)$ and $P_\tau(x_1|x_2)$ both only have statistically relevant contributions for paths of a given free energy class (ref. Eq. 40), then

$$\mu(x_2) - \mu(x_1) \approx -k_B T \ln \left(\frac{P_\tau(x_2|x_1)p^{(s)}(x_1)}{P_\tau(x_1|x_2)p^{(s)}(x_2)} \right) \quad (42)$$

Thus, the free energy profile locally provides a measure of deviation of detailed balance conditions.¹⁴ Regions of approximately equal free energy potential are nearly at equilibrium conditions, and regions with steep free energy gradients have strongly irreversible underlying trajectories.

¹³ ΔG includes contributions to the free energy from any external reactions and any external work done in a cycle of the device.

¹⁴This is obvious for a single chemical transition (ref. the pairwise affinity in Eq. 23).

CHAPTER III

FOUNDATIONS OF RECTIFIED BROWNIAN MOTION

An argument for the ubiquity of Brownian motion-based mechanisms in nanoscale biology follows from an appreciation for the rapidity of diffusive transport at the nanoscale in conjunction with the thermodynamic formalism reviewed in Section 2.2. RBM is defined as a particular class of Brownian motion mechanisms, providing a viable alternative to both power stroke models and Brownian ratchets. This definition is inspired from the principle of how irreversibility is related to Brownian motion and other fluctuation-based mechanisms.

Sections 3.1 and 3.2 outlines results relating to characteristic time and length scales that accompany diffusive motion, including preliminary statements concerning the role of power stroke versus Brownian motion transport. Section 3.3 applies several non-equilibrium results in the context of the enzymatic systems, in particular discussing the relevance of boundary driven systems in the principle of rectification. Sections 3.4 and 3.5 formulate proposed definitions for RBM and power strokes that are consistent with these principles.

3.1 Viscosity and Thermal Noise

An appreciation for the immense effects of viscosity and thermal fluctuations at the nanoscale is critical in the understanding of cellular and intracellular dynamics [62]. Low Reynolds number behavior imposes heavy viscous damping that quickly eliminates inertial effects,¹ but thermal fluctuations provide a vigorous means to generate rapid spatial displacements in the form of diffusion [90]. As discussed presently, an

¹Systems that are too small, i.e. those that begin to become comparable to the molecular size of water, may require special consideration.

examination of the interplay between viscous drag and thermal heat provides insight into how a RBM scheme can power a molecular device. Preliminary comments are also made on how Brownian motion-based versus power stroke-based mechanisms can be distinguished.

The effects of viscous drag on a nanoscale body can be made once drag tensors have been obtained for the linear equations of low Reynolds number flow [44, 46]. For definiteness, consider the lowest order solution for flow around a spherical body (first derived by Stokes) with mass m , radius R , and a position described by a linear coordinate x . If the drag force is written $F_{drag} = -\Gamma\dot{x}$, where \dot{x} is the velocity, then

$$\Gamma = 6\pi\eta R \quad (43)$$

is the drag coefficient for a sphere in a medium with dynamic viscosity η . The corresponding relaxation time $\tau = m/\Gamma$ to dissipate a mean initial velocity v_0 (ignoring diffusive effects) is incredibly short for nanoscale systems, consistent with a small mean inertial range $v_0\tau$ in most systems. For example, if the head domain of a kinesin head is approximated by a sphere with radius $R = 6$ nm and a mass $m = 6 \times 10^{-23}$ kg, the inertial lifetime is only picoseconds in water with $\eta = 1$ cp [21]. Even if such a body was launched forward with kinetic energy equal to the entire free energy of ATP, the resulting inertial displacement would be a small fraction of the 16 nm distance required for kinesin's functionality.

An overdamped description is thus appropriate when analyzing nanoscale dynamics. The addition of thermal fluctuations does not alter this result, but investigation of inertial dynamics in light of thermal noise leads to simple, but useful, results for diffusional displacement and inertial energetics. Consider a particle with viscous drag coefficient Γ (e.g. from Eq. 43) with thermal noise modeled by a second-order Langevin equation (ref. Section 2.1.2 and [23])

$$m\ddot{x} = -\Gamma\dot{x} + F + \xi(t) \quad (44)$$

where $\xi(t)$ is a stochastic Gaussian white noise modeling fluctuations from the thermal bath, and F is an applied constant external force. $\xi(t)$ is both an unbiased and uncorrelated in time, such that (as before with Eq. 3)

$$\begin{aligned}\langle \xi(t) \rangle &= 0 \\ \langle \xi(t_1)\xi(t_2) \rangle &= A\delta(t_1 - t_2)\end{aligned}\tag{45}$$

where A is the magnitude of the noise (to be defined shortly in Eq. 47), and angular brackets $\langle \cdot \rangle$ denote averaging over realizations of the noise. The solution to Eq. 44 is straightforward

$$\begin{aligned}x(t) - x(0) &= \frac{1}{m} \int_0^t dt_1 \int_0^{t_1} dt_2 e^{(t_2-t_1)/\tau} \xi(t_2) \\ &+ (v_0 - v_F) \tau (1 - e^{-t/\tau}) + v_F t\end{aligned}\tag{46}$$

$v_F = F/\Gamma$ the asymptotic mean velocity due to F , and $\tau = m/\Gamma$ again the relaxation time. Eq. 46 determines all relevant averages for the system, as demonstrated in Section 2.1.2 and Appendix A.1. A is then fixed by ensuring that the asymptotic variance of the velocity $A\tau/2m^2$ equals the squared thermal velocity $v_T^2 = k_B T/m$, i.e.

$$A = 2\Gamma k_B T\tag{47}$$

A similar treatment of the positional variance at zero force sets the diffusion constant $D = \langle \Delta x^2(t \rightarrow \infty) \rangle / 2t$

$$D = \frac{k_B T}{\Gamma}\tag{48}$$

Equations 47 and 48 may also be derived from the more general fluctuation-dissipation relations by Onsager and Einstein.

Two sources of power input drive the Brownian particle in Eq. 44: the mechanical power by the constant force F and the power of thermal fluctuations. The mechanical power rapidly (for times greater than τ) approaches the deterministic value

$\langle \dot{W} \rangle = Fv_F$. The power due to thermal noise is a much larger constant

$$\langle \dot{Q}_{in}(t) \rangle \equiv \langle \xi(t)\dot{x}(t) \rangle = \frac{k_B T}{\tau} \quad (49)$$

The ratio of these is

$$\frac{\langle \dot{W} \rangle}{\langle \dot{Q}_{in} \rangle} = \frac{v_F \tau}{L_F} \quad (50)$$

where the characteristic length $L_F = k_B T / F$ has been used. The inertial-like distance $v_F \tau$ in a nanoscale system is typically orders of magnitude smaller than L_F , indicating that thermal power is by far the dominant source of power input. However, thermal power is balanced by equally large viscous drag dissipation heat

$$\dot{Q}_{out} = \Gamma \dot{x}^2 \quad (51)$$

that approaches $\frac{k_B T}{\tau}$ for ensembles near thermal equilibrium. The imbalance between viscous drag output and thermal power input rapidly approaches the mean drag heat Γv_F , which is relatively small compared to the thermal power itself.²

While viscous drag and thermal fluctuations set the dominant power scales of all Brownian dynamics, this does not determine the relevance of thermal diffusion in the actual generation of spatial displacements. Specifically, compare the ‘‘power stroke’’ time $\tau_{PS} = L\Gamma/F$ (the time to travel a distance L at velocity v_F) to the Brownian motion time $\tau_{BM} = L^2/2D$ (the time for the diffusional width $\sqrt{2Dt}$ to equal L). The ratio τ_{BM}/τ_{PS} is

$$\frac{\tau_{BM}}{\tau_{PS}} = \frac{L}{2L_F} \quad (52)$$

where $L_F = k_B T / F$ as before. Brownian motion is thus the dominant mode of transport for distances much shorter than L_F . An alternate interpretation of Eq. 52 is that power stroke principles dominate when the viscous heat $F L$ generated by the force

²Notice that the mean irreversible heat dissipation in this case rapidly approaches the work done on the particle (a statement of energy balance). This last observation is familiar from overdamped deterministic dynamics but fails to be true in general (consider equilibrium systems).

F is much greater than $k_B T$. This last observation will again appear in Section 3.3 in a different context.

The relative contribution of power stroke and Brownian motion components in the abstracted flagellar propulsion of an E. coli bacterium can already be examined at this level of complexity, without recourse to elaborate equilibrium theory.³ Notice, however, the molecular mechanism itself is more complicated and may receive significant contributions from Brownian motion [102]. Following H. Berg [4], E. coli is approximated by a sphere of radius $1 \mu\text{m}$ with the density of water. The bacterium propels itself in runs that last approximately $\tau_{tot} = 1 \text{ s}$, with a secular velocity approximately $v = 2 \times 10^{-5} \text{ m/s}$. Motion takes place in a fluid with $\eta = 1 \text{ cp}$ at temperature $T = 298 \text{ K}$. The mean drift distance $v\tau_{tot} = 20 \mu\text{m}$ accumulated during a given run is many times the diffusional distance $\sqrt{2D\tau_{tot}} = 0.7 \mu\text{m}$. Consistently, a viscous drag heat of $2000 k_B T$ also indicates a power stroke (by Eq. 52). Flagellar propulsion as an abstract mechanism thus exemplifies a power stroke. Indeed, this must be true if E.coli is to effectively overcome diffusion in order to seek out food sources in chemotaxis. The situation is quite different for the diffusion of a kinesin head, which can freely diffuse the required 16 nm stepping distance in only $2 \mu\text{s}$. This rate is rapid compared to the overall rate of kinesin, which is of order milliseconds.

3.2 Simple Models of Rectified Brownian Motion

The inclusion of non-equilibrium boundary conditions is sufficient to rectify Brownian motion. The implementation of rectification is frequently done by the imposition of effectively absorbing and reflecting boundary conditions that respectively promote and inhibit diffusing trajectories to transition into other regions of state space. These boundaries can be established by the coupling of a few essentially irreversible events,

³E.coli is indeed overdamped. Its inertial lifetime is estimated to be $\tau = 0.2 \mu\text{s}$. Once propulsion has ceased, the mean inertia from flagellar propulsion would in this time have the bacterium drift less than an angstrom on average. [4]

e.g. a statistically favorable chemical reaction, to mechanical progression in the system.

A straightforward and illustrative example is one-dimensional overdamped⁴ diffusion in a potential. Supposing a coordinate x , a force potential $U(x)$, and a diffusion constant D , the mean first passage time (MFPT) for a diffusive process to travel from a reflecting boundary at $x = 0$ to an absorbing boundary at $x = L$ is [23]

$$\tau_{MFPT} = \frac{1}{D} \int_0^L dy \int_0^y dz e^{(U(y)-U(z))/k_B T} \quad (53)$$

The characteristic times τ_{PS} and τ_{BM} from free diffusion are faithfully reproduced by Eq. 53 for $U(x) = -Fx$ ($FL \gg k_B T$) and a constant potential, respectively. Rectification produces more pronounced effects once an uphill potential barrier is instead considered. If $U(x) = Fx$ ($FL \gg k_B T$), then τ_{MFPT} become exponentially large

$$\tau_{MFPT} \approx \frac{L_F^2}{D} e^{FL/k_B T} \quad (54)$$

as would be expected from transition state theory [30]. Mechanical work can thus be generated from thermal fluctuations in the presence of rectification. An early RBM model for kinesin utilized this approach to oppose 3 pN over a 16 nm stepping distance, i.e. a $12 k_B T$ potential barrier, with a characteristic time of milliseconds⁵. Generally, the utilization of rectification to bring about thermally-driven barrier penetration is a recurrent scheme in nano-biology.

While the introduction of reflecting and absorbing boundaries considerably simplifies the analysis of a diffusive process, there are several unphysical artifacts that arise. The most obvious is the irreversibility at these boundaries, which can be interpreted as an infinite expenditure of free energy. A physical system always has some probability for reversing a transition. Two artifacts more closely tied to diffusion are

⁴Recall that the assumption of overdamped dynamics is needed for the NESS formalism used in this thesis.

⁵Notice that this model assumes external force is applied directly to a tethered head, rather than at some intermediate point between the heads.

the divergences of the NESS free energy profile $\mu(x)$ and ensemble velocity $v(x)$ near an absorbing boundary (ref. Section 2.2). By definition, the probability density at an absorbing boundary is zero. If ϵ is a distance to the boundary, a linear approximation of the probability density near the boundary leads to a $\mu \sim \ln(\epsilon)$ divergence and a $v \sim 1/\epsilon$ divergence. These two divergences are related, e.g. by Eq. 34, and signal a breakdown of the overdamped formalism assumed presently. Indeed, if an absorbing boundary was imposed instead on the inertial dynamics of Section 3.1, the maximum velocity expected at the absorbing boundary would be limited in scale by the equilibrium thermal velocity $\sqrt{k_B T/m}$.

3.3 Steady State Properties of Nanoscale Biological Processes

Cellular enzymes are isothermal motors that spontaneously perform tasks by virtue of a coupling to available free energy. On the assumption that the enzyme state and ambient chemical concentrations provide a complete description of the system,⁶ a non-equilibrium thermodynamic approach to enzyme kinetics can be constructed [32, 65]. Such a non-equilibrium theory was reviewed in Section 2.2, primarily emphasizing mathematical relations that generally hold for stochastic systems. Revisiting the content of Section 2.2 with a physical interpretation is an important step in appreciating the role of irreversibility, particularly as it relates to defining RBM systems.

In contrast to the mathematical approach in Section 2.2.2, where paths in state space were the natural objects, the most basic thermodynamic objects in fluctuating non-equilibrium thermodynamics are cycles. The decomposition of global free energy expenditure in terms of fundamental cycles (each with an associated thermodynamic force) has been long known [32, 80], in analogy to theorems in circuit theory. An enzyme that performs a cyclic motion \mathcal{C} in state space must only leave the environment

⁶The environment is thus assumed to quickly equilibrate in response to changes in the enzyme.

changed, with an assumed environmental free energy difference ΔG . The cycle free energy is accordingly defined $\Delta\mu(\mathcal{C}) = \Delta G$. Since each enzyme typically only couples to a finite number of distinct reactions, all such ΔG should arise from a finite set of fundamental free energies (ref. Eq. 39).

The affinity-based version of the cycle free energy (ref. Eq. 25) is identified with this physical picture, providing ties between thermodynamics and irreversibility. Namely, the steady state weight of a cyclic path in state space is exponentially biased by free energy expenditure

$$\frac{P_\tau(\mathcal{C})}{P_\tau(\mathcal{C}^R)} = e^{-\Delta\mu(\mathcal{C})/k_B T} \quad (55)$$

Such an emphasis on cycles is consistent with the ability for localized rectification to induce global non-equilibrium currents. As long as $\mu(\mathcal{C}) < 0$ for a cycle, energetically uphill actions can be statistically biased forward. Compare this view to the macroscopic “power stroke” view of thermodynamics, which forbids autonomous processes that require an observable increase in free energy, i.e. a macroscopic activation, to function.⁷ That is, mechanical work in a power stroke model is generated only by means of a continual expenditure of free energy. RBM requires the much weaker condition based on Eq. 55, and thus, RBM is a natural approach for basic molecular processes.

The generalization of cycle free energies to path free energies is somewhat less inspired from macroscopic thermodynamics and instead is based on kinetic relations. The affinity-based path free energy (ref. Eq. 24) allows a detailed description of irreversibility, via [47]

$$\frac{P_\tau(\mathcal{P})}{P_\tau(\mathcal{P}^R)} = e^{-\Delta\mu(\mathcal{P})/k_B T} \quad (56)$$

Related advantages of this formulation for the free energy expenditure are discussed

⁷The fact that a power stroke has rather specific kinetic and thermodynamic characteristics, compared to general stochastic processes, is a key motivation for the definition of a power stroke in Section 3.5.

in Section 2.2.2. An alternative, though not preferred, choice for the path free energy is the “physical” free energy difference (ref. Eq. 16)

$$\Delta U(\mathcal{P}) = -k_B T \ln \frac{w_t(\mathcal{P})}{w_t(\mathcal{P}^R)} \quad (57)$$

which is more directly measured by examining short time propagation outside of steady state.⁸ The two are simply related by

$$\Delta\mu(\mathcal{P}) - \Delta U(\mathcal{P}) = k_B T \ln \frac{p^{(s)}(x_f)}{p^{(s)}(x_i)} \quad (58)$$

for initial and final states x_i and x_f , respectively. Transitions can satisfy $\Delta U \approx \Delta\mu$ (in the sense of relative magnitudes) if both $|\Delta U| \gg k_B T$ and the endpoints of the steady state distribution are not exponentially different. Since these conditions frequently occur for macroscopic processes, intrinsic irreversibility of macroscopic free energy transduction is sensible, and the two versions of the free energy do not need to be distinguished. The asymptotically long trajectories in fluctuations theorems have a similar correspondence between the two free energies.

The existence of a free energy potential (either of the $\mu(x)$ or $U(x)$ variety) is both natural and useful in the study of nanoscale systems coupled to a finite number of free energy sources (ref. Section 2.2.4). However, despite the ubiquity of potentials, the degree that a potential affects steady state flow should not be underestimated. A primary consequence is that a region \mathcal{R} with a potential $\mu(x)$ is a boundary driven process (this is discussed for a reaction network in Appendix A.2). Essentially, the existence of a potential $\mu(x)$ in a region \mathcal{R} implies that the irreversible heat production rate \dot{Q}_{irr} associated with \mathcal{R} reduces to boundary terms. For a continuous system, defining the thermodynamic force $\vec{\Pi} = -\vec{\nabla}\mu$ and the steady state current \vec{J} , the kernel $\vec{\Pi} \cdot \vec{J}$ in the integrand for \dot{Q}_{irr} reduces to a divergence

$$\vec{J} \cdot \vec{\Pi} = -\vec{J} \cdot \vec{\nabla}\mu = -\vec{\nabla} \cdot (\mu\vec{J}) \quad (59)$$

⁸When ΔU is globally derived from a potential $U(x)$, the Boltzmann distribution of $U(x)$ provides the equilibrium distribution. This is of course consistent with $U(x)$ being the free energy of the quasi-equilibrium state x .

where the steady state condition $\vec{\nabla} \cdot \vec{J} = 0$ has been used. Eq. 59 makes clear why regions with a potential are boundary driven.

Boundary driven processes are quite common in practice, e.g. occurring in all diffusive processes driven by a finite number of fundamental cycles (ref. Section 2.2.4). However, a special type of boundary driven process, which we label a “rectified process,” frequently describes diffusive transport in nanoscale biological mechanisms. A rectified process in a region \mathcal{R} is defined as a boundary driven process that supports probability current at two boundaries, $\partial\mathcal{R}_1$ and $\partial\mathcal{R}_2$, that are separated in state space. By Eq. 59 and Eq. 28, the free energy expenditure and current in \mathcal{R} can be interpreted as a boundary rectification phenomenon if one boundary is held at a higher $\mu(x)$ potential than the other. Indeed, if the boundaries in a rectified process are defined as equipotential surfaces of $\mu(x)$, then probability current between the boundaries is always rectified to flow towards the surface of lower free energy. Section 3.5 will use this interpretation of rectification in the definition of RBM, defining RBM in the class of processes that are suitably approximated by a rectified process. H. Qian has already emphasized the interpretation of rectification in terms of boundary driven processes, but rectified processes are presently adopted for their directional structure [66].

Due to the relevance of this point in the definition of RBM, notice that an approximate boundary driven process may not share certain features that accompany a true boundary driven process. For example, there may not exist boundary conditions for an approximate boundary driven process that lead to equilibrium conditions. What is shared in both cases is a typical tight coupling between the mechanical state and free energy expenditure, by definition of the validity of an approximate free energy potential $\mu(x)$. The validity of $\mu(x)$ is equivalent to the statistical dominance of trajectories from a single free energy class, in the sense of Eq. 40, for stochastically observed trajectories. This free energy class of trajectories can be interpreted as the boundary

driven portion of the system. A system with aberrant trajectories pruned from the dynamics produces an exact boundary driven system that statistically approximates the real process. It is in this sense that we interpret an approximate rectified process.

3.4 *Regions of Reversibility*

A useful concept to be used shortly is that of a region of approximate reversibility. Supposing that a potential $\mu(x)$ exists, a local region of approximate reversibility ϵ may be defined for the state x_0

$$\mathcal{R}(x_0, \epsilon) = \{x : |\mu(x) - \mu(x_0)| < \epsilon \text{ , } x \text{ connected to } x_0\} \quad (60)$$

where the last condition is to ensure $\mathcal{R}(x_0, \epsilon)$ is a connected region containing x_0 . For example, $\epsilon = k_B T$ is such a choice, though smaller values are equally useful. Such regions have bounded affinities between all interior points, and for sufficiently small ϵ , they can be shown to approach local equilibrium.

Consider this in the case of diffusion. One-dimensional diffusion at steady state from $x = 0$ to an absorbing barrier at $x = L$ (ref. Section 3.2) has a linearly varying probability density, with an associated logarithmic free energy profile

$$\Delta\mu(x) \equiv \mu(x) - \mu(0) = k_B T \ln \frac{L-x}{L} \quad (61)$$

If x_n is defined such that $\Delta\mu(x_n) = -nk_B T$, Brownian motion can be described by intervals of approximate irreversibility

$$\Delta x_n \equiv x_n - x_{n-1} = L(e^{-1} - 1)e^{-n} \quad (62)$$

Each interval Δx_n is $(1 - e^{-1}) \approx 63\%$ the remaining forward distance $L - x_{n-1}$ to the absorbing barrier, with the implication that the boundary-related irreversibility of a purely diffusive process follows from approximately reversible regions of length comparable to the distance to the boundary. These large regions of reversibility are

typical of diffusion-based spatial transport, and appear even in the most severe case of an absorbing boundary.

Regions of reversibility along a given direction of mechanical progress form the definitions for power strokes and RBM in Section 3.5 (though the notation in Eq. 60 will be avoided).

3.5 Rectified Brownian Motion, Power Strokes, and Brownian Ratchets

The distinction between power stroke and Brownian motion based mechanisms in nano-biology has frequently been done in the literature, especially concerning molecular motors [93]. Such a division is intuitively clear in many examples, but a set of precise criteria has been largely lacking for the general case. The NESS approach fortunately provides several compelling criteria that can be used for this purpose, leading here to a set of proposed distinguishing characteristics for all of RBM, power strokes, and Brownian ratchets.⁹

Recall that a power stroke is intuitively a continual and directional release of stored internal energy that is used to push the system through the viscous medium and possibly used to generate mechanical work. Free energy expenditure in this case continuously compels a power stroke forward by means of a “force,” which in this case is interpreted as a free energy gradient that strongly biases propagation (ref. Eq. 42). A power stroke forbids large fluctuations from providing productive spatial transport, since this would necessarily imply a Brownian motion based mechanism.¹⁰ A power stroke for characteristic spatial resolution δ is thus characterized by the absence of regions of reversibility (in the sense of Section 3.4) longer than δ along the power stroke. This condition of progressive irreversibility at a resolution δ is a necessary

⁹There exist several competing definitions for what constitutes a Brownian ratchet, and so a particular such definition will be adopted.

¹⁰More properly, this would be a thermal fluctuation based mechanism, but this distinction is largely unnecessary for physical systems.

condition for any power stroke.

The most direct method to identify progressive irreversibility is by means of examining the path free energy of a representative path \mathcal{P}_{PS} along the power stroke.¹¹ By the assumption of progressive irreversibility, \mathcal{P}_{PS} can be partitioned into many smaller paths \mathcal{P}_i that each progress a distance δ and satisfy

$$-\Delta\mu(\mathcal{P}_i) \gtrsim k_B T \quad (63)$$

Such a decomposition naturally arises in simple Fokker-Planck models for a power stroke, and Appendix A.3 outlines the details for the one-dimensional case. A second necessary condition for a power stroke follows

$$-\Delta\mu(\mathcal{P}_{PS}) \gg k_B T \quad (64)$$

i.e. power strokes must be essentially irreversible as a whole (this is the “power” in a power stroke). Failure of either Equations 63 or 64 to apply signals the absence of a power stroke. For an example that will be revisited in Section 4.1, the diffusive spatial transport in ubiquinone has a heat production per traversal that is many orders of magnitude smaller than $k_B T$ and thus clearly not a power stroke.

A secondary concern for a power stroke is the ability to persist forward during application of an opposing external force (the role of a power stroke in macroscopic motors is often to overcome external loads). Robustness of progressive irreversibility under a given range of external forces can be imposed as an additional condition for a power stroke, if desired. However, this complication will not be explored presently.

The condition of progressive irreversibility in Equations 63 and 64 is usually not sufficient to identify a power stroke. “Futile heat,” which is not associated with the observed irreversibility of spatial displacements, may lead to spurious directional irreversibility. This concern can be alleviated in the case of rectified processes (ref.

¹¹Such a path may be sampled from the steady state of the system.

Section 3.3). Approximate rectified processes occur relatively often in many nanoscale biological mechanisms of interest, e.g. for molecular motors with tight mechanochemical coupling (ref. Section 2.2.4). A free energy potential $\mu(x)$ must then exist. Thus, there is not futile heat, in the sense that free energy expenditure and mechanical progression are tightly coupled.¹² Given the existence of a rectified process, a proposed definition for a power stroke is a process with progressive irreversibility along a given direction. This definition can be refined (e.g. with the above condition for the robustness under external force), but it satisfies the basic notion that a power stroke compels the system forward by a continual expenditure of free energy.

The failure of progressive irreversibility implies that there exists a large region of approximate reversibility in the direction of mechanical progression. With this motivation, a spatial motion in a mechanism governed by a rectified process is said to be RBM when power strokes are inadequate to explain the mechanism, e.g. that the irreversibility of the mechanism is not explained by a few dominating power strokes.¹³ RBM is thus defined to be complementary to power stroke mechanisms in the set of rectified processes. Examples of RBM mechanisms are largely consistent with this definition [20, 21, 36, 52]. The seeming lack of a strong biological selection for power stroke systems, in light of the robustness of diffusion at the nanoscale, would appear to make the special condition of progressive irreversibility unnecessary for the fundamental mechanisms of nano-biology. RBM is thus conjectured to be prevalent in nano-biology. Only when the required distance of diffusive spatial transport is large, e.g. many microns, does the failure of thermal diffusion relative to drift-based schemes truly occur.

Brownian ratchets can be compared with the above definition above for RBM. The well-known Brownian ratchets, as defined by Reimann and Hänggi [69], typically

¹²Mechanical progression may in this case be measured by equipotential surfaces of $\mu(x)$.

¹³This definition can be refined for a particular set of models, but the basic notion of RBM remains clear.

are taken to obey the one-dimensional reaction-diffusion equation (periodic in some spatial length L)

$$\begin{aligned}\frac{\partial p_i}{\partial t} &= -\frac{\partial J_i}{\partial x} + \sum_j K_{ij}p_j - \sum_j K_{ji}p_i \\ J_i &= -D_i \left(\frac{1}{k_B T} \frac{\partial U_i}{\partial x} + \frac{\partial}{\partial x} \right) p_i\end{aligned}\tag{65}$$

with J_i the i^{th} species spatial probability current, D_i the diffusion constant, U_i the periodic force potential function, and K_{ji} the periodic position-dependent transition rate from species i to j . Brownian ratchets are restricted to those systems that include Brownian motion as an essential component, i.e. the power stroke picture is insufficient in a Brownian ratchet mechanism. Periodicity of the potentials implies that nonzero cycle free energies only arise from cycles that twist around the reaction coordinate (ref. Section 3.3), and these reactions can be coupled to mechanical movement.

The dynamics in Eq. 65 typically has a loose correspondence between mechanical progression and free energy expenditure [68], and this fact excludes the existence of an underlying rectified process for mechanical progression. Brownian ratchets thus lack an interpretation in terms of boundary rectification (in the sense of the path free energy), and they are accordingly distinct from RBM mechanisms. The type of rectification in Brownian ratchets instead occurs in the statistical sense of a net drift that arises from breaking the detailed balance symmetry of an equilibrium system [68].¹⁴

It should be made clear that Brownian ratchets also generally differ from RBM mechanisms on a simpler basis. Namely, Brownian ratchets require a periodic ratchet potential, while RBM mechanisms do not require any such ratchet potential. Ubiquinone and rotary enzymes, for example, are RBM mechanisms that lack spatially periodic

¹⁴This is Curie's principle, which asserts that an effect not prohibited *a priori* from symmetry principles should be expected to occur. [69]

potentials (ref. Chapter 4). RBM mechanisms are in this respect more general than Brownian ratchets.

A closing word on the definitions for power strokes and RBM is in order. While there exists room to improve on the above definitions, a feature that appears to be firm in the present approach is that power strokes are best understood as distinct objects in a mechanism. A different approach, notably that characterized by the works of Peskin, Wang, and Oster [60, 100], assumes that general mechanisms can be decomposed into simple percentages of power stroke and Brownian motion-based motion.¹⁵ That is, some simple measurement provides the values ρ_{PS} and ρ_{BM} that quantify the importance of power stroke and Brownian motion, respectively (Eq. 52 is an example for such a measurement in a very simple setting). These are complementary, satisfying $\rho_{PS} + \rho_{BM} = 1$. While sensible in certain circumstances, such a decomposition encounters difficulty in general situations.¹⁶ For example, consider the proposed strain-induced bias amplification mechanism in conventional dimeric kinesin (ref. Section 5.1), which depends critically on the existence of both diffusion and the so-called neck linker zippering [71], the latter of which is often thought to be a power stroke component. Supposing that this mechanism can be decomposed into Brownian motion and power stroke components risks erroneously asserting the independence of such components.

¹⁵In these cited works, the term “Brownian ratchet” is used to describe Brownian motion-based mechanisms.

¹⁶Some of these problems are related to the arbitrariness of the measure used. A measure may be ill fit to the basic notion of what a power stroke actually entails.

CHAPTER IV

UBIQUINONE AND ROTARY ENZYMES

The simplest application and interpretation of RBM arises in two systems fundamental to cellular metabolism: the ubiquinone shuttle and rotary enzymes [85]. Spatial transport in both systems is achieved exclusively through thermal fluctuations, while rectification follows from reactions at the boundaries of thermal diffusion. The conceptual aspects of RBM can be simply explored through these systems.

Simple models for ubiquinone and a rotary enzyme are discussed in Sections 4.1 and 4.2, respectively. The appearance of a rectified process naturally arises in these models. Section 4.3 revisits the discussion of rotary enzymes in the case of biotin, including a summarized account of results from molecular dynamics simulations. Characteristic properties of biotin diffusion are presented from these simulations.

4.1 Ubiquinone Model, Revisited

The ubiquinone shuttle is an essential step in the biased facilitated diffusion of protons across a membrane barrier. Two electrons and two protons are transferred to ubiquinone by a donor reaction near one side of the membrane and taken again by an acceptor reaction near the other side. Free energy from this redox reaction takes part in the energetically uphill task of building a large proton concentration gradient across the boundary [85]. Ubiquinone's structure consists of a reactive head that participates in redox reactions that is connected to a long, hydrophobic isoprenoid tail that gives ubiquinone the overall hydrophobic character necessary to reside in a lipid bilayer. The model for this situation is taken from an earlier paper [20], and consists of one-dimensional diffusion of the two forms of ubiquinone between two reactive sites (ref. Fig. 1). Discussion of this model will mostly be a review of results that arise

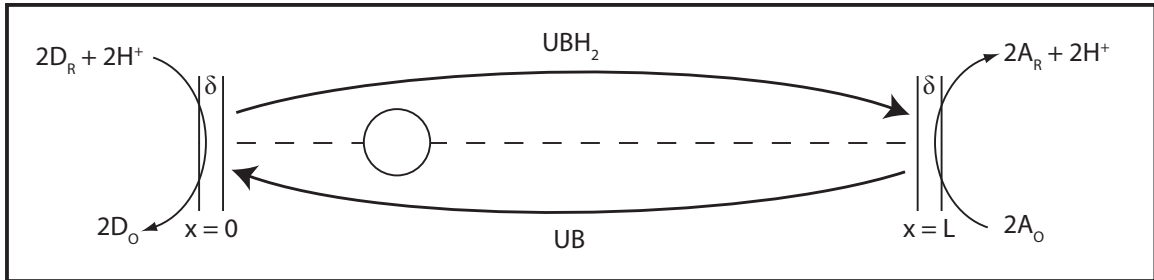


Figure 1: A model for the ubiquinone shuttle [20]. The ubiquinone molecule in this simplified model functions as an intermediate carrier of protons and electrons between donor and acceptor molecules on opposite sides of a lipid membrane bilayer. Oxidized (UQ) and reduced (UQH_2) forms of ubiquinone are interconverted via redox reactions between donor molecules (oxidized form D_O , reduced form D_R) and acceptor molecules (oxidized form A_O , reduced form A_R). Redox reactions are assumed to occur at a reactive site of small width δ around the membrane boundaries. Ubiquinone undergoes free diffusion in a coordinate x between the two boundaries at locations $x = 0$ and $x = L$, and this diffusion is rectified by non-equilibrium redox reactions that drive the flow of electrons from donor to acceptor molecules on average.

from the solution found in the earlier paper [20].

Ubiquinone is modeled to be a spherical particle of radius $R = 0.75$ nm, immersed in a lipid medium of viscosity $\eta = 25$ cP (the approximate viscosity of an oleate lipid medium). Viscous drag on ubiquinone is thus given by the Stokes formula Eq. 43.¹ Parameters for this model can be derived on the assumption that the ubiquinone tail is wrapped around the hydrophilic head in a compact structure, e.g. as a shield to the hydrophilic core. However, molecular dynamics simulations suggest ubiquinone diffuses with the long isoprenoid tail in an extended structure [84]. The assumptions of the simpler spherical model are not severe in terms of order of magnitude estimates, since diffusion will be demonstrated to be mostly transparent from a free energy standpoint.

The free energy difference that drives ubiquinone is given as usual by the contributions of standard redox free energy potentials and by concentration terms. For the

¹The Stokes formula can be considered an order of magnitude estimate.

donor reaction, ubiquinone is reduced with free energy (per reaction)

$$\Delta G_D = \Delta G_D^{(0)} + k_B T \ln \left(\frac{[D_O]^2 [UQH_2]}{[D_R]^2 [UQ]} \right) \quad (66)$$

where $[\cdot]$ are concentrations, and $\Delta G_D^{(0)}$ is a pH-dependent redox free energy. The acceptor reaction oxidizes ubiquinone with free energy (per reaction)

$$\Delta G_A = \Delta G_A^{(0)} + k_B T \ln \left(\frac{[A_R]^2 [UQ]}{[A_O]^2 [UQH_2]} \right) \quad (67)$$

The total free energy for the ubiquinone cycle is $\Delta\mu = \Delta G_D + \Delta G_A$ and satisfies $\Delta\mu < 0$ if the process is spontaneous in the forward direction.

The diffusive motion for both oxidized and reduced forms of ubiquinone are governed by two purely diffusive Fokker-Planck equations with probability densities $g(x)$ and $f(x)$, respectively. The small boundary layer of length δ near the membrane surfaces interconverts these forms by reactions between effective chemical states

$$X_0 = f(0) \delta \quad X_L = f(L) \delta \quad (68)$$

$$Y_0 = g(0) \delta \quad Y_L = g(L) \delta$$

such that diffusion is biased by the boundary chemical kinetics

$$\begin{aligned} \dot{X}_0 &= -\alpha_0 X_0 + \beta_0 Y_0 + D \frac{\partial f}{\partial x}(0, t) \\ \dot{Y}_0 &= \alpha_0 X_0 - \beta_0 Y_0 + D \frac{\partial g}{\partial x}(0, t) \end{aligned} \quad (69)$$

$$\dot{X}_L = -\alpha_L X_L + \beta_L Y_L - D \frac{\partial f}{\partial x}(L, t)$$

$$\dot{Y}_L = \alpha_L X_L - \beta_L Y_L - D \frac{\partial g}{\partial x}(L, t)$$

with rate constants consistent with Equations 66 and 67. Solution of the steady state can be done with straightforward algebraic manipulations and will not be provided

here. The natural diffusive rate constant

$$r = D/L\delta \quad (70)$$

arises in the steady state solution, and the rapidity of diffusion is characterized by the fact that r is physically many orders of magnitude smaller than the chemical reaction rates. Ubiquinone in this model thus diffuses between the boundaries many times before partaking in a chemical reaction. The use of effective states in Eq. 68 is consistent with a reaction-limited model.

Despite the rapid transport of a ubiquinone between boundaries of a membrane, this motion is highly reversible in nature. Consider the irreversible heat production rate \dot{Q}_{irr} due to non-equilibrium diffusion. Evaluation of \dot{Q}_{irr} for a given ubiquinone form reduces to a boundary term (ref. Eq. 59)

$$\begin{aligned} \dot{Q}_{irr} &= J(k_B T \ln p_s(0) - k_B T \ln p_s(L)) \\ &= J(\mu(0) - \mu(L)) = -J\Delta\mu \end{aligned} \quad (71)$$

where $-\Delta\mu$ is the heat production associated with the steady state traversal of the membrane. Substituting the steady state solution into Eq. 71, the free energies for diffusion in the reduced and oxidized species are

$$\begin{aligned} \Delta\mu_f/k_B T &= (\mu_f(L) - \mu_f(0))/k_B T \\ &= \ln\left(1 + \frac{\beta_L(\alpha_0 + \beta_0)}{r(\beta_0 + \beta_L)}\right) - \ln\left(1 + \frac{\beta_0(\alpha_L + \beta_L)}{r(\beta_0 + \beta_L)}\right) \end{aligned} \quad (72)$$

$$\begin{aligned} \Delta\mu_g/k_B T &= (\mu_g(L) - \mu_g(0))/k_B T \\ &= \ln\left(1 + \frac{\alpha_L(\alpha_0 + \beta_0)}{r(\alpha_0 + \alpha_L)}\right) - \ln\left(1 + \frac{\alpha_0(\alpha_L + \beta_L)}{r(\alpha_0 + \alpha_L)}\right) \end{aligned}$$

Assuming that r is much larger than the reaction rates, Eq. 72 is approximately

$$\begin{aligned}\Delta\mu_f/k_B T &\approx \frac{\beta_L(\alpha_0 + \beta_0) - \beta_0(\alpha_L + \beta_L)}{r(\beta_0 + \beta_L)} \\ \Delta\mu_g/k_B T &\approx \frac{\alpha_L(\alpha_0 + \beta_0) - \alpha_0(\alpha_L + \beta_L)}{r(\alpha_0 + \alpha_L)}\end{aligned}\tag{73}$$

Thus, the characteristic heat production due to non-equilibrium diffusion is here several orders of magnitude smaller than $k_B T$ per cycle, with a corresponding irreversibility $e^{-\Delta\mu/k_B T}$ of the same magnitude. The concentration terms for each form of ubiquinone in Equations 66 and 67 can accordingly be approximated by constants, and the ubiquinone shuttle from a free energy standpoint appears to be a simple intermediate chemical state.

The characteristic heat production rate \dot{Q}_{irr} can be compared to other characteristic heat production rates in ubiquinone's diffusion. If ubiquinone was a uniformly moving body at the characteristic diffusion velocity $v_L = L/\tau_{BM} = 2D/L$, then the frictional dissipation rate $\dot{Q}_{uniform}$ (ref. Section 3.1) is²

$$\dot{Q}_{uniform} = \Gamma v_L^2 = \frac{2k_B T}{\tau_{BM}}\tag{74}$$

i.e. a large heat production rate of $2k_B T$ per diffusional time τ_{BM} . The still larger (and primarily reversible) heat $\dot{Q}_\tau = k_B T/\tau$ due to thermal fluctuations is of order $k_B T$ per nanosecond. These quantities satisfy the strong inequalities

$$\dot{Q}_\tau \gg \dot{Q}_{uniform} \gg \dot{Q}_{irr}\tag{75}$$

Heat production due to Brownian motion by far dominates other characteristic scales, as usual for nanoscale mechanisms, while the relative largeness of $\dot{Q}_{uniform}$ is due to the reaction-limited nature of diffusion.

² $\dot{Q}_{uniform}$ is a measure of the the minimal irreversible heat production of a uniform power stroke before diffusive motion becomes the dominant mode of transport (e.g. ref. Eq. 52)

4.2 Simple Rotary Enzyme Model

The analysis of ubiquinone is similar to that of the rotary enzymes [20]. Rotary enzymes are flexible, chain-like prosthetic groups that facilitate the transport of reaction intermediates between spatially separated catalytic regions on a much larger protein (for simplicity, reactions during diffusion between catalytic sites are ignored). These occur in several varieties, including biotin, lipoamide, and phosphopantetheine [85], each of which has a specific reactive terminus.³ Rotary enzymes all have a low molecular weight, equivalent to only a few amino acids, but their extended structure exaggerates the effects of drag from the surrounding aqueous environment, such that an approximate diffusive interpretation of motion is possible.

A simple model for a rotary enzyme replaces the reactive head with an overdamped particle in a three-dimensional conservative force field $-\nabla U$, with U derived from the entropic and enthalpic contributions of the flexible chain.⁴ In this manner, the flexible portion of the chain is treated in a mean-field sense. The catalytic sites that support chemical changes of the head correspond to a set of two-dimensional surfaces Σ_i on the protein, where the forward sense of the reaction is directed from catalytic site i to $i + 1$ (excepting in the final reaction of the periodic chemical cycle). The rotary enzyme's chemical state is similarly ordered, with the reaction between chemical states i and $i + 1$ occurring at Σ_i .

Since the entropy production kernel for such diffusion reduces to a divergence (ref. Eq. 59), irreversible heat dissipation due to the $\Sigma_i \rightarrow \Sigma_{i+1}$ diffusional mode is a boundary term

$$\dot{Q}_{irr}(i \rightarrow i + 1) = \int_{\Sigma_i} \mu_i \vec{j}_i \cdot d\vec{S}_i - \int_{\Sigma_{i+1}} \mu_i \vec{j}_i \cdot d\vec{S}_{i+1} \quad (76)$$

with forwardly oriented (in the direction of the reaction) surface elements $d\vec{S}_i$, the i^{th}

³Phosphopantetheine is also known as a long group in coenzyme A.

⁴Effective drag tensors and diffusion tensors of the head also have contributions from the chain.

species NESS chemical potential μ_i , and current density \vec{j}_i . Like ubiquinone, reaction rates may be considered much slower than diffusional times, such that approximate equilibration of a diffusive state occurs and free energy expenditure due to diffusion is small. Of course, if diffusion tends to get trapped in effective bound states at a catalytic site (neglected in the above model), a more detailed treatment is necessary.

The simplest variant of the catalytic site model is that of a rigid rotor with a single rotational degree of freedom θ that diffuses between two catalytic sites, e.g. $\theta_1 = 0$ and $\theta_2 = \pi$. This model can be mapped exactly to the ubiquinone model in Section 4.1. Supposing diffusive forces alone, basic estimates of the diffusion time to subtend this angle are of roughly of order nanoseconds for biotin or lipoamide.⁵

4.3 Biotin Rotary Enzyme Molecular Dynamics Simulation

The simple rotary enzyme model in Section 4.2 is useful for outlining free energy expenditure, but a proper explanation of motion is lacking. For instance, there are at least two different limits for a rotary enzyme: free thermally driven diffusion (stiff chain with a loose pivot) and discrete conformational diffusion (transitions between a discrete number of bond angles along the chain). Each of these provides a potentially different characteristic timescale for diffusion.

In this interest, a molecular dynamics simulation of the biotin rotary enzyme (biocytin) was done to probe its behavior. Biocytin is a biotinylated lysine amino acid (ref. Fig. 2) and functions as a carrier of activated CO₂ [85]. Several informative results from this simulation are given in the following sections. The lipoamide rotary enzyme is structurally identical to biotin with respect to its chain, and consequently, many of the results are expected to apply to lipoamide as well.

⁵Estimates can be derived from a bead-model assumption [16].

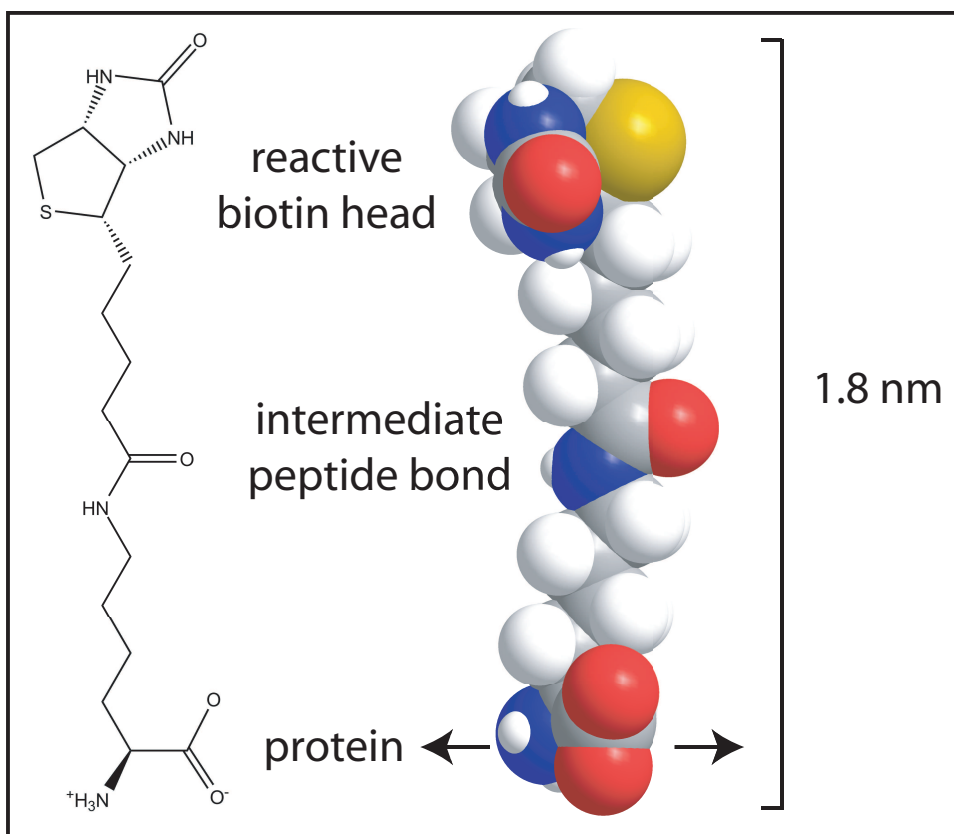


Figure 2: Biocytin is constructed by a peptide linkage between the amino acid lysine and biotin. The distal ureido hydrogen (attached to nitrogen) on the reactive head can be exchanged for a carboxyl group, providing a means for a facilitated transfer of CO_2 . The base of lysine connects to the remainder of the protein through peptide linkages.

4.3.1 Simulation Details

To investigate the dynamics of the biotin rotary enzyme in the presence of water, two molecular dynamics simulations of 8 ns each were performed using the NAMD package [61]. A 2 fs timestep was used. Rigid bonds were taken for hydrogen atoms. An all atom OPLS force field parameter set (dated November 2000) governed the dynamics of water and lysine portions [38, 53], with additional OPLS parameters for biotin from a different source [49]. The method of parameterization for the rotary enzyme is briefly discussed in Fig. 3.

A collection of 798 TIP3P water molecules made the aqueous environment [51].⁶ Cubic periodic boundary conditions were applied, with a periodic length approximately 2.912 nm that was determined by an initial simulation at temperature 298 K and pressure 1 atm.⁷ An initial thermalization unique to each of the two simulations was done at fixed volume for 100 ps, with subsequent simulations done at fixed energy and volume. Actual average initial temperatures vary between 297 to 302 K, with a positive drift of roughly 2 K over 8 ns. Initial average (group) pressures range from roughly 15 to 85 atm, with a drift of roughly 40 atm.⁸ These conditions may vary too greatly to form precise estimates, but examination of biocytin’s motion did not reveal a reason to question order of magnitude estimates.

A neutral variant of the biocytin was used for the model, where the amine and carboxyl groups at the base of the lysine portion were replaced with neutral nitrogen and carbon atoms, respectively. The four atoms that constitute the base (hydrogen, two carbons, and a nitrogen) of the rotary enzyme were fixed in space to simulate attachment to a much larger body (a protein). The initial configuration of biocytin in each simulation resembled the upright configuration in Fig. 2.

4.3.2 Results

The qualitative motion by biotin in both simulations displayed several expected traits. For example, the carbon-carbon bonds in the chain have a considerable dihedral interaction that fixes their position to an effectively discrete number of states at the given temperature, while the rigid peptide bond structure has relatively significant angular freedom for rotations about the bounding carbon atoms (this has been checked, e.g.

⁶The TIP3P water model has its own difficulties. For example, the self-diffusion constant of TIP3P water as used is already factor of 2 too large compared to normal water [51].

⁷This is not so far removed from the expected 1.8 nm maximum length of biocytin, but this length is expected to provide sufficient room to avoid strong self interaction through the periodic boundaries.

⁸Estimates of pressure fluctuations can be estimated to be roughly 270 atm in magnitude. Pressure estimates for small, essentially incompressible systems are expected to fluctuate greatly.

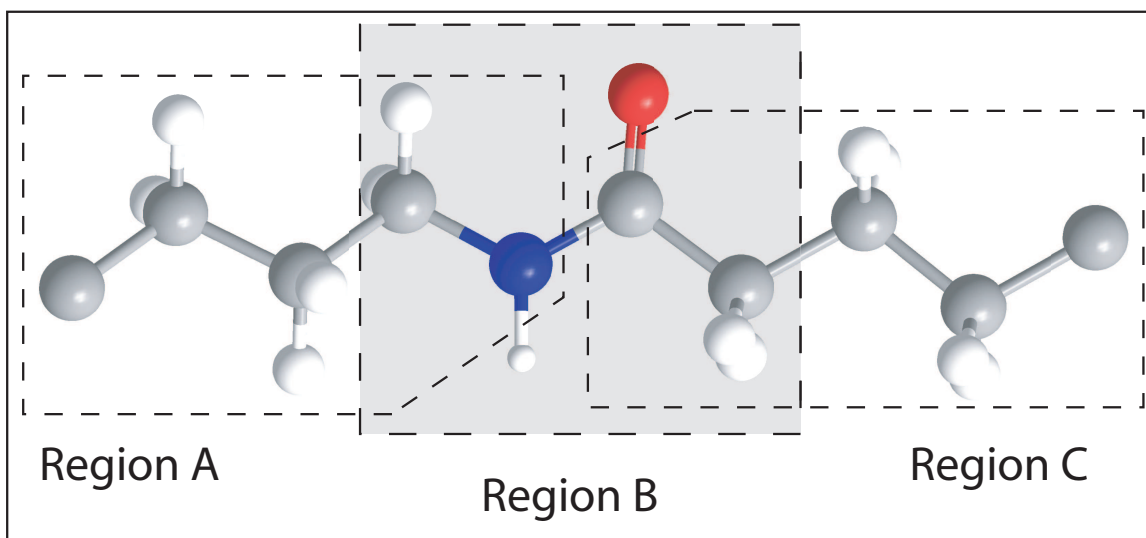


Figure 3: Construction of the parameterization for biotin follows from the patching between three regions: (A) the lysine residue, (B) the peptide linkage, and (C) biotin. If (B) is assumed to locally resemble a repeating glycine polypeptide, parameterization from available sets for each region can essentially be taken from known parameter sets. Where there is an ambiguity in or a lack of a given interaction in the separate regions of a patch (this is particularly troublesome for dihedral interactions), preference is given towards maintaining regions A and C over region B.

by investigation with the *ab initio* program *GAMESS* [79]). Motion is thus characterized by three primary effects: discrete changes between equilibrium positions of carbon-carbon bonds (roughly occurring somewhere in the chain several times every 100 picoseconds), diffusion due to the partial rotational freedom of the peptide bond, and diffusive fluctuations contributed from the finite rigidity of the carbon-carbon bonds. The latter two effects appear to be significant for the fine diffusive fitting of the reactive head into catalytic site, while global diffusion appears to be primarily due to changes in the carbon-carbon dihedral angles. Diffusion of the reactive head across essentially its entire range of motion was observed in each of the 8 ns simulations, such that a potentially successful diffusive search for a nearby catalytic site is expected to occur on the order of tens of nanoseconds. Global diffusion thus occurs on a slower timescale than the perfect rotor at the end of Section 4.2.

A measurement of interest is the effective rotational diffusion constant for short-time motion. The effective rotational diffusion constant for the reactive head gives a characteristic time for the head to explore the immediately available state space. This measurement was performed by creating a normalized vector $\vec{n}(t)$ from the central (alpha) carbon of the lysine base to the center of the biotin head (taken to be the bond adjacent to the two heterocycles), and then measuring the mean angular deviation of this vector in increments of $\tau = 200$ fs. If the time increments are sufficiently small, the rotational diffusion constant for isotropic rotational diffusion (rotational diffusion constant D) on a sphere is [4]

$$\langle |\Delta\vec{n}(\tau)|^2 \rangle \equiv \langle |\vec{n}(t + \tau) - \vec{n}(t)|^2 \rangle \approx 4D\tau \quad (77)$$

This “point” measurement, done in both simulations, is found to be $D = 0.87$ rad²/ns, with a relative difference between simulations of approximately 2%. This measurement can be compared to the histogram of the variable $|\Delta\vec{n}(\tau)|^2$, which is exponentially distributed in the case of pure rotational diffusion. Fit of an exponential to such a histogram produces an estimate of D approximately 5 to 8% lower than the point measurement (ref. Fig. 4), with again the two simulations producing close results. Again, diffusional searches of the local state space with a timescale of several nanoseconds is expected. Note that a difficulty with the rotational diffusion picture is that biotin occasionally wraps around to bring the head near the base, amplifying the effect of spatial fluctuations on angular measurements. Additionally, this measure misses any anisotropy of diffusion that may be significant in the mechanism.

In short, these results support that global diffusion is primarily governed by dihedral bond angle transitions, with significant local flexibility of the chain for each of these dihedral configurations. The free energy formalism of the previous sections of course applies to this more complicated picture of diffusion as well, and the assurance of a potential $\mu(x)$ for the biocytin dynamics follows from the assumption that reactions occur only at catalytic sites (ref. Section 4.2). Further analysis of these

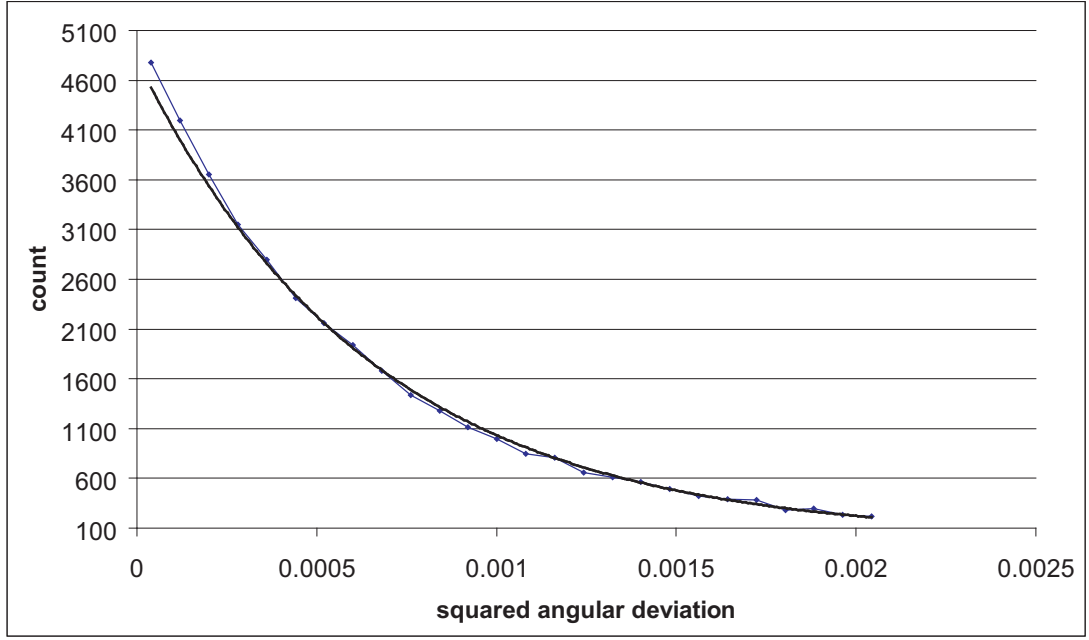


Figure 4: A histogram for the $\tau = 200$ fs distribution of $|\Delta\vec{n}(\tau)|^2$. Dots are bin counts centered horizontally on each respective interval of the histogram, while the smooth line is a best fit exponential that corresponds to $D \approx 0.8$ rad²/ns.

simulations or of analogous simulations may be released in the future.

CHAPTER V

MOLECULAR MOTORS

The diffusive transport harnessed in ubiquinone and rotary enzymes is ideal for nanometer transport, but a typical biological cell may be many micrometers in diameter and may additionally require the organization of large vesicles.¹ The characteristic time for diffusion scales quadratically in the transport distance and linearly in the radius of a spherical body; an increase in scale of either of these distances can lead to problematically large diffusion times. A cellular mechanism designed to overcome this difficulty is the active transport of cellular cargo by means of molecular motors. Molecular motors consume free energy to direct motion of the cargo [91], such that transport can be achieved in a time that scales linearly in transport distance. Additionally, the biased fluctuating motion of these molecular motors is responsible in higher organisms for producing muscular contraction [98]. These functions make molecular motors worthy of the intense study they have received in the literature.

The molecular motors kinesin and myosin V have become key figures in the study of molecular motors in general [93, 5, 92, 6, 8], owing in part to their interesting property (processivity) that a single motor can linearly transport attached cargo for long distances before dissociation of the motor from its track. The essential configurational aspects of forward motion have been established for conventional kinesin and myosin V as a “hand over hand” stepping pattern [103, 101]. This pattern is reminiscent of ordinary human walking, since the track binding domains (heads) alternatively bind in front of one another. The detailed physical mechanism underlying these motors has long been a matter of debate, particularly concerning the relevance of Brownian

¹The axons of certain nerve cells are macroscopic in length.

motion versus power stroke principles.² This chapter pursues the argument that RBM is a likely candidate for both motors.

5.1 *Rectified Brownian Motion Model*

The power stroke description of molecular motors is characterized by a large configurational free energy decrease associated with the motion of a tethered head in the forward direction, e.g. as favored in [92, 81]. Diffusion functions here only in an assisting role to orient the head appropriately for binding. In the case of kinesin (ref. Fig. 5), adoption of the power stroke view was seriously challenged by the determination of a small associated neck linker zippering energy (“power stroke” energy) [70], with an associated “power stroke” force generation smaller than that seen in experiment.³

This failure of power stroke arguments to predict this so-called amplified stepping bias does not violate thermodynamics, but rather, emphasizes the role of whole cycles in small system thermodynamics (ref. Eq. 55). The existence of essentially irreversible transitions associated with bound states, e.g. phosphate release after ATP hydrolysis, in either kinesin or myosin V provide significant contributions to the overall free energy expenditure in a typical stochastic trajectory. Indeed, if the free energy expenditure, via Eq. 56, due to bound state transitions is comparable to the total free energy expenditure in a standard mechanical cycle, the residual free energy remaining for spatial motion need not be large. A proper account of irreversibility can in this way be used to discount a power stroke scheme as the primary contributor of irreversibility in a mechanism. Such an analysis can be done due to the “gated” tight mechanochemical coupling of these motors [93], which allows approximate construction of a system-wide free energy profile for an analogous system that neglects

²In the case of myosin V, recent experiments have measured diffusional effects directly [82].

³Force generation is here measured in terms of the ability for a molecular motor to move against a given external load.

rare backwards binding events (ref. Section 2.2.4).

A recent study (included as part of this thesis) has indeed found many attractive qualities for an RBM model of kinesin, including a simultaneous explanation for both chemical coordination and bias amplification through the presence of internal strain between the two kinesin heads [52].⁴ The essence of this approach lies in the ability for small effects (i.e. neck linker zippering), which slightly change the ensemble averaged position of a diffusing tethered head, to exponentially change the frequency of relatively rare binding events. In short, a diffusing head binds forward most often because it visits that site most often, and these visitation probabilities can be controlled with a weak neck linker zippering energy. The details of this argument are presented anew in the latter part of this section in the case of myosin V, but the essential picture for kinesin is presented in Fig. 5. It is not insignificant that experimental investigations may have also determined an entirely similar RBM mechanism for ribosomes [48], where a small energetic difference between the acceptance of cognate tRNA and near-cognate tRNA is proposed to induce a spatial shift in the tRNA position that amplifies relatively rare diffusive fluctuations of a tRNA molecule.

The details of chemical coordination and bias amplification in myosin V (ref. Fig. 6) are similar to kinesin, in that both effects may be simultaneously explained by the presence of internal torques between the two heads. This approach presents an alternative model to power stroke models of myosin V. For these purposes, consider an actin-bound myosin V head (head 1) that anchors the otherwise free myosin motor, such that the tethered head (head 2) is unbound and able to diffuse. The present RBM approach to myosin V requires that this intermediate tethered head 2 must strongly prefer forward binding over backward binding if forward motion is to be ensured. This can be measured by the ratio of forward to backward binding rates, termed the bias ξ , for the diffusing head 2. In kinesin, ξ predicts the bias from

⁴Notice that this model appears in Chapter 6.

an intermediate “parked state” [28, 1], though the role of ξ in a detailed myosin V mechanism may differ. Demonstrating that ξ is large for our RBM model, using only small changes in internal configuration, is done presently.

As in previous models of myosin V [45, 96], interaction between these two heads occurs in part or in whole through the elastic strain of the myosin necks (the flexibility of the hinge connecting the two myosin necks may also be considered). The free energies $E^{(f)}$ and $E^{(b)}$ for the elastic strain when head 2 is in a forward or backward binding configuration, respectively, are functions of the angles θ_1 and θ_2 , as depicted in Fig. 6. $E^{(b)}$ is related to $E^{(f)}$ by the exchange of θ_1 and θ_2 . The rate for head 2 to bind either forward or backward is assumed to obey a simple form of Kramer’s rate law [30]

$$k = k_0 e^{-U(\theta_1, \theta_2)/k_B T} \quad (78)$$

such that the binding rate k is proportional, up to a multiplicative constant k_0 , to the Boltzmann factor of the elastic strain free energy $U(\theta_1, \theta_2)$ for a given binding configuration. This approach predicts that a symmetry state with $\theta_1 = \theta_2$ will bind forward or backward with equal probability.

Suppose the existence of two nucleotide-dependent states that impose given values on θ_1 and θ_2 : an uncocked state with angle θ_0 , and a cocked state with angle $\theta_0 + \delta\theta$ that is lower in energy by the value ϵ . Some may refer to the uncocked and cocked states as pre-power stroke and post-power stroke states, respectively, with ϵ being the power stroke energy, but this view will be seen not to be appropriate for the model at hand.

Using Eq. 78 to determine binding rates for a given pair nucleotide states, the total rate of forward binding is taken to be the weighted sum of forward rates from the uncocked and cocked states, such that cocked states are $e^{\epsilon/k_B T}$ more likely. Backwards binding is treated similarly. With head 2 restricted to be in the uncocked state, the

bias ξ is

$$\xi = \frac{e^{-E^{(f)}(\theta_0, \theta_0)/k_B T} + e^{\epsilon/k_B T} e^{-E^{(f)}(\theta_0 + \delta\theta, \theta_0)/k_B T}}{e^{-E^{(b)}(\theta_0, \theta_0)/k_B T} + e^{\epsilon/k_B T} e^{-E^{(b)}(\theta_0 + \delta\theta, \theta_0)/k_B T}} \quad (79)$$

where the overall prefactor k_0 in Eq. 78 vanishes for this simple model. Upon simplifying Eq. 79 by identifying through symmetry $E^{(f)}(\theta_0, \theta_0) = E^{(b)}(\theta_0, \theta_0) = E_0$, the general expression for the stepping bias in the present context is

$$\xi = \frac{1 + e^{\epsilon/k_B T} e^{-[E^{(f)}(\theta_0 + \delta\theta, \theta_0) - E_0]/k_B T}}{1 + e^{\epsilon/k_B T} e^{-[E^{(b)}(\theta_0 + \delta\theta, \theta_0) - E_0]/k_B T}} \quad (80)$$

A few assumptions on the system simplify Eq. 80 into a form more suitable for interpretation. The first of these is to suppose dominance of the elastic strain free energy terms, in the sense that the numerator is approximated by $e^{\epsilon/k_B T} e^{-[E^{(f)}(\theta_0 + \delta\theta, \theta_0)]/k_B T}$ while the denominator is approximated by 1. This assumption relies on the existence of large elastic free energy changes upon variation of θ_1 and θ_2 (demonstrated for a particular model at the end of this section). A further assumption that the Taylor expansion $E^{(f)}(\theta_0 + \delta\theta, \theta_0) \approx E_0 - \mathcal{T} \delta\theta$ is valid, where $\mathcal{T} = -\frac{\partial E^{(f)}}{\partial \theta_1}(\theta_0, \theta_0)$ is an effective internal torque, finally reduces Eq. 80 to

$$\xi \approx e^{\epsilon/k_B T} e^{\mathcal{T} \delta\theta/k_B T} \quad (81)$$

The usual factor $e^{\epsilon/k_B T}$ is recognized as the estimate of the stepping bias in the power stroke scheme (ref. Appendix A.3 and Eq. 107), such that $e^{\mathcal{T} \delta\theta/k_B T}$ is interpreted as a bias amplification factor. Eq. 81 demonstrates, as with kinesin, how the stepping bias of a system may depend strongly on the presence of internal strain (cf. [52]).

To assume that the internal torque \mathcal{T} is a large quantity is consistent with the known coordinating role of internal strain, which has been experimentally observed in the form of force-activated chemical gates within a myosin head [95, 63, 94]. The chemical states of each head are in this manner kept out of phase to prevent the rapid dissociation of myosin V from actin and to keep myosin V highly processive. Large \mathcal{T} would then also lead to bias amplification through Eq. 81. The observation that

bias amplification and coordination may be tied to a common cause (internal strain) is a compelling feature of an RBM approach to myosin V.

How does this ability for forward motion change in light of a given retarding load on the system? Power stroke models address this issue by assuming that the anchored head domain has a highly energetic change in conformation that pushes the system forward - an external force is overcome directly. However, the analysis of an RBM model is not so singularly focused. Estimates of the ability for myosin V to oppose an external load require analysis of, among other things, the bias amplification factor, the susceptibility of the elastic necks themselves, and the natural unit of torque for the cocked state $\mathcal{T}_\epsilon = \epsilon/\delta\theta$. (In contrast to power stroke models, an RBM model of myosin can take $\delta\theta$ small, such that \mathcal{T}_ϵ can readily become comparable to the torques generated on the neck by several-piconewton external forces.) Estimates of these factors appear to allow a strong RBM component in the mechanism of myosin V. For instance, if we assume a temperature 300 K, $\delta\theta = 10$ degrees, and a single myosin neck length of 30 nm, then a moderate energy of $\epsilon = 2.5 k_B T$ is sufficient for \mathcal{T}_ϵ to oppose 2 pN loads on a myosin neck. Even when this estimate fails, bias amplification factors can ensure stepping remains forward, for similar reasons that forward bias may persist in Eq. 81 even if $\epsilon < 0$.

As a numerical example of bias amplification in myosin V, the link model and parameters adopted by Lan and Sun are used [45] (that of Vilfan is also viable [96]), such that the elastic energy of the necks is assumed to be given by minimization of the energy function

$$E_l = -k_B T \sum_{i=2}^6 \frac{l_p}{a^3} \left[\vec{r}_i^{(1)} \cdot \vec{r}_{i-1}^{(1)} + \vec{r}_i^{(2)} \cdot \vec{r}_{i-1}^{(2)} - 2a^2 \right] + C(\vec{r}_i^{(1)}, \vec{r}_i^{(2)}) \quad (82)$$

where $\vec{r}_i^{(j)}$ is the displacement vector of the i^{th} link for the myosin neck bound to head j , $a = 5.0$ nm is the length of a single link for a neck, $l_p = 120$ nm is the persistence

length of the necks, and $C(\vec{r}_i^{(1)}, \vec{r}_i^{(2)})$ is a constraint such that $\sum_{i=1}^6 \vec{r}_i^{(1)} = \sum_{i=1}^6 \vec{r}_i^{(2)}$. All vectors are taken, for simplicity, to exist in a two-dimensional plane. The angles θ_1 and θ_2 from the previous discussion are identified with the angle of the first link in each chain (ref. Fig. 6), and these act as constraints on the minimization of the energy Eq. 82. The “vertical” uncocked angle $\theta_0 = \pi/2$ is chosen for definiteness. Estimates of \mathcal{T} for this particular model provide $\mathcal{T} \approx 13 k_B T / rad$, such that bias amplification factors of an order of magnitude readily arise from $\delta\theta$ of a mere ten degrees. Hence, the small configurational changes due to the cocked state provide a bias amplification that can readily account for a significant order of magnitude or larger discrepancy between the power stroke estimate and the actual bias ξ .

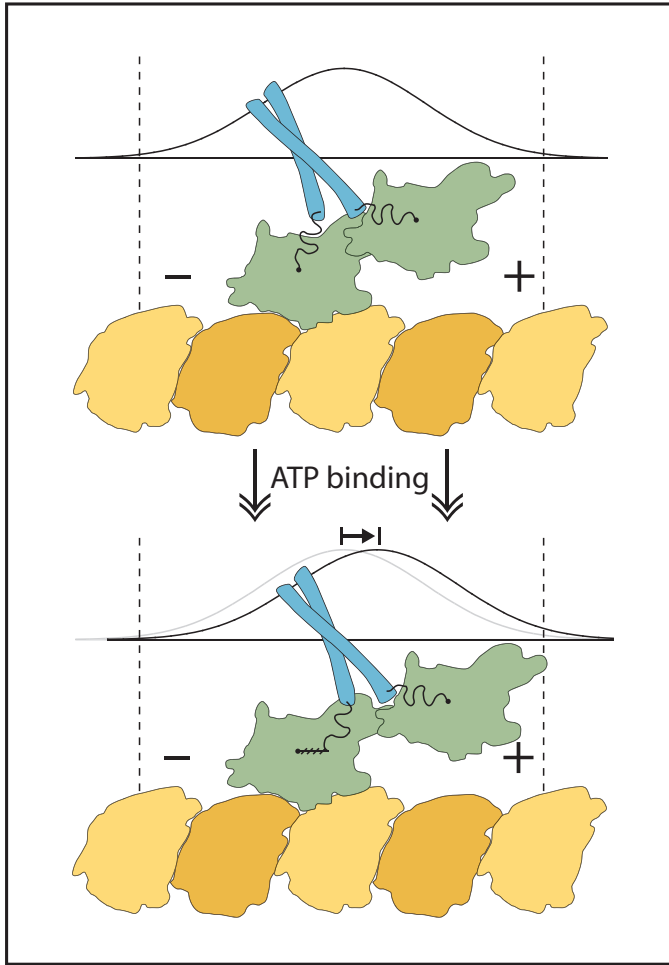


Figure 5: Kinesin moves along microtubule in the plus direction by alternately attaching each head to the beta-tubulin subunits (light orange), producing a 16 nm translation for a given head and a 8 nm translation for the center of mass of the kinesin dimer. The two heads are approximately 6 nm in diameter and can together move forward against externally applied retarding forces up to 7 pN [6]. Kinesin is attached by a polypeptide neck linker (black lines) to the coiled-coil stalk, which binds cargo. This neck linker can either be free (left head, top) or bound weakly to a head in a zippered state (left head, bottom), depending on the nucleotide state of the head. Entropic and enthalpic contributions from the neck linkers and the coiled-coil provide tensions between the heads. Illustrated above is the spatial displacement step, occurring by means of strain-induced bias amplification. In the unzipped state of kinesin, the probability distribution (the unimodal curve) of the kinesin head does not favor either the forward (plus end) or backward (minus end) binding site, by symmetry. However, the small change induced by neck linker zippering is amplified by an exponential relative increase of the probability distribution near the forward binding site. This is related to the slope of the distribution near bound states, i.e. related to a force. Since a kinesin head visits the forward site more often, irreversible binding (rectification) can keep the head at the binding site to produce a forward step. Power stroke models cannot explain such a mechanism, due to the weakness of neck linker zippering.

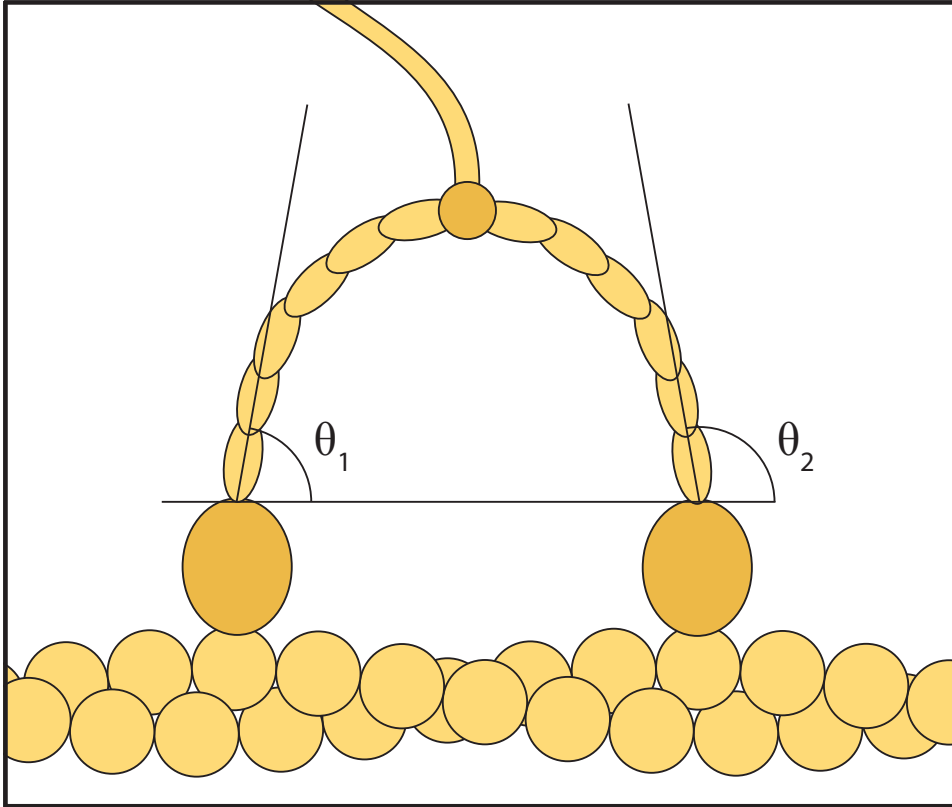


Figure 6: An illustration of myosin V head domains bound to actin, with semi-flexible necks meeting at a common hinge and myosin head domains binding 36 nm apart at the actin pseudo-repeat length. The forward sense of motion is to the right, and the labeling of the angles corresponds to forward binding (backward binding would exchange the order of θ_1 and θ_2 in the diagram). Given these angles, the elastic free energy may be determined for a given model of the myosin necks, e.g. that of Lan and Sun used in the text [45]. Notice that this picture does not take into account the observed ability for myosin V to bind at lengths unequal to the pseudo-repeat length of actin [8, 45], but this complication does not seriously affect the argument in the text.

CHAPTER VI

RECTIFIED BROWNIAN MOTION MODEL FOR KINESIN

The approach to bias amplification models in Section 5.1 is sufficiently complex to present the basic idea that boundary rectification can produce a stepping bias much larger than power stroke thinking can provide. A more developed model was developed by us in the case of kinesin [52]. Bias amplification in kinesin is distinct from myosin V in that a rather large *entropic* component (due to the neck linkers, ref. Fig 7) is expected to contribute to internal strain.¹ Thermal fluctuations are thus responsible for both elastic potentials and motility.

The remaining sections in this chapter reproduce (essentially verbatim) this work done for kinesin in [52]. Motivation for the kinesin model follows from known structural and chemical functional elements (discussed in Section 6.1). An experimentally characterized force-dependent chemical gate, which we label T-gate, serves in this model to both ensure chemical coordination and to explain the tapering of kinesin's velocity for increasing external load forces. The model itself is split into two different portions: the bias amplification mechanism that determines stepping bias (discussed in Sections 6.2 and 6.3, with many of the details for the full model in Appendix B.1), and the waiting mechanism that determines the rate of ATP hydrolysis for a head (discussed in Section 6.4). This separation is possible due to the rapidity of the diffusive step under a wide range of external loads. Concluding remarks appear in Section 6.5.

¹Enthalpic contributions also have reason to arise from unwinding of the coiled-coil stalk that binds cargo, but these contributions were mostly ignored in this kinesin model.

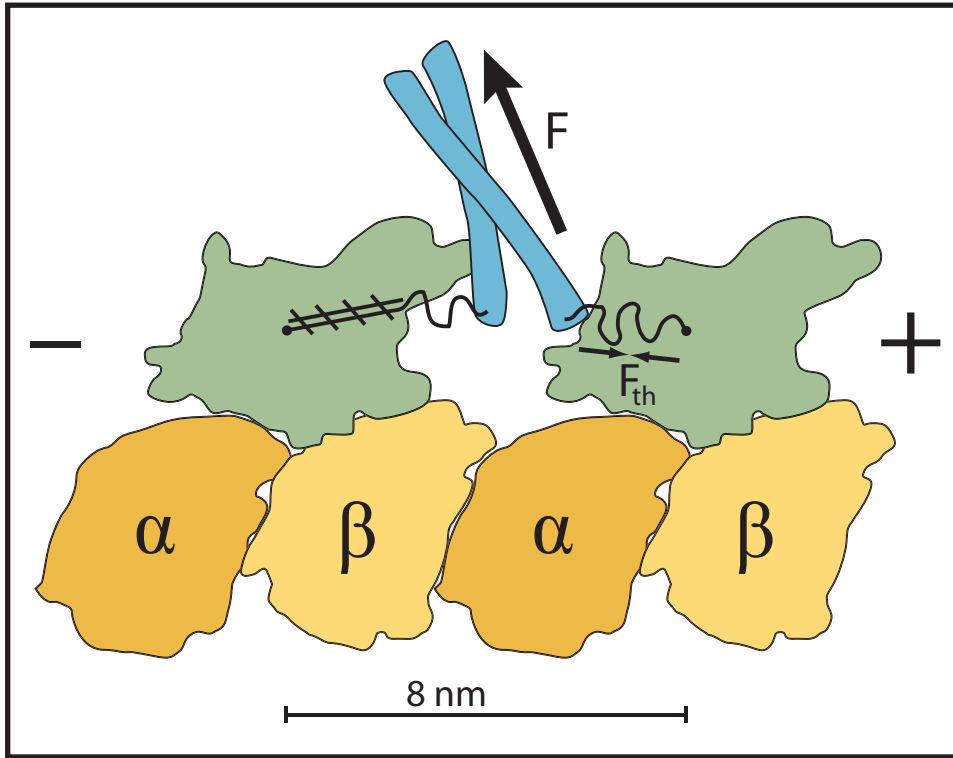


Figure 7: A doubly-bound kinesin dimer oriented with the microtubule plus-end to the right. The N-terminal kinesin heads can bind to tubulin [33, 34, 93, 39]. The kinesin heads are connected by two neck linkers, ~ 15 amino acids (a.a.) each [71], and these neck linkers end in a coiled-coil “stalk” that can connect cargo through light chains and mediate tension, indicated by \mathbf{F} (the load force). Entropic considerations for the neck linkers suggest a thermal force, \mathbf{F}_{th} , which resists neck linker extension. A microtubule-bound head in an ATP or hydrolyzed ATP (ADP.P) state will initiate immobilization (zippering) of its neck linker onto itself through a series of hydrogen bonds, schematically indicated by hatched lines. This figure outlines structures found in Protein Data Bank file: 1IA0 [39].

6.1 Structural and Chemical Functional Elements

Experiments have isolated several components that participate in kinesin’s forward cycle. Our model incorporates a number of these components through simplified representations that are appropriate for our level of detail. Here, the more involved discussion of our model is preceded with several brief treatments of the elements in kinesin’s modeling.

6.1.1 Neck Linkers and the Coiled-Coil Neck

Of central importance to the understanding of kinesin’s cycle are the elements that connect the two kinesin heads, namely, the two non-rigid neck linkers that together merge into a fairly stable coiled-coil neck [71]. The coiled-coil was originally supposed to provide, through its unwinding, an essential ingredient for the existence of kinesin’s forward motion, but experiments do not support such a theory [73]. Neck linkers are then assumed to provide the leading functional contributions, in part by forming entropic springs that generate a force by virtue of thermal fluctuations alone. These entropic springs supply an “internal strain” that guides kinesin’s functioning [13], e.g. by coordinating chemical states through activation of T-gate (ref. Section 6.1.4).

For the neck linker entropic force, a model from the study of polymers will be called upon to approximate our $\sim 12 - 15$ amino acid (a.a.) neck linker chain. Though the length of a neck linker is far removed from the length of most polymers, the 12 – 15 neck linker units may already be sufficient for common polymer statistical mechanical chains models to apply when fluctuations are included (e.g. the variance of extension for a forced, diffusing neck linker is allowed to be comparable to the mean extension). The most appropriate standard model for a peptide backbone is the freely-rotating-chain [18], due to the axial nature of peptide bonds (if the bond angle is very small, then results are known as the worm-like-chain (WLC) [42, 77]). Instead, an effective freely-jointed-chain (FJC) model is used for the sake of simplicity [43, 18]. The reduction of a chain force to an effective FJC or WLC is not uncommon, e.g. for DNA [10].

A computationally friendly form of the FJC force model utilizes a rational polynomial approximation that gives the correct asymptotic results for large and small extensions of length x [9]:

$$f(x) = \eta \frac{k_B T}{a} K(x/Na), \quad K(\alpha) \equiv \frac{\alpha(3 - \alpha^2)}{(1 - \alpha^2)} \quad (83)$$

where α is the relative extension x/Na , a is a link length for one amino acid, N is the number of amino acids in a neck linker, and η is a fitting parameter to set the correct linear regime dependence. The linear regime force constant, $3\eta k_B T/Na^2$, can readily scale to several piconewtons per nanometer for parameters describing peptide bonds. The x-integral of this force function provides a free energy potential that defines the single-chain Boltzmann probability density, ρ_N :

$$\rho_N(x) = Z_N^{-1} e^{-\eta N G(x/Na)} \quad (84)$$

$$G(\alpha) \equiv \frac{1}{2} \alpha^2 - \ln(1 - \alpha^2)$$

where Z_N is a normalization constant. Expected values for the model parameters are η of order unity and the virtual peptide bond length $a \approx 0.38$ nm (compare to $a = 0.35$ nm for the axial distance per amino acid in a β -sheet).

Though coiled-coil unwinding was not found essential for the forward motion of kinesin [73], steric aspects of the coiled-coil and its unwinding contribute substantially to bias calculations. Our modeling assumes that the width of the coiled-coil (possibly partially unwound) provides a given length Δd to the head-to-head extension in addition to the neck linkers. Acting upon the one-dimensional representation to be used for kinesin's diffusive step (akin to a reaction coordinate, ref. Section 6.2 and Appendix B.1), the coiled-coil prompts modeling of the tethered head's diffusion within an effective *reduced* interval, $[-d, d] = [-d_0 + \Delta d, d_0 - \Delta d]$, where $d_0 \sim 8.2$ nm is the original binding distance. This reduced interval minimally accounts for the extra reach due to the width of the coiled-coil. Notice that though the coiled-coil extension in the real system will dynamically change in response to entropic neck linker forces, this time-dependent effect is ignored in our model. Our model similarly ignores the restoring force due to coiled-coil unwinding (a static element that produces no intrinsic force).

6.1.2 Neck Linker Zippering

Estimated only to possess a free energy difference of $\sim 2 k_B T$ [70, 99], neck linker zippering is surprisingly essential for kinesin’s processive motor function [71, 7, 87]. Our modeling of neck linker zippering borrows from work done in protein folding, specifically the formation of β -hairpins. From statistical-mechanical investigations, β -hairpins exhibit bistable cooperative behavior due to competition between hydrogen bond formation and the configurational entropy of a solvated chain [17, 55, 54]. This bistability inspires a finite two-state zippering model (the kinematics are made more precise in Appendix B.1), where the state with several formed hydrogen bonds is labeled the “zippered” state, and the absence of zippered bonds is labeled the “unzippered” state.

The basic purpose of zippering is to immobilize neck linker links in the microtubule plus direction, thus shifting the anchoring point (point of emanation) for the microtubule-bound head’s neck linker toward the forward binding site. Supposing that N_z is the number of immobilized links in the zippered state, the act of zippering is modeled by a change that simultaneously shifts this anchoring point a plus-directed distance $\Delta x = N_z a$ and reduces the number of solvated neck linker links for the microtubule-bound head by N_z .

Since the external load will tend to place a strain on the neck linker, a Bell form [3] is taken for the Boltzmann probability of being in the zippered state (probability P_z) vs. the unzippered state (probability P_u)²

$$P_z/P_u = e^{-\Delta\mu_{zu}/k_B T} \tag{85}$$

$$\Delta\mu_{zu} = \Delta\mu_0 + F\delta_{zu}$$

²Notice that the notation here differs from that in earlier sections. This chapter does not make use of the affinity-based free energy.

with $\Delta\mu_{zu}$ the free energy of zippering, $\Delta\mu_0$ the free energy at zero load, F the external load, and δ_{zu} the characteristic distance for zippering. Our model takes $\delta_{zu} = \gamma N_z a$, with N_z the number of zippered links, a the link length, and γ is a pure number. For $\gamma = 1$, δ_{zu} is then the length of the zippered segment.

At biological temperatures, $F_{zu} = k_B T / \delta_{zu}$ defines a characteristic force of $F_{zu} \sim 2$ piconewtons if $\delta_{zu} \sim 2$ nanometers (approximately 5 zippered neck linker links). Zippering then remains forwardly biased for loads up to ~ 4 pN for zippering energies of magnitude $2 k_B T$. Reaching this force does not necessarily imply that kinesin has stalled, since a small probability to be in a zippered state can be sufficient for an overall forward bias (ref. Section 6.2 for an explanation of this, as a result of the amplification of bias).

6.1.3 Weak Binding

When a kinesin head is in the ADP nucleotide state, the bonding strength of the head with tubulin is observed to be markedly lower than in other states, and consequently, the microtubule-bound ADP state has been labeled weak binding (strong binding has higher bonding strength and is associated with the ATP and no-nucleotide states). Measurements were done by Uemura et al. to determine weak state unbinding rates when a weakly bound head is under external forcing [89, 88], finding that a natural forward bias exists in weak state unbinding. Our model uses a more symmetric form of weak state unbinding rates that is directionally independent:

$$k^W(F) = (1 \text{ s}^{-1}) \cdot e^{F \cdot 3.0 \text{ nm} / k_B T} \quad (86)$$

with F the applied force magnitude. Eq. 86 approaches the rates of other internal processes, e.g. 150 s^{-1} , when $F \sim 7$ pN. Such forces are attainable with entropic neck linker tensions.

6.1.4 T-gate

Chemical coordination between the heads of a doubly-bound kinesin dimer has been linked to internal strain activating a gate (T-gate) that prevents the binding of ATP to the plus-end head [75, 74, 13]. This coordinating mechanism allows the forward head to remain in the no-nucleotide state until the rearward head releases phosphate and detaches, thereby relieving the rearward force on the forward head and allowing ATP to bind. Without this coordination, kinesin would be unable to take more than a few steps before dissociation. T-gate thus establishes an important link between mechanical forces and chemical rates.

Further effects of T-gate are discussed in Section 6.4, within the context of the waiting mechanism.

6.2 *Bias Amplification Mechanism Revisited*

Much of kinesin’s functionality can be explained by the bias amplification argument in Section 5.1. Only the basic details for this argument are again presented, such that the parameters for the bias ξ in Eq. 81 can be deduced.

Kinesin’s stepping bias is derived from the probability for the tethered kinesin head to strongly bind either forward or backward once ATP has bound to the microtubule-bound head.³ The likelihood of a tethered kinesin head to bind either forward or backward is directly related to the frequency (probability) for this head to visit each respective binding site. This visitation probability may be predicted by the free energy Boltzmann factor that corresponds to system configurations with a kinesin head near a given binding site (this approach is similar to that in transition state theory).

Suppose, as described in Section 6.1.2, that a small “shift” in the tethered head

³This depends on previously mentioned “parked state” in Hackney’s gate [28], which prevents a tethered ADP-bound head from binding to microtubule until ATP binds to the microtubule-bound head. Hackney’s gate continues to provide intriguing experimental results [1].

probability density towards the microtubule plus-direction results when the neck linker is in the zippered state. The required energy to ensure this shift against an applied external load is accordingly small up to a limiting load value, such that zippering itself remains a weak effect. This internal strain sensitizes kinesin to the small changes due to zippering, by the argument in Section 5.1.

A function $U(x)$ is identified with the free energy for kinesin in the unzipped state to have a given head-to-head extension x along the microtubule, where the one-dimensional coordinate x is positive for extensions toward the microtubule plus-end. $U(x)$ is assumed to be an even function in x , where evenness is motivated by the expectation to find approximately neutral intrinsic stepping bias for an unzipped state (neck linker zippering would not be needed otherwise). In relation to the unzipped state, the zippered state free energy function is given through a translation of the neck linker origin and the addition of the energy difference $\Delta\mu_0$ corresponding to the zippering energy, i.e. $U(x) \rightarrow U(x - \Delta x) + \Delta\mu_0$. Translations are sufficient to introduce asymmetric favorability of the forward binding site, such that exponentially large biasing changes will appear. A translation only approximates the effect of zippering, since physically, zippering also alters the shape of $U(x)$ by reducing the number of solvated chain links (ref. Section 6.1.2). Forward and backward binding are defined to occur at $x = d$ and $x = -d$, respectively.

Assuming that a Taylor expansion to first order is valid for the energy function in the transition rate, i.e. $U(d - \Delta x) \approx U(d) - \lambda\Delta x$, then we can again derive the expression $\xi \sim e^{-\Delta\mu_0/k_B T} e^{\lambda\Delta x/k_B T}$ in the limit of strong biasing (up to subexponential terms that would be used in Kramer's formula). Thus, $e^{\lambda\Delta x/k_B T}$ can be interpreted as the amplification factor of the naive zippering energy Boltzmann term. Numerical values of the amplification factor can be readily estimated. The choice $\Delta x = 2$ nm is made for the zippering distance, corresponding to approximately 5 zippered neck linker links. $\lambda = \frac{\partial U}{\partial x}(d)$ is related to an effective internal strain of the system near

the boundary. By consideration of entropic neck linker forces (Eq. 83), $\lambda = 10$ pN is chosen as an example effective force. These values lead to an amplification factor of 130 at biological temperatures ($\xi \approx 1000$ if $\Delta\mu_0 = -2 k_B T$).

The strength of this simple model is its presentation of the origin of bias. However, certain relevant elements of kinesin’s cycle (e.g. weak state binding and unbinding) have been ignored for the purpose of conceptual clarity. Section 6.3 and Appendix B.1 resolve these shortcomings with a more detailed consideration of kinesin’s functional elements.

6.3 Detailed Biasing Mechanism

The heuristic model of biasing in Section 6.2 can be expanded into a detailed model that considers carefully the roles of weak binding, zippering, and entropic neck linker forces. Elaboration on the structural and mathematical details of this biasing mechanism are found in Appendix B.1. Conclusions of this detailed model are similar to earlier assertions: that the rate for the diffusing head to weakly bind during the biasing mechanism is proportional to the stationary probability density p_s for this head in the vicinity of the binding site (ref. Equations 78, 110, and 118), and that the stepping bias $\xi(F)$ at load F generally also depends on weak state unbinding rates (ref. Equations 86 and 119). A convenient numerical observation, that the biases $\xi(F)$ for physically relevant parameters satisfy an approximate Bell form (as in experiment [56, 6]), allows a parameterization of $\xi(F)$ in terms of the zero-load bias and stall force. In this manner, all provided examples of this section are selected to match the “measured” bias Bell form with a zero load bias of 1000 (i.e. 99.9% forward) and a stall force of 7.0 pN.

Two useful cases arise for the parameters of the biasing mechanism: those lacking and those retaining weak state unbinding. Elimination of weak binding effects in the former case emphasizes the diffusional origins of bias utilized by the heuristic model.

To demonstrate specific solutions of the modeling parameters for both of these cases, example parameter sets that match the measured bias are presented below.

Both of these examples share the parameters: $T = 300$ K, $N = 13$ (13 total neck linker links), $a = 0.38$ nm (virtual link length), $d_0 = 8.2$ nm (distance to the next binding site), $\Delta\mu_0 = -2 k_B T$ (zippering energy), and $k^S = 300$ s⁻¹ (the strong binding rate constant used in Eq. 119). The remaining parameters were made variable and matched to the “measured” bias Bell form with the construction in Appendix B.1: η (neck linker force constant in Eq. 83), N_z (number of zippered links in the zippered state), Δd (static extension of the coiled-coil in Section 6.1.1), and γ (a scaling parameter for δ_{zu} , the Bell length of zippering in Eq. 85). For the case lacking weak state unbinding, these are: $\eta = 1.4$, $N_z = 4$, $\Delta d = 4.6$ nm, and $\gamma = 1.0$. For the case with weak state unbinding, these are: $\eta = 0.86$, $N_z = 5$, $\Delta d = 5.0$ nm, and $\gamma = 0.5$. Other example parameter sets that match the measured bias certainly exist, but they are not explored here. Further details for the example lacking weak state unbinding are given in Fig. 9.

Evident in these numerical examples are the large predicted coiled-coil extensions. However, this observation may not translate well into the corresponding physical statement that large coiled-coil unwinding exists during the biasing mechanism. This problem arises due to the ignored restoring forces that are generated by unwinding of the coiled-coil, where these forces will alter bias calculations. Introduction of a force-extension model for the coiled-coil (not an entirely trivial task) would better address susceptibility of the coiled-coil to large extensions. Regardless of these technicalities, a 10-fold reduction in kinesin’s processivity has been attributed to experimental stabilization of the coiled-coil (to prevent unwinding) [73], which indicates that some coiled-coil unwinding is natural in kinesin’s normal forward cycle and should appear in modeling. Large Δd values may then be reasonable.

Results of our model also indicate that the biasing mechanism remains a fast

step within kinesin’s cycle as the external load is increased. Relevant to this is the rate for a diffusing head to weakly bind, with forward and backward binding rates k_+^D and k_-^D , respectively. The most rapid rate of these at a given external load, i.e. $\max(k_+^D, k_-^D)$, approximates the rate of the biasing mechanism’s diffusional step. Numerical examples (e.g. the above examples) indicate that this maximum rate tends to not decrease by more than a factor of 20 at increasing loads - a factor small enough to leave the diffusional step relatively fast. In contrast, the diffusional bias k_+^D/k_-^D undergoes larger changes through the combined effect of k_+^D decreasing and k_-^D increasing. Numerical examples further suggest that these observations are not drastically altered with the inclusion of weak state unbinding events.

The combination of entropic neck linker forces and weak binding states in this biasing mechanism provides an avenue for the exploration of the ADP gate discovered by Hackney [28]. Hackney observed that in the combined absence of ATP (i.e. without zippering) and external load, the free head of a singly-bound kinesin dimer binds to microtubule only slowly, if at all. This situation is a “parked” state [6]. Judging from similarities between the unzipped state in the biasing mechanism and this parked state, e.g. that each lacks neck linker zippering, Hackney’s gate should be a consequence of long lifetimes for an unzipped-like state (compare to the unzipped zero-load state in Fig. 9). Long parked lifetimes in Hackney’s experiment may then occur, for instance, if weak state unbinding becomes much faster than the strong binding rate k^S . The analysis of this approach is not done here, but this path to Hackney’s gate remains attractive.

6.4 *Waiting Mechanism*

The biasing mechanism of Section 6.3 is primarily suitable for describing the direction of stepping. Since biasing remains relatively fast, the dwell times for kinesin’s cycle are rather taken to arise from the chemical steps that occur outside of biasing -

collectively labeled the “waiting mechanism.” Some important technicalities in the logical separation of biasing and waiting are presented in Fig. 10. T-gate’s mechanochemical coupling is invoked as the principal contributor to the waiting mechanism at rate limiting conditions, directly coupling the stress of an external load (in a geometry similar to frame 5 of Fig. 8) to the rate at which kinesin binds ambient ATP. Rate limiting aspects of kinesin’s cycle, at either high load or low [ATP], are then determined by ATP binding rates.

A common element in the numerous models for dwell times is a Bell length of magnitude 2 – 3 nm that is responsible for rate-limiting behavior at external loads of several piconewtons [56, 6]. Supposing that T-gate indeed manages dwell times, then this Bell exponent characterizes the load dependence of T-gate. This identification is consistent in magnitude with the fact that T-gate’s coordinating mechanism is activated by internal strain on order of several piconewtons. A rate model, presented in Fig. 11, is based on the ansatz chosen for a natural lifetime within T-gate:

$$\tau(F) = \tau_0 \left\{ \left(\frac{R_0}{R_0 + 1} \right) e^{-F\delta_T/k_B T} + \left(\frac{1}{R_0 + 1} \right) \right\}^{-1} \quad (87)$$

with τ_0 , R_0 , and δ_T constants to be determined. Eq. 87 is intentionally similar to Eq. 3 used by Nishiyama et al. [56], though Eq. 87 is an *ad hoc* way to implement a ceiling in T-gate’s ability to inhibit ATP (e.g. due to higher loads altering the accessibility of the nucleotide pocket differently). The placement of $\tau(F)$ within our rate model is similar to Fig. 2 of Block et al. [5], with their k_{-2} set to zero. Additional details are in Fig. 11.

Further development of the waiting mechanism would inappropriately shift emphasis away from the central topics of this chapter, i.e. the origin of bias and the role of T-gate. No doubt that a more detailed rate model could be developed to describe dwell times, but this has been done many times previously.

6.5 *Concluding Comments on the Kinesin Model*

Kinesin’s biasing mechanism harnesses RBM principles to amplify neck linker zippering by effectively altering boundary conditions, that is, by altering the exponentially sensitive probabilities to visit forward and backward binding sites. At low loads, kinesin’s step then is a process that is biased by virtual absorbing and reflecting boundaries (such boundary conditions were taken *ad hoc* in a previous work [21]), though at high loads and particularly at stall, absorbing and reflecting boundaries are a poor approximation. The remainder of kinesin’s stepping is largely orchestrated by T-gate, including the coordination of chemical steps and the appearance of large dwell times at rate-limiting conditions.

There exist several improvements to this kinesin model that should be incorporated in future models of kinesin. The most obvious is the need for a detailed treatment of the forces that would arise from extension of the coiled-coil and neck linker forces, e.g. done through molecular dynamics simulations. Additionally, the stability of the “parked” state in Hackney’s gate that precedes ATP uptake has not been directly addressed by the results of this model. Addressing each of these concerns will lead to welcome refinements.

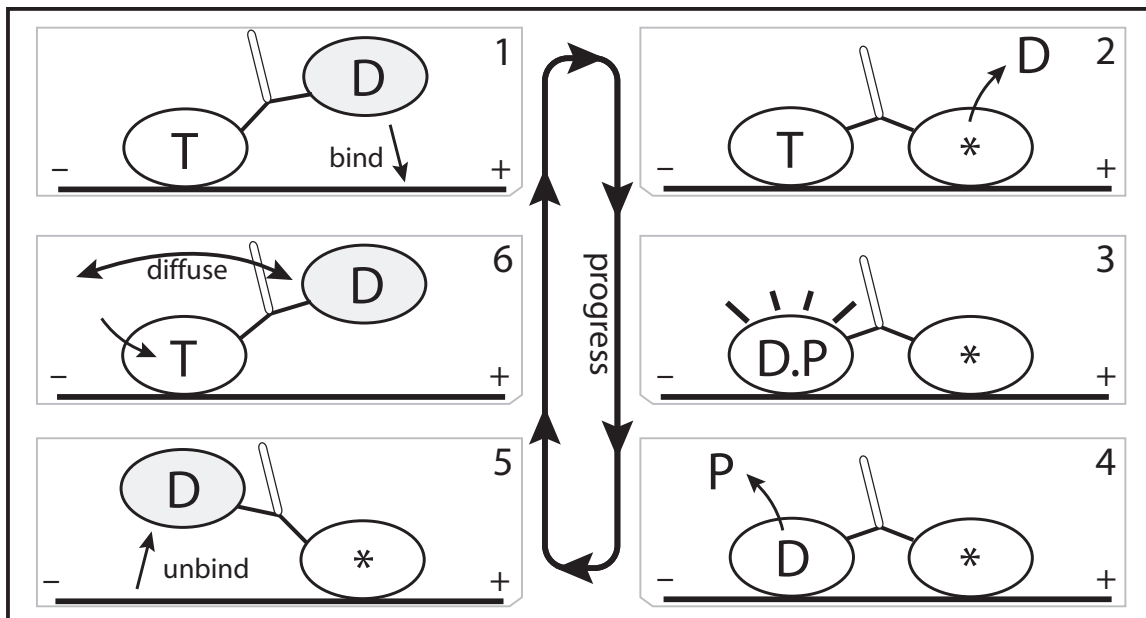


Figure 8: Key aspects of kinesin’s forward (plus-end) cycle have been elucidated through a varied multitude of experiments, including cryo-EM, x-ray structural, force bead, and others [97, 71, 7, 75, 29, 83, 14, 41]. This process is briefly reviewed, where “**T**” labels the ATP nucleotide state, “**D**” the ADP nucleotide state, “*****” the nonucleotide state, and “**P**” the phosphate after ATP hydrolysis. The free head is shaded to clarify motion between frames. Frames 1,2: the free head weakly binds to the plus-end binding site, leading to strong binding once ADP is released. ATP binding to the plus-end head is inhibited by a coordinating mechanism (labeled T-gate, ref. Section 6.1.4) that is activated by the internal strain. Frames 3–5: hydrolysis of ATP in the minus-end head leads to an intermediate ADP-phosphate state, “**D.P.**,” and phosphate release alters the binding of the minus-end head into weak binding, which allows rapid release of the minus-end head from tubulin [13]. Frame 5 is to be identified with the parked state in Carter and Cross [6]. Frame 6: the free head tends not to strongly bind until ATP binds to the microtubule-bound head [28]. ATP binding initiates zippering of the microtubule-bound head’s neck linker, coinciding with a large acceleration of the rate for the free head to bind onto microtubule. This entire forward cycle consumes one ATP and moves the center of mass of the system ~ 8 nm.

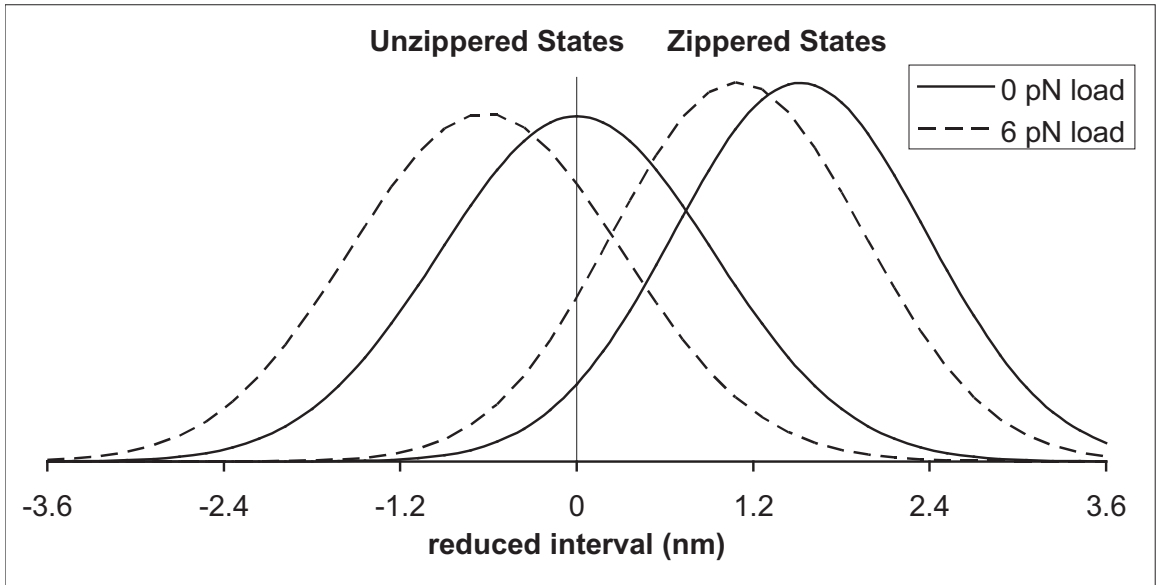


Figure 9: Plots of zippered and unzipped stationary probability densities (in arbitrary units) vs. the *reduced* interval $[-d, d]$ (ref. Section 6.1.1 and Eq. 110), for the case example in Section 6.3 that ignores the effects of weak state unbinding. The use of the reduced interval, which subtracts the coiled-coil extension, hides the fact that zippering is a small change (~ 2 nm) compared to the distance travelled by one head (~ 16 nm). Zippering probabilities, e.g. Eq. 85, are not represented in these plots. As discussed in Section 6.2, the small and decreasing tails of the distribution are responsible for the generation of large biases. Apparent in these plots are the competing influences of zippering, which shifts the density towards the plus-end, and of loads, which shifts the density towards the minus end. Stall occurs when all these effects balance one another. The inclusion of weak state unbinding in the model preserves many of the features presented here.

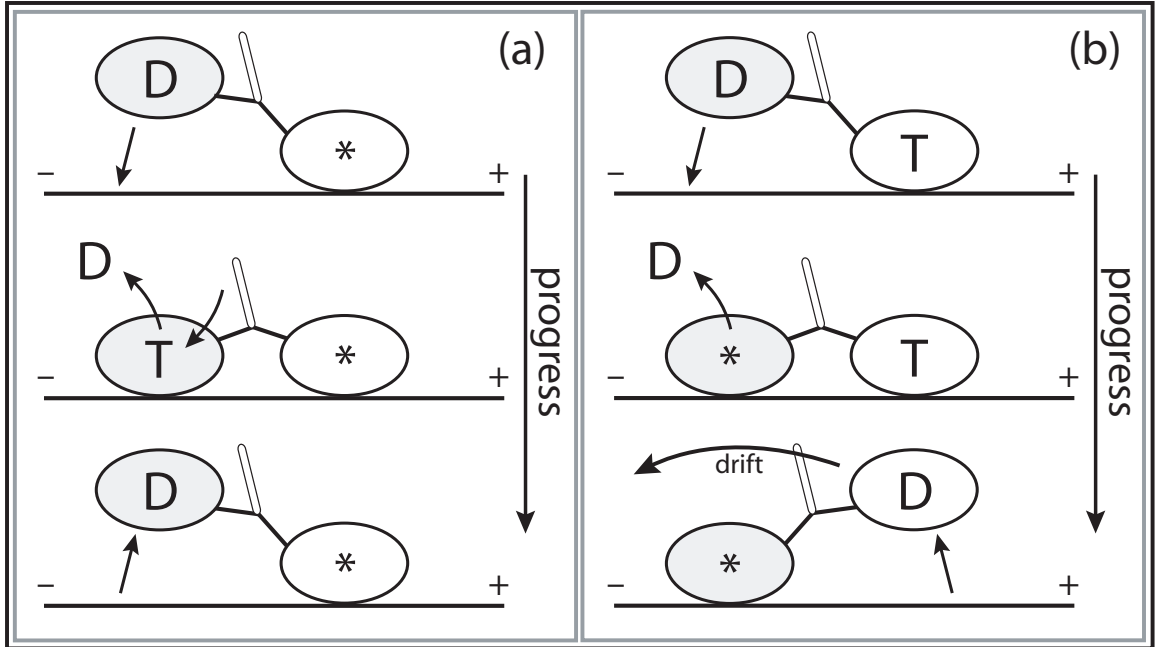


Figure 10: Much of the biasing mechanism is assumed to occur in the parked geometry of frame 5 in Fig. 8, where the external load acting on the microtubule-bound head leads to long dwell times (ref. Section 6.4). However, the free head could have, in the time before ATP uptake, an opportunity to bind rearward during a period when forward binding is virtually excluded (due to no zippering). Thus, bias would then be $[ATP]$ dependent due to $[ATP]$ dependence of the waiting mechanism. In (a), a fast step is outlined that corrects this undesired backward stepping. Since the forward head experiences strain due to the rearward-bound head, ATP uptake is greatly inhibited in the forward head, and thus, there exists a much larger probability that the rearward head detaches first (at the expense of one ATP hydrolysis). In contrast, (b) outlines how a “real” backward step may occur once the waiting mechanism has ended, i.e. once ATP has bound to the microtubule-bound head. Notice that if the rearward head binds as in (b), the forward head is at least one chemical step ahead of the rearward head. With a few assumptions, the forward head in (b) may then be expected to release first on average. Events in (b) where instead the rearward head unbinds will alter the simple relation between binding and stepping direction, but these (potentially uncommon) events are ignored at the level of detail in this model.

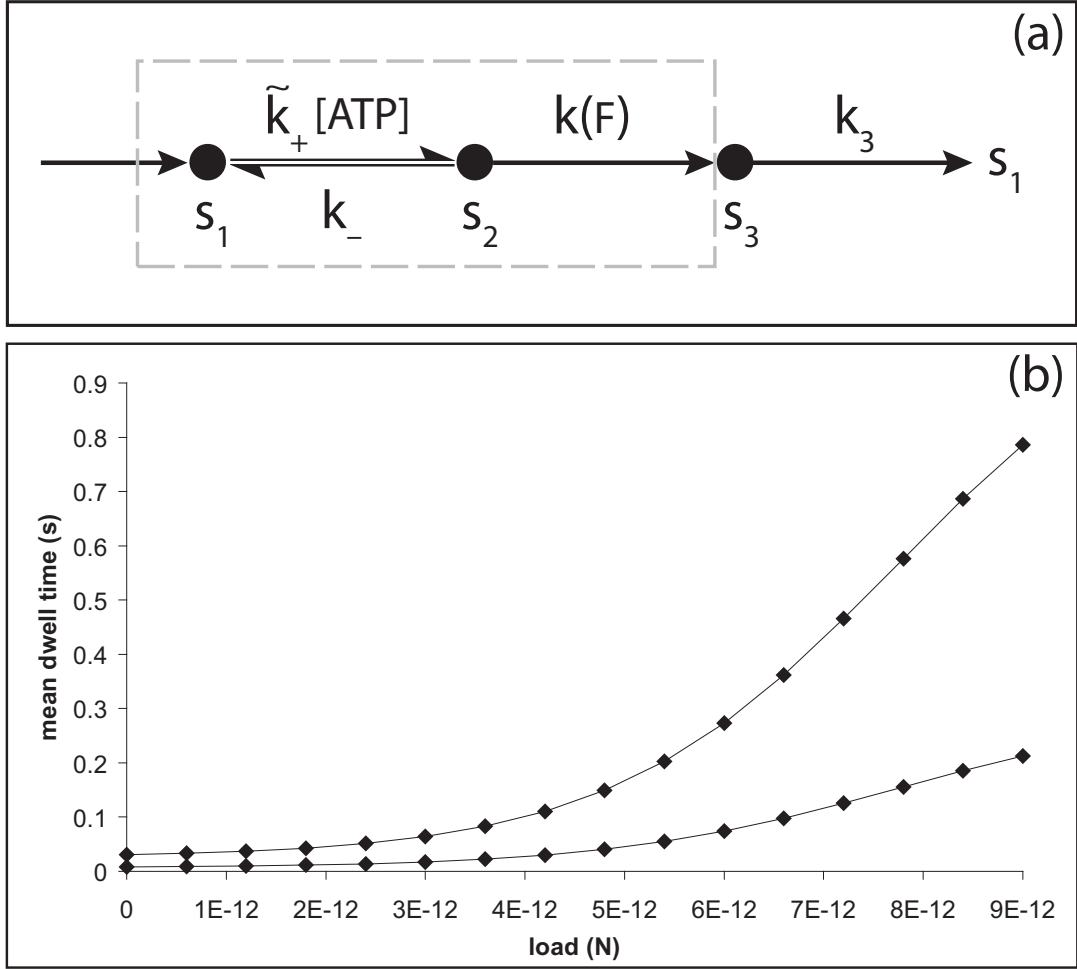


Figure 11: Part (a) illustrates a rate model to minimally describe T-gate's effect on dwell times (actually, the steady-state natural lifetime). Such a simple model would doubtfully predict detailed measurements, e.g. the randomness [86]. The dashed region that contains abstract states s_1 and s_2 describes the overall ATP uptake mechanism, which includes T-gate within a Michaelis-Menton structure. The state s_3 represents the remainder of kinesin's chemical cycle. A particular form of the force dependent rate, $k(F) = 1/\tau(F)$, is taken from Eq. 87. Part (b) provides a plot of dwell times from the rate model in part (a) with parameters deduced by fitting to the model of Nishiyama et al. [56], fitting with better than visual accuracy. That the agreement with Nishiyama et al. is excellent is likely a result of the choice in Eq. 87, but this is not to state that our rate model is identical with theirs (e.g. in the manner $[\text{ATP}]$ dependence is included). Used in part (b): $\delta = 3.10$ nm, $R_0 = 193$, $\tilde{k}_+ = 5.08$ s $^{-1}$ μM^{-1} , $k_- = 137$ s $^{-1}$, $k(0) = 857$ s $^{-1}$, $k_3 = 137$ s $^{-1}$, and $T = 300$ K.

CHAPTER VII

CONCLUSION

This thesis has examined RBM anew from several different aspects, including examining physical scales, non-equilibrium constructs, and biological examples. The notion that RBM provides a natural and robust framework for nanoscale biological systems has been supported by these arguments. Emphasis has been placed on the path and cycle free energies as a powerful route to provide insight into the advantages and widespread applicability of RBM compared to the macroscopic alternative: the power stroke. Indeed, power stroke schemes should be viewed as the exception in very small biological systems, since they appeal incorrectly to deterministic ideals. A further distinction with RBM was also made in reference to Brownian ratchets, which we present as a distinct class of systems on the basis of free energy structure, notably the failure of a boundary-driven interpretation for Brownian ratchets. Examples of RBM were provided for ubiquinone, rotary enzymes, and molecular motors, listed in the order of increasing complexity of the underlying mechanism. In particular, bias amplification was found to be a functional alternative to power stroke and Brownian ratchet approaches.

RBM, being a general scheme, has room for future work in both the refinement of its precise definition and in the elucidation of new mechanisms. The definition presented in this thesis has the compelling feature of following directly from NESS measures of irreversibility, rather than through some arbitrary measure that is inspired by model power strokes. A primary difficulty in this definition was an appeal to a logical sense of mechanical progression in a power stroke, along which the non-equilibrium free energy profile could be examined. Refinements on this definition are

indeed welcome. New RBM mechanisms grounded in a compelling definition of RBM also offer interesting prospects. For example, how might the technology for efficient manmade nano-machines be inspired from cellular mechanisms? Such questions are currently left to speculation.

APPENDIX A

FOUNDATIONS OF RBM

A.1 Example: Brownian Motion

The calculation of averages for the Brownian particle using the Langevin equations in Section 3.1 follows from the combination of white noise averages Eq. 45 and the solution Eq. 46 [90]. For example, the heat input due to thermal noise is derived to be

$$\begin{aligned}\langle \dot{Q}_{in} \rangle &\equiv \langle \xi(t) \dot{x} \rangle \\ &= \left\langle \xi(t) \left(\frac{1}{m} \int_0^t dt_2 e^{(t_2-t)/\tau} \xi(t_2) \right. \right. \\ &\quad \left. \left. + (v_0 - v_F) e^{-t/\tau} + v_F \right) \right\rangle \\ &= \frac{A}{m} \left(\int_0^t dt_2 e^{(t_2-t)/\tau} \delta(t - t_2) + 0 \right) \\ &= \frac{A}{m} \int_0^t dt_2 \delta(t - t_2) \\ &= \frac{A}{2m} = \frac{k_B T}{\tau}\end{aligned}\tag{88}$$

i.e. a constant. Similar procedures can demonstrate that the average of the trajectory follows the deterministic relaxation:

$$\langle v(t) \rangle = (v_0 - v_F) e^{-t/\tau} + v_F\tag{89}$$

where, as before, v_0 is the initial velocity at $t = 0$, and $v_F = F/\Gamma$ is the asymptotic velocity. The velocity correlation function is readily derived as well

$$\begin{aligned} \langle v(t_1)v(t_2) \rangle - \langle v(t_1) \rangle \langle v(t_2) \rangle = \\ v_T^2 (e^{-|t_1-t_2|/\tau} - e^{-(t_1+t_2)/\tau}) \end{aligned} \quad (90)$$

with $v_T = \sqrt{k_B T/m}$ the thermal velocity. In particular, the variance of $v(t)$ is:

$$\langle v(t)^2 \rangle - \langle v(t) \rangle^2 = v_T^2 (1 - e^{-2t/\tau}) \quad (91)$$

which approaches the usual value v_T^2 of equilibrium thermodynamics for time $t \gg \tau$. Other averages, e.g. the diffusion constant $\langle x^2 \rangle - \langle x \rangle^2$, are completely analogous.

Supposing that the initial velocity v_0 is averaged over the Boltzmann distribution (represented by $\{ \cdot \}$) simplifies many results. Equations 89 and 91 become

$$\{ \langle v(t) \rangle \} = v_F (1 - e^{-t/\tau}) \quad (92)$$

$$\{ \langle v(t)^2 \rangle \} - \{ \langle v(t) \rangle \}^2 = v_T^2 \quad (93)$$

Equations 92 and 93 can be applied to investigate the average power delivered to the particle under the influence of the force F

$$\{ \langle F v(t) \rangle \} = F \{ \langle v(t) \rangle \} = F v_F (1 - e^{-t/\tau}) \quad (94)$$

and also the difference between thermal power input and dissipative drag output to the medium

$$\left\{ \left\langle \dot{Q}_{in} - \Gamma v(t)^2 \right\rangle \right\} = -F v_F (1 - e^{-t/\tau})^2 \leq 0 \quad (95)$$

Notice that the large factors of $k_B T/\tau$ due to Brownian fluctuations exactly cancel in Eq. 95, suggesting that the average heat exchange with the medium is a sensible quantity in the overdamped limit (ref. Eq. 34 in the next section). The diffusional growth of the positional variance also simplifies in this case

$$\frac{d}{dt} \{ \langle x^2 \rangle \} = 2D(t) \quad (96)$$

for the time-dependent diffusion constant $D(t) = D(1 - e^{-t/\tau})$ and $D = k_B T/\Gamma$. This result approaches the standard $\frac{d}{dt} \{\langle x^2 \rangle\} = 2D$ for $t \gg \tau$, and is more generally known as the Ornstein-Fürth formula [90].

A.2 Irreversible Heat Production and Boundary Driven Processes

The irreversible heat production rate \dot{Q}_{irr} in Eq. 27 is a useful quantity in chemical kinetics. If the contribution in the summation for \dot{Q}_{irr} is zero for any given set of transitions, these transitions must support zero steady state current. If transitions between all states in an entire region \mathcal{R} are associated with zero irreversible heat production, then \mathcal{R} must have null internal steady state current (a form of local equilibrium) [80].

A special class of systems, i.e. those with a NESS free energy potential for the path free energy, have a special interpretation in terms of \dot{Q}_{irr} . To see this, suppose a region \mathcal{R} in a reaction network has the potential μ_i . \dot{Q}_{irr} can be decomposed into

$$\dot{Q}_{irr} = -\frac{1}{2} \sum_{i \in \mathcal{R}} \sum_{j \in \mathcal{R}} \Delta\mu_{ij} J_{ij} - \sum_{i \in \mathcal{R}} \sum_{j \notin \mathcal{R}} \Delta\mu_{ij} J_{ij} - \frac{1}{2} \sum_{i \notin \mathcal{R}} \sum_{j \notin \mathcal{R}} \Delta\mu_{ij} J_{ij} \quad (97)$$

The term for transitions within \mathcal{R} is simplified by use of the divergentless condition for steady state currents (derived from the master equation)

$$\sum_i J_{ij} = \sum_j J_{ij} = 0 \quad (98)$$

which implies

$$\begin{aligned} \frac{1}{2} \sum_{i \in \mathcal{R}} \sum_{j \in \mathcal{R}} \Delta\mu_{ij} J_{ij} &= \frac{1}{2} \sum_{i \in \mathcal{R}} \sum_{j \in \mathcal{R}} (\mu_i - \mu_j) J_{ij} = \sum_{i \in \mathcal{R}} \sum_{j \in \mathcal{R}} \mu_i J_{ij} \\ &= \sum_{i \in \mathcal{R}} \mu_i \sum_{j \in \mathcal{R}} J_{ij} = \sum_{i \in \mathcal{R}} \mu_i \left(\sum_j - \sum_{j \notin \mathcal{R}} \right) J_{ij} \\ &= - \sum_{i \in \mathcal{R}} \sum_{j \notin \mathcal{R}} \mu_i J_{ij} \end{aligned} \quad (99)$$

i.e. the heat contribution for transitions between states in \mathcal{R} reduces to a boundary term. If the potential for states at this boundary is constant, a second application of Eq. 98 demonstrates the heat production rate in Eq. 99 is zero. Thus, \mathcal{R} is internally at equilibrium if and only if its boundary is at equilibrium, and the process within \mathcal{R} is a boundary driven process.

Boundary driven systems can also be discussed in terms of the path affinity for a process with a potential (ref. Eq. 28). The path affinity is zero between states of equal μ_i potential, and in particular, a region with an equipotential boundary cannot have biased internal trajectories. The appearance of the heat generation as a non-equilibrium potential function can similarly be used to approach boundary driven systems [67].

A.3 Power Strokes in the Deterministic Limit of Fokker-Planck Equations

The spatial displacements in a mechanism are often approximated suitably by a Fokker-Planck equation. When the dynamics additionally are dominated by the deterministic drift portion of the Fokker-Planck equation, the dynamics can be shown to have progressive irreversibility (ref. Equations 63 and 64) and to thus typically satisfy the proposed definition of a power stroke in Section 3.5. This is outlined for a simple one-dimensional example, where all statements can in principle be explored explicitly.

The one-dimensional Fokker-Planck equation, Eq. 31, is used to formulate a simple example of a power stroke. The power stroke starts at position $x = 0$ and ends at $x = L$, and can be taken to have the steady state probability distribution

$$p^{(s)}(x) = \frac{e^{(\mu(x)-U(x))/k_B T}}{\int_0^L ds e^{(\mu(s)-U(s))/k_B T}} \quad (100)$$

that has been normalized for simplicity. A positive probability current J is taken (in the direction of the power stroke), such that by Eq. 34, the free energy function $\mu(x)$

is monotonically decreasing. The potential energy function $U(x)$ is assumed to be monotonically decreasing, with a “power stroke energy” $\Delta U = U(L) - U(0)$ many times larger in magnitude than $k_B T$. Furthermore, the force $F = -\partial U/\partial x$ is always sufficiently large and varies slowly throughout the power stroke (these conditions can be made precise). These restrictions on $U(x)$ can be relaxed in some cases that are not explored here. The NESS free energy difference $\Delta\mu(x) = \mu(x) - \mu(0)$ is determined from Eq. 33 to be

$$e^{\Delta\mu(x)/k_B T} = 1 - (1 - e^{\Delta\mu_0/k_B T}) \frac{\int_0^x ds e^{U(s)/k_B T}}{\int_0^L ds e^{U(s)/k_B T}} \quad (101)$$

for a total free energy expenditure $\Delta\mu(L) = \Delta\mu_0$. Equations 100 and 101 provide all the relevant information to explore this proposed power stroke in this section.

The dynamics here need not arise purely from explicit forces and interactions with the medium (in the sense of the discussion in Section 3.1), where changes in the free energy profile are interpreted as arising from irreversible viscous heat production. Let the probability current $J(x)$ of the stationary probability distribution $p^{(s)}(x)$ instead be defined by

$$J(x) = \left(V(x) - D \frac{\partial}{\partial x} \right) p^{(s)}(x) \quad (102)$$

for drift velocity $V(x)$ and diffusion constant D . Then, the drag constant Γ and force $F = -\partial U/\partial x$ can be defined by $\Gamma = D/k_B T$ and $F = \Gamma V$, respectively. Eq. 34 still holds, i.e. $\partial\mu/\partial x = -\Gamma v$, such that Γ provides an effective drag force constant that provides the irreversible heat generation for a given non-equilibrium ensemble velocity v . This generalization may be useful in systems where chemical transitions contribute to the fluctuations already imposed by the viscous medium, which may arise from the many chemical interactions in a molecular power stroke mechanism [58]. Whether irreversible heat is primarily chemical or viscous drag in nature is inconsequential here.

Progressive irreversibility for this model follows from the conditions on $U(x)$ along

with a further condition

$$\Delta\mu_0 \approx \Delta U \quad (103)$$

The results here are mostly insensitive to moderate violations of Eq. 103, where, for example, the case with $\Delta U < \Delta\mu_0$ requires care primarily for values of x that satisfy $\Delta U(x) \lesssim \Delta\mu_0$ (this is a region where the power stroke has allowed approximate thermal equilibration). The most basic observation is that the steady state velocity profile

$$v(x) = \frac{F(x)}{\Gamma} - D \frac{\partial}{\partial x} \ln p^{(s)}(x) \quad (104)$$

is dominated in most regions by the deterministic term. That is, deterministic drift follows

$$v(x) \approx \frac{F(x)}{\Gamma} \quad (105)$$

Thus, Brownian motion can be demonstrated directly to be mostly irrelevant for steady state dynamics, such that a deterministic limit is approached. By Eq. 34, the gradient in the NESS free energy potential for a power stroke is dominated by dissipation due to explicit forces

$$\frac{\partial\mu}{\partial x}(x) \approx -F(x) \quad (106)$$

or upon integration

$$\Delta\mu(x) \approx \Delta U(x) \quad (107)$$

The heat generated by the viscous dissipation thus arises from a release of internal energy, as would be predicted by macroscopic thermodynamics. Due to the assumed functional form for $U(x)$, the system is also progressively irreversible. The interval $0 < x < L$ can be partitioned into many path segments \mathcal{P}_i that satisfy

$$-\Delta\mu(\mathcal{P}_i) \sim k_B T \quad (108)$$

where the spatial width of each \mathcal{P}_i is approximately

$$L_F(x_i) = k_B T / F(x_i) \quad (109)$$

for a representative point x_i in \mathcal{P}_i . Eq. 109 reiterates the conclusion in Eq. 52: irreversibility sets in when irreversible viscous drag heat exceeds $k_B T$.

APPENDIX B

RBM KINESIN MODEL

B.1 Extended Model of Biasing

This section develops a model to explain kinesin's bias in a manner more complete than the heuristic model in Section 6.2. The roles of weak binding, diffusion, and internal strain in these dynamics are incorporated through the considerations of Section 6.1. Key results are congruent with those from transition state theory.

The framework of the present model, as with the heuristic model, utilizes a coordinate x along the microtubule that represents the position of an unbound kinesin head relative to the microtubule-bound head. x is restricted to exist on the reduced interval $x \in [-d, d]$ (ref. Section 6.1.1), and the boundaries $x = -d, d$ of this reduced interval represent binding sites that can induce transitions to and from weak binding states. Connecting the two heads are the neck linkers, which join at a neck linker junction (i.e. an effective coiled-coil) that is located at some point y in the reduced interval. Load is exerted at this junction by the coiled-coil stalk, such that a factor $e^{-Fy/k_B T}$ weights neck linker contributions in the probability density calculations (ref. Eq. 110 below).

The combined influence of neck linkers and external load supplies a free energy landscape for the variable x , as partitioned into the stationary Boltzmann distributions $p_{z,s}(x)$ and $p_{u,s}(x)$ for the zippered and unzipped states, respectively. These

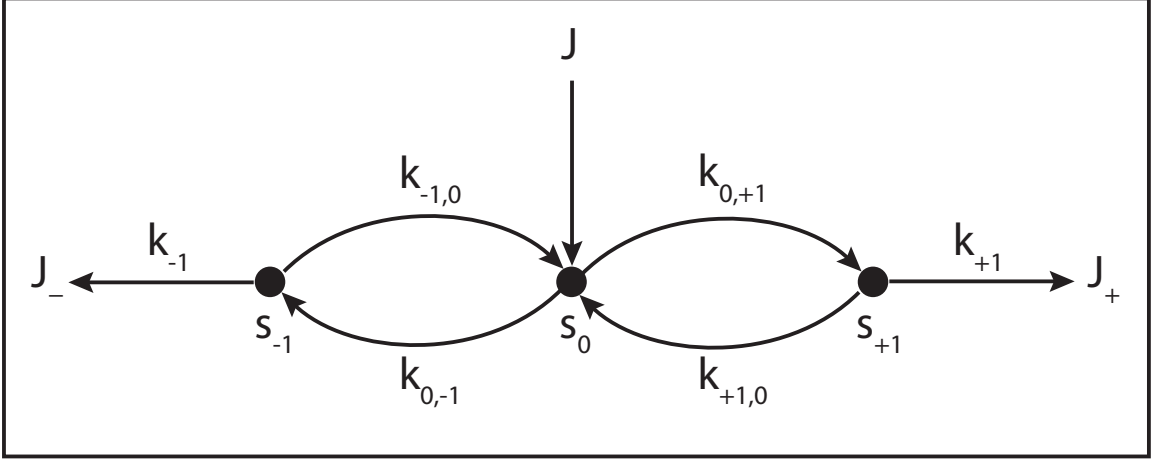


Figure 12: A network diagram to describe the bias of kinesin's step, providing the rates necessary for Eq. 119. s_0 represents the reduced interval, the state where one kinesin head remains unbound. s_+ and s_- represent the plus and minus-end weak binding states, respectively. J is the steady state probability current entering the process (due to kinesin binding ATP to the microtubule-bound head), and J_+ , J_- are the exiting currents (due to strong binding transitions). The labels k_{\pm}^D are given to the rates of weak binding from a diffusing state, k_{\pm}^W to the rates of weak state unbinding (e.g. from Eq. 86), and k_{\pm}^S to the rates of strong binding. As a simplification, the strong binding rates equal a constant k^S that is independent of load. The essential irreversibility of the strong binding step corresponds to a large free energy decrease for strong binding transitions (consistent with the RBM principle).

distributions are obtained through the convolution:

$$p_{z,s}(x) = Z_z^{-1} \int_{-\infty}^{\infty} \rho_{N-N_z}(y - N_z a) \rho_N(x - y) e^{-Fy/k_B T} dy \quad (110)$$

$$p_{u,s}(x) = Z_u^{-1} \int_{-\infty}^{\infty} \rho_N(y) \rho_N(x - y) e^{-Fy/k_B T} dy$$

with N the number of peptide units per neck linker, ρ_N the neck linker density (ref. Eq. 84), F the load force at the junction of the neck linkers, and a the link length. Z_z and Z_u are constants at a given load, with their ratio determined by the free energy of zippering $\Delta\mu_{zu}$ (ref. Eq. 85):

$$P_z / P_u = \frac{\int p_{z,s}(x) dx}{\int p_{u,s}(x) dx} = e^{-\Delta\mu_{zu}/k_B T} \quad (111)$$

Once Z_z and Z_u are determined by normalization of the total probability $P_z + P_u$, the stationary probability distribution for the unbound state is known.

For the loads and parameter ranges considered, the distributions in equations 110 and 111 have a single most probable zippering state in the neighborhood of each binding site (zippered for plus-directed binding, unzipped for minus-directed binding). An approximation used routinely below is then to assume that only zippered states bind forward and only unzipped states bind rearward, i.e. to neglect contributions of the less favorable zippering state. Relaxation of this assumption is simple but clutters the details of the model.

Kinetic aspects of our model are included to determine binding and unbinding rates. This kinetic portion in the reduced interval obeys a pair of coupled, one-dimensional Fokker-Planck equations that reproduce the stationary densities in Eq. 110. Define $U_z(x)$ and $U_u(x)$ to be the respective free energy functions that generate these densities at a given load - that is:

$$\begin{aligned} p_{z,s}(x) &= e^{-U_z(x)/k_B T} \\ p_{u,s}(x) &= e^{-U_u(x)/k_B T} \end{aligned} \quad (112)$$

Using these definitions, the non-stationary zippered and unzipped densities $p_z(x, t)$ and $p_u(x, t)$, respectively, are taken to satisfy:

$$\begin{aligned} \frac{\partial p_z(x, t)}{\partial t} &= -D \frac{\partial}{\partial x} \left(-\frac{1}{k_B T} \frac{\partial U_z}{\partial x} p_z - \frac{\partial p_z}{\partial x} \right) + W_{uz}(x) p_u - W_{zu}(x) p_z \\ \frac{\partial p_u(x, t)}{\partial t} &= -D \frac{\partial}{\partial x} \left(-\frac{1}{k_B T} \frac{\partial U_u}{\partial x} p_u - \frac{\partial p_u}{\partial x} \right) - W_{uz}(x) p_u + W_{zu}(x) p_z \end{aligned} \quad (113)$$

$$W_{uz}(x) / W_{zu}(x) = e^{-\Delta U_{zu}(x)/k_B T}$$

with $\Delta U_{zu}(x) = U_z(x) - U_u(x)$, D the diffusion coefficient, and $W_{zu}(x)$ and $W_{uz}(x)$ the transition rates between zippering states. Direct substitution verifies that Eq. 112 is the stationary solution to Eq. 113.

Implicit in Eq. 113 is the peculiarity that the head-to-head separation x is assumed to change on a timescale much slower than the position y of the neck linker

junction (y is integrated out). This assumption can be considered merely a modeling simplification, consistent in spirit with the choice to use a reduced interval in place of the coiled-coil (ref. Section 6.1.1).

Weak binding states in our model may transform to and from diffusing states via weak unbinding and binding, respectively, at the boundaries of the reduced interval ($x = \pm d$). Coupling relations are here given for the plus-end binding site, while behavior for the minus-end site is supposed identical. At a given time, there exists a probability P_W to exist in the weakly bound state. Coupling between the continuously diffusing system and the weak binding state is achieved through the introduction of boundary conditions that linearly relate P_W to the values $p_z(x)$ and $\frac{\partial p_z}{\partial x}(x)$ at the plus-end boundary (ref. Appendix B.2 for an alternative, discrete approach). This linear relation is established via two parameters, v_+ and \hat{v}_- , such that:

$$\frac{dP_W}{dt} = -v_+P_W + \hat{v}_-p_z(d) \tag{114}$$

$$\frac{dP_W}{dt} = J(d), \quad J(x) = -D \left(\frac{1}{k_B T} \frac{\partial U_z}{\partial x}(x) + \frac{\partial}{\partial x} \right) p_z(x)$$

where $J(x)$ is understood to be the probability current in the continuum. Eq. 114 implies both $\frac{dP_W}{dt} = J(d)$, which is the statement of probability conservation, and $-v_+P_W + \hat{v}_-p_z(d) = J(d)$, which provides the aforementioned linear boundary condition. \hat{v}_- is interpreted as the affinity to weakly bind when near a binding site, with binding rate $\hat{v}_-p_z(d)$. v_+ is the rate for a weak state to unbind back into the reduced interval at position $x = d$. In our model, \hat{v}_- is assumed to be a constant, while v_+ may vary with internal strain according to Eq. 86 (thus requiring the calculation of the entropic neck linker force on a weakly bound kinesin head at a given load).

Binding and unbinding rates may now be calculated via approximations similar to those in transition state theory, where as a simplification, rates most strongly depend on configurations near the binding site [104]. The rate formulae below are in this way

explored with an uncoupled approach that considers only the single most probable zippering state in the vicinity of each binding site. For conciseness, only the plus-end boundary $x = d$ will be considered. Analogous results apply to the minus-end boundary.

Transition rates between meta-stable states often reduce to a knowledge of mean first passage times (MFPT's) [104, 23], which for our problem are the mean times for the system to either weakly bind or unbind. Letting $\tau(x)$ be the MFPT for a given process (either binding or unbinding) that at initial time has the position x within the reduced interval, the function $\tau(x)$ for a one-dimensional, zippered state head in the potential $U_z(x)$ satisfies [23]:

$$-\frac{1}{k_B T} \frac{\partial U_z}{\partial x}(x) \frac{\partial \tau}{\partial x}(x) + \frac{\partial^2 \tau}{\partial x^2}(x) = -\frac{1}{D} \quad (115)$$

such that a set of boundary conditions (related to weak binding) define a unique solution for $\tau(x)$. Eq. 115 is solvable with straightforward integrals.

Denote x_0 as some typical point in the reduced interval away from the boundaries (e.g. $x_0 = 0$), and W as the plus-end weak binding state (not to be confused with the rates W_{zu}, W_{uz}). The MFPT for a given process starting at this weak binding state is denoted τ_W . Weak state binding, i.e. the process starting at x_0 and ending at W , is denoted $x_0 \rightarrow W$, while unbinding, i.e. the process starting at W and ending at x_0 , is denoted $W \rightarrow x_0$. The MFPT for each of these may be calculated using Eq. 115 with the boundary conditions:

$$x_0 \rightarrow W : \quad \tau_W = 0, \quad \frac{\partial \tau}{\partial x}(d) = -\frac{\hat{v}_-}{D} \tau(d), \quad \frac{\partial \tau}{\partial x}(-d) = 0 \quad (116)$$

$$W \rightarrow x_0 : \quad \tau_W = \tau(d) + \frac{1}{v_+}, \quad \frac{\partial \tau}{\partial x}(d) = \frac{1}{D} \frac{\hat{v}_-}{v_+}, \quad \tau(x_0) = 0$$

as may be derived from consideration of the backwards equation [23]. A brief outline of the derivation that leads to Eq. 116 can be found in Appendix B.2.

With a few assumptions, related to the free energy profile near the boundary, these MFPT's can be expressed using:

$$\delta_- \equiv D/\hat{v}_- , \quad \delta_{th} \equiv \int_{x_0}^d \frac{p_s(d)}{p_s(x)} dx \quad (117)$$

to give:

$$\tau(x_0 \rightarrow W) \approx \frac{\delta_{th} + \delta_-}{D p_s(d)} \quad (118)$$

$$\tau(W \rightarrow x_0) \approx \frac{1}{v_+} \left(1 + \frac{\delta_{th}}{\delta_-} \right)$$

Using Eq. 118, the low affinity ($\delta_{th} \ll \delta_-$) and high affinity ($\delta_- \ll \delta_{th}$) limits are clearly expressed.

The low affinity limit is taken for our modeling, such that δ_{th} need not be known. On physical grounds, this limit reflects that there exists an entropic barrier before the onset of binding, e.g. due to the orientational specificity of binding that is excluded from the one-dimensional model. As expected from transition state theory, the low affinity limit predicts that the rates of weak binding ($\hat{v}_- p_s(\pm d)$) and unbinding (v_+) are equal to the quasi-equilibrium rate of crossing the state boundaries $x = \pm d$. In contrast, the high affinity limit problematically hinders escape from the boundaries $x = \pm d$, as indicated by the reduction of the weak state unbinding rate from the desired value v_+ .

Once binding and unbinding rates have been determined, calculation of the total bias in our model follows from the rate diagram in Fig. 12, where the rates k_+^D , k_+^W , and k_+^S are defined in the figure caption. In steady state, the bias (i.e. the ratio of the probability currents J_+ and J_- for forward and backward binding, respectively)

is then:

$$\xi_{tot} \equiv \frac{J_+}{J_-} = \xi_D \xi_W \tag{119}$$

$$\xi_D \equiv \frac{k_+^D}{k_-^D}, \quad \xi_W \equiv \frac{1 + (k_-^W/k_-^S)}{1 + (k_+^W/k_+^S)}$$

with ξ_D representative of the bias due to diffusion leading to weak binding and ξ_W representative of transitions from weak binding states. As expected, if weak binding states are long-lived compared to strong binding transitions (not generally true), the overall bias is purely a diffusional/zippering effect. Notice that the parameter \hat{v}_- disappears from Eq. 119, due to taking the ratio k_+^D/k_-^D (this assumes \hat{v}_- is equal at each binding site).

Numerical calculation of the stationary distribution $p_s(x)$, needed in Eq. 118, was done with the convolution in Eq. 110. Both Eq. 110 and its normalization can be evaluated through direct numerical integration. For estimates of weak state unbinding (from Eq. 86), the force on a weakly bound head must be known. This may be done by finding the equilibrium position $y = y^*$ of the neck linker junction, such that the forces on this junction (due to the load and the forces of the neck linkers) are balanced for kinesin's doubly-bound configuration. The entropic neck linker force in Eq. 83 was in this way used to find y^* with a simple root finding routine, which then provided the needed force that determines the rate of weak state unbinding.

B.2 Mean First Passage Time Boundary Conditions

The boundary conditions in Eq. 116, used for the calculation of mean first passage times in Appendix B.1, are not all obvious at first glance. Their derivation is readily achieved through consideration of a discrete rate theory in the limit of a small grid spacing. Basic steps of this reasoning are presented in the following text, though some well-known results are only cited. A different treatment exists that avoids the limit of

a discrete theory. However, such an approach is somewhat less straightforward than the discrete approach.

Consider a series of states labeled with index i . A probabilistic process with one-dimensional, nearest-neighbor transitions is taken to evolve as:

$$\frac{\partial P_i}{\partial t} = P_{i-1}w_{i-1}^+ + P_{i+1}w_{i+1}^- - P_i(w_i^+ + w_i^-) \quad (120)$$

with t the time, P_i the probability to be in state i , and w_i^\pm the transition rates from state i to states $i \pm 1$. Points of exit for this process may be created through the creation of an absorbing state, such that $P_j = 0$ is imposed for some state j .

The mean first passage time problem for Eq. 120 is readily solved. In analogy to the continuous case, the mean first passage time function τ_i is the mean time for a process that starts in state i to first exit via an absorbing state. The function τ_i can be shown to satisfy the recurrence relation [23]:

$$-1 = w_i^+(\tau_{i+1} - \tau_i) + w_i^-(\tau_{i-1} - \tau_i) \quad (121)$$

A unique solution to Eq. 121 follows from appropriate boundary conditions, such as $\tau_j = 0$ when there exists an absorbing state at j .

A useful continuous limit exists for a choice of transition rates in Eq. 120. Using the new variable $x_i = i\delta$ in the limit $\delta \rightarrow 0$, the rates:

$$w_i^+ = \frac{A(x_i)}{2\delta} + \frac{D}{\delta^2}, \quad w_i^- = -\frac{A(x_i)}{2\delta} + \frac{D}{\delta^2} \quad (122)$$

reproduce the distribution of the continuous stochastic process with velocity field $A(x)$ and diffusion constant D [23]. Likewise with the above rates, the continuous limit of Eq. 121 is Eq. 115 if $A(x) = -\frac{D}{k_B T} \frac{\partial U}{\partial x}(x)$.

With the above developments, construction of a system with mixed continuous and discrete parts may be analyzed with a discrete approach. For the current demonstration of weak binding and unbinding, a weakly bound state is identified with $i = -1$,

while the continuously diffusing states of an unbound tethered head are identified with $i \geq 0$. Transitions to and from the weakly bound state are defined:

$$w_{-1}^- = 0, \quad w_{-1}^+ = v_+, \quad w_0^- = \frac{\hat{v}_-}{\delta}, \quad w_0^+ = \frac{A(x_0)}{2\delta} + \frac{D}{\delta^2} \quad (123)$$

with Eq. 122 defining the remaining transition rates for $i > 0$. It can be demonstrated that with these definitions, the dynamical boundary conditions Eq. 114 in Appendix B.1 are satisfied. Thus, the dynamics of this system are as supposed. Additionally, Eq. 121 then straightforwardly leads to both the boundary conditions Eq. 116 and the continuous equation Eq. 115 for the mean first passage time problem, where the cases of weak binding and unbinding in Eq. 116 correspond to the presence or absence, respectively, of an absorbing state at $i = -1$.

REFERENCES

- [1] ALONSO, M. C., DRUMMOND, D. R., KAIN, S., HOENG, J., AMOS, L., and CROSS, R. A., “An ATP gate controls tubulin binding by the tethered head of kinesin-1,” *Science*, vol. 316, pp. 120–123, Apr. 2007.
- [2] ANDRIEUX, D. and GASPARD, P., “Fluctuation theorems and the nonequilibrium thermodynamics of molecular motors,” *Phys. Rev. E*, vol. 74, p. 011906, July 2006.
- [3] BELL, G. I., “Models for specific adhesion of cells to cells,” *Science*, vol. 200, no. 4342, pp. 618–627, 1978.
- [4] BERG, H., *Random Walks in Biology*. Princeton University Press, New Jersey, 1993.
- [5] BLOCK, S. M., ASBURY, C. L., SHAEVITZ, J. W., and LANG, M. J., “Probing the kinesin reaction cycle with a 2D optical force clamp,” *Proc. Natl. Acad. Sci. U.S.A.*, vol. 100, no. 5, pp. 2351–2356, 2003.
- [6] CARTER, N. J. and CROSS, R. A., “Mechanics of the kinesin step,” *Nature*, vol. 435, no. 7040, pp. 308–312, 2005.
- [7] CASE, R. B., RICE, S., HART, C. L., LY, B., and VALE, R. D., “Role of the kinesin neck linker and catalytic core in microtubule-based motility,” *Curr. Biol.*, vol. 10, no. 3, pp. 157–160, 2000.
- [8] CLEMEN, A. E. M., VILFAN, M., JAUD, J., ZHANG, J. S., BARMANN, M., and RIEF, M., “Force-dependent stepping kinetics of myosin-V,” *Biophys. J.*, vol. 88, pp. 4402–4410, June 2005.
- [9] COHEN, A., “A Pade approximant to the inverse Langevin function,” *Rheol. Acta*, vol. 30, no. 3, pp. 270–273, 1991.
- [10] CONROY, R. S. and DANILOWICZ, C., “Unravelling DNA,” *Contemp. Phys.*, vol. 45, no. 4, pp. 277–302, 2004.
- [11] CROOKS, G. E., “Entropy production fluctuation theorem and the nonequilibrium work relation for free energy differences,” *Phys. Rev. E*, vol. 60, pp. 2721–2726, Sept. 1999.
- [12] CROOKS, G. E., “Path-ensemble averages in systems driven far from equilibrium,” *Phys. Rev. E*, vol. 61, pp. 2361–2366, Mar. 2000.
- [13] CROSS, R. A., “The kinetic mechanism of kinesin,” *Trends Biochem.*, vol. 29, no. 6, pp. 301–309, 2004.

- [14] CROSS, R. A., “Molecular motors: Kinesin’s interesting limp,” *Curr. Biol.*, vol. 14, no. 4, pp. R158–R159, 2004.
- [15] CVITANOVIĆ, P., ARTUSO, R., MAINIERI, R., TANNER, G., and VATTAY, G., *Chaos: Classical and Quantum*. Copenhagen: Niels Bohr Institute, 2004. <http://ChaosBook.org> (July 2007).
- [16] DELATORRE, J. G., NAVARRO, S., MARTINEZ, M. C. L., DIAZ, F. G., and CASCALES, J. J. L., “Hydro: a computer-program for the prediction of hydrodynamic properties of macromolecules,” *Biophys. J.*, vol. 67, pp. 530–531, Aug. 1994.
- [17] DINNER, A. R., LAZARIDIS, T., and KARPLUS, M., “Understanding β -hairpin formation,” *Proc. Natl. Acad. Sci. U.S.A.*, vol. 96, no. 16, pp. 9068–9073, 1999.
- [18] FLORY, P., *Statistical Mechanics of Chain Molecules*. Hanser Publishers, New York, 1989.
- [19] FOX, R. F., “Gaussian stochastic processes in physics,” *Phys. Rep.*, vol. 48, no. 3, pp. 179–283, 1978.
- [20] FOX, R. F., “Rectified Brownian movement in molecular and cell biology,” *Phys. Rev. E*, vol. 57, no. 2, pp. 2177–2203, 1998.
- [21] FOX, R. F. and CHOI, M. H., “Rectified Brownian motion and kinesin motion along microtubules,” *Phys. Rev. E*, vol. 63, no. 5, p. 051901, 2001.
- [22] GALLAVOTTI, G. and COHEN, E. G. D., “Dynamical ensembles in nonequilibrium statistical-mechanics,” *Phys. Rev. Lett.*, vol. 74, pp. 2694–2697, Apr. 1995.
- [23] GARDINER, C., *Handbook of Stochastic Methods*. Springer-Verlag, New York, 2004.
- [24] GASPARD, P., “Fluctuation theorem for nonequilibrium reactions,” *J. Chem. Phys.*, vol. 120, pp. 8898–8905, May 2004.
- [25] GASPARD, P., “Brownian motion, dynamical randomness and irreversibility,” *New J. Phys.*, vol. 7, p. 77, Mar. 2005.
- [26] GASPARD, P., “Hamiltonian dynamics, nanosystems, and nonequilibrium statistical mechanics,” *Physica A*, vol. 369, pp. 201–246, Sept. 2006.
- [27] GASPARD, P., *Chaos, Scattering and Statistical Mechanics*. Cambridge University Press, 1998.
- [28] HACKNEY, D. D., “Evidence for alternating head catalysis by kinesin during microtubule-stimulated ATP hydrolysis,” *Proc. Natl. Acad. Sci. U.S.A.*, vol. 91, no. 15, pp. 6865–6869, 1994.

- [29] HACKNEY, D. D., STOCK, M. F., MOORE, J., and PATTERSON, R. A., “Modulation of kinesin half-site ADP release and kinetic processivity by a spacer between the head groups,” *Biochemistry*, vol. 42, no. 41, pp. 12011–12018, 2003.
- [30] HANGGI, P., TALKNER, P., and BORKOVEC, M., “Reaction-rate theory: 50 years after Kramers,” *Rev. Mod. Phys.*, vol. 62, pp. 251–341, Apr. 1990.
- [31] HATANO, T. and SASA, S., “Steady-state thermodynamics of Langevin systems,” *Phys. Rev. Lett.*, vol. 86, pp. 3463–3466, Apr. 2001.
- [32] HILL, T. L., *Free Energy Transduction in Biology*. Academic Press, 1977.
- [33] HIROSE, K., LOCKHART, A., CROSS, R. A., and AMOS, L. A., “Three-dimensional cryoelectron microscopy of dimeric kinesin and ncd motor domains on microtubules,” *Proc. Natl. Acad. Sci. U.S.A.*, vol. 93, no. 18, pp. 9539–9544, 1996.
- [34] HIROSE, K., LOWE, J., ALONSO, M., CROSS, R. A., and AMOS, L. A., “Congruent docking of dimeric kinesin and ncd into three-dimensional electron cryomicroscopy maps of microtubule-motor ADP complexes,” *Mol. Biol. Cell*, vol. 10, no. 6, pp. 2063–2074, 1999.
- [35] HOWARD, J., “Protein power strokes,” *Curr. Bio.*, vol. 16, pp. R517–R519, July 2006.
- [36] HUXLEY, A. F., “Muscle structure and theories of contraction,” *Prog. Biophys. Mol. Biol.*, vol. 7, pp. 255–318, 1957.
- [37] IKEDA, N. and WATANABE, S., *Stochastic Differential Equations and Diffusion Processes*. North-Holland, Amsterdam, 1989.
- [38] JØRGENSEN, W. L., MAXWELL, D. S., and TIRADORIVES, J., “Development and testing of the OPLS all-atom force field on conformational energetics and properties of organic liquids,” *J. Am. Chem. Soc.*, vol. 118, pp. 11225–11236, Nov. 1996.
- [39] KIKKAWA, M., SABLIN, E. P., OKADA, Y., YAJIMA, H., FLETTERICK, R. J., and HIROKAWA, N., “Switch-based mechanism of kinesin motors,” *Nature*, vol. 411, no. 6836, pp. 439–445, 2001.
- [40] KLEINERT, H., *Path Integrals in Quantum Mechanics, Polymer Physics, and Financial Markets*. World Scientific Publishing Co. Pte. Ltd., 2004.
- [41] KLUMPP, L. M., HOENGER, A., and GILBERT, S. P., “Kinesin’s second step,” *Proc. Natl. Acad. Sci. U.S.A.*, vol. 101, no. 10, pp. 3444–3449, 2004.
- [42] KRATKY, O. and POROD, G., “Röntgenuntersuchung geloster Fadenmoleküle,” *Recl. Trav. Chim. Pay. B.*, vol. 68, no. 12, pp. 1106–1122, 1949.

- [43] KUHN, W. and GRUN, F., “Relations between elastic constants and the strain birefringence of high-elastic substances,” *Kolloid-Z.*, vol. 101, no. 3, pp. 248–271, 1942.
- [44] LAMB, H., *Hydrodynamics*. Dover, 1932.
- [45] LAN, G. H. and SUN, S. X., “Dynamics of myosin-V processivity,” *Biophys. J.*, vol. 88, no. 2, pp. 999–1008, 2005.
- [46] LANDAU, L. and LIFSHITZ., E., *Fluid Mechanics*. Pergamon Press, New York, 2003.
- [47] LEBOWITZ, J. L. and SPOHN, H., “A Gallavotti-Cohen-type symmetry in the large deviation functional for stochastic dynamics,” *J. Stat. Phys.*, vol. 95, pp. 333–365, Apr. 1999.
- [48] LEE, T.-H., BLANCHARD, S. C., KIM, H. D., PUGLISI, J. D., and CHU, S., “The role of fluctuations in tRNA selection by the ribosome,” *Preprint for Biophys. J.*, 2007.
- [49] LEI, Y., LI, H. R., ZHANG, R., and HAN, S. J., “Molecular dynamics simulations of biotin in aqueous solution,” *J. Phys. Chem. B*, vol. 108, pp. 10131–10137, July 2004.
- [50] MAGNASCO, M. O., “Molecular combustion motors,” *Phys. Rev. Lett.*, vol. 72, pp. 2656–2659, Apr. 1994.
- [51] MARK, P. and NILSSON, L., “Structure and dynamics of the TIP3P, SPC, and SPC/E water models at 298 K,” *J. Phys. Chem. A*, vol. 105, pp. 9954–9960, Nov. 2001.
- [52] MATHER, W. H. and FOX, R. F., “Kinesin’s biased stepping mechanism: Amplification of neck linker zippering,” *Biophys. J.*, vol. 91, pp. 2416–2426, Oct. 2006.
- [53] McDONALD, N. A. and JORGENSEN, W. L., “Development of an all-atom force field for heterocycles. properties of liquid pyrrole, furan, diazoles, and oxazoles,” *J. Phys. Chem. B*, vol. 102, pp. 8049–8059, Oct. 1998.
- [54] MUNOZ, V., HENRY, E. R., HOFRICHTER, J., and EATON, W. A., “A statistical mechanical model for β -hairpin kinetics,” *Proc. Natl. Acad. Sci. U.S.A.*, vol. 95, no. 11, pp. 5872–5879, 1998.
- [55] MUNOZ, V., THOMPSON, P. A., HOFRICHTER, J., and EATON, W. A., “Folding dynamics and mechanism of β -hairpin formation,” *Nature*, vol. 390, no. 6656, pp. 196–199, 1997.
- [56] NISHIYAMA, M., HIGUCHI, H., ISHII, Y., TANIGUCHI, Y., and YANAGIDA, T., “Single molecule processes on the stepwise movement of ATP-driven molecular motors,” *Biosystems*, vol. 71, no. 1-2, pp. 145–156, 2003.

- [57] OONO, Y. and PANICONI, M., “Steady state thermodynamics,” *Prog. Theor. Phys. Supp.*, vol. 130, pp. 29–44, 1998.
- [58] OSTER, G. and WANG, H. Y., “Rotary protein motors,” *Trends In Cell Biology*, vol. 13, pp. 114–121, Mar. 2003.
- [59] PESKIN, C. S., ODELL, G. M., and OSTER, G. F., “Cellular motions and thermal fluctuations: the Brownian ratchet,” *Biophys. J.*, vol. 65, pp. 316–324, July 1993.
- [60] PESKIN, C. S. and OSTER, G., “Coordinated hydrolysis explains the mechanical-behavior of kinesin,” *Biophys. J.*, vol. 68, no. 4, pp. S202–S211, 1995.
- [61] PHILLIPS, J. C., BRAUN, R., WANG, W., GUMBART, J., TAJKHORSHID, E., VILLA, E., CHIPOT, C., SKEEL, R. D., KALE, L., and SCHULTEN, K., “Scalable molecular dynamics with NAMD,” *J. Comput. Chem.*, vol. 26, pp. 1781–1802, Dec. 2005.
- [62] PURCELL, E. M., “Life at low Reynolds-number,” *Am. J. Phys.*, vol. 45, no. 1, pp. 3–11, 1977.
- [63] PURCELL, T. J., SWEENEY, H. L., and SPUDICH, J. A., “A force-dependent state controls the coordination of processive myosin V,” *Proc. Natl. Acad. Sci. U.S.A.*, vol. 102, pp. 13873–13878, Sept. 2005.
- [64] QIAN, H., “Nonequilibrium steady-state circulation and heat dissipation functional,” *Phys. Rev. E*, vol. 6402, p. 022101, Aug. 2001.
- [65] QIAN, H., “Entropy production and excess entropy in a nonequilibrium steady-state of single macromolecules,” *Phys. Rev. E*, vol. 65, p. 021111, Feb. 2002.
- [66] QIAN, H., “Motor protein with nonequilibrium potential: Its thermodynamics and efficiency,” *Phys. Rev. E*, vol. 69, p. 012901, Jan. 2004.
- [67] QIAN, H., “Nonequilibrium potential function of chemically driven single macromolecules via Jarzynski-type log-mean-exponential heat,” *J. Phys. Chem. B*, vol. 109, pp. 23624–23628, Dec. 2005.
- [68] REIMANN, P., “Brownian motors: noisy transport far from equilibrium,” *Phys. Rep.*, vol. 361, pp. 57–265, Apr. 2002.
- [69] REIMANN, P. and HANGGI, P., “Introduction to the physics of Brownian motors,” *App. Phys. A*, vol. 75, pp. 169–178, Aug. 2002.
- [70] RICE, S., CUI, Y., SINDELAR, C., NABER, N., MATUSKA, M., VALE, R., and COOKE, R., “Thermodynamic properties of the kinesin neck-region docking to the catalytic core,” *Biophys. J.*, vol. 84, no. 3, pp. 1844–1854, 2003.

- [71] RICE, S., LIN, A. W., SAFER, D., HART, C. L., NABER, N., CARRAGHER, B. O., CAIN, S. M., PECHATNIKOVA, E., WILSON-KUBALEK, E. M., WHITTAKER, M., PATE, E., COOKE, R., TAYLOR, E. W., MILLIGAN, R. A., and VALE, R. D., “A structural change in the kinesin motor protein that drives motility,” *Nature*, vol. 402, no. 6763, pp. 778–784, 1999.
- [72] RISKEN, H., *The Fokker-Planck Equation: Methods of Solution and Applications*. Springer-Verlag, 1996.
- [73] ROMBERG, L., PIERCE, D. W., and VALE, R. D., “Role of the kinesin neck region in processive microtubule-based motility,” *J. Cell Biol.*, vol. 140, no. 6, pp. 1407–1416, 1998.
- [74] ROSENFELD, S. S., FORDYCE, P. M., JEFFERSON, G. M., KING, P. H., and BLOCK, S. M., “Stepping and stretching: How kinesin uses internal strain to walk processively,” *J. Biol. Chem.*, vol. 278, no. 20, pp. 18550–18556, 2003.
- [75] ROSENFELD, S. S., XING, J., JEFFERSON, G. M., CHEUNG, H. C., and KING, P. H., “Measuring kinesin’s first step,” *J. Biol. Chem.*, vol. 277, no. 39, pp. 36731–36739, 2002.
- [76] SACK, S., MULLER, J., MARX, A., THORMAHLEN, M., MANDELKOW, E. M., BRADY, S. T., and MANDELKOW, E., “X-ray structure of motor and neck domains from rat brain kinesin,” *Biochemistry*, vol. 36, pp. 16155–16165, Dec. 1997.
- [77] SAITO, N., TAKAHASHI, K., and YUNOKI, Y., “Statistical mechanical theory of stiff chains,” *J. Phys. Soc. Jpn.*, vol. 22, no. 1, pp. 219–227, 1967.
- [78] SASA, S. I. and TASAKI, H., “Steady state thermodynamics,” *J. Stat. Phys.*, vol. 125, pp. 125–227, Oct. 2006.
- [79] SCHMIDT, M. W., BALDRIDGE, K. K., BOATZ, J. A., ELBERT, S. T., GORDON, M. S., JENSEN, J. H., KOSEKI, S., MATSUNAGA, N., NGUYEN, K. A., SU, S. J., WINDUS, T. L., DUPUIS, M., and MONTGOMERY, J. A., “General atomic and molecular electronic-structure system,” *J. Comp. Chem.*, vol. 14, pp. 1347–1363, Nov. 1993.
- [80] SCHNAKENBERG, J., “Network theory of microscopic and macroscopic behavior of master equation systems,” *Rev. Mod. Phys.*, vol. 48, no. 4, pp. 571–585, 1976.
- [81] SELLERS, J. R. and VEIGEL, C., “Walking with myosin V,” *Curr. Opin. Cell Biol.*, vol. 18, pp. 68–73, Feb. 2006.
- [82] SHIROGUCHI, K. and KINOSHITA, K., “Myosin V walks by lever action and Brownian motion,” *Science*, vol. 316, pp. 1208–1212, May 2007.

- [83] SKINIOTIS, G., SURREY, T., ALTMANN, S., GROSS, H., SONG, Y. H., MANDELKOW, E., and HOENGER, A., “Nucleotide-induced conformations in the neck region of dimeric kinesin,” *EMBO J.*, vol. 22, no. 7, pp. 1518–1528, 2003.
- [84] SODERHALL, J. A. and LAAKSONEN, A., “Molecular dynamics simulations of ubiquinone inside a lipid bilayer,” *J. Phys. Chem. B*, vol. 105, pp. 9308–9315, Sept. 2001.
- [85] STRYER, L., *Biochemistry*. W.H. Freeman and Co., 1995.
- [86] SVOBODA, K., MITRA, P. P., and BLOCK, S. M., “Fluctuation analysis of motor protein movement and single enzyme-kinetics,” *Proc. Natl. Acad. Sci. U.S.A.*, vol. 91, no. 25, pp. 11782–11786, 1994.
- [87] TOMISHIGE, M. and VALE, R. D., “Controlling kinesin by reversible disulfide cross-linking: Identifying the motility-producing conformational change,” *J. Cell Biol.*, vol. 151, no. 5, pp. 1081–1092, 2000.
- [88] UEMURA, S. and ISHIWATA, S., “Loading direction regulates the affinity of ADP for kinesin,” *Nat. Struct. Biol.*, vol. 10, no. 4, pp. 308–311, 2003.
- [89] UEMURA, S., KAWAGUCHI, K., YAJIMA, J., EDAMATSU, M., TOYOSHIMA, Y. Y., and ISHIWATA, S., “Kinesin-microtubule binding depends on both nucleotide state and loading direction,” *Proc. Natl. Acad. Sci. U.S.A.*, vol. 99, no. 9, pp. 5977–5981, 2002.
- [90] UHLENBECK, G. E. and ORNSTEIN, L. S., “On the theory of the Brownian motion,” *Phys. Rev.*, vol. 36, pp. 0823–0841, Sept. 1930.
- [91] VALE, R. D., “The molecular motor toolbox for intracellular transport,” *Cell*, vol. 112, pp. 467–480, Feb. 2003.
- [92] VALE, R. D., “Myosin V motor proteins: marching stepwise towards a mechanism,” *J. Cell Biol.*, vol. 163, no. 3, pp. 445–450, 2003.
- [93] VALE, R. D. and MILLIGAN, R. A., “The way things move: Looking under the hood of molecular motor proteins,” *Science*, vol. 288, no. 5463, pp. 88–95, 2000.
- [94] VEIGEL, C., SCHMITZ, S., WANG, F., and SELLERS, J. R., “Load-dependent kinetics of myosin-V can explain its high processivity,” *Nat. Cell Bio.*, vol. 7, pp. 861–869, Sept. 2005.
- [95] VEIGEL, C., WANG, F., BARTOO, M. L., SELLERS, J. R., and MOLLOY, J. E., “The gated gait of the processive molecular motor, myosin V,” *Nat. Cell Bio.*, vol. 4, pp. 59–65, Jan. 2002.
- [96] VILFAN, A., “Elastic lever-arm model for myosin V,” *Biophys. J.*, vol. 88, pp. 3792–3805, June 2005.

- [97] VISSCHER, K., SCHNITZER, M. J., and BLOCK, S. M., “Single kinesin molecules studied with a molecular force clamp,” *Nature*, vol. 400, no. 6740, pp. 184–189, 1999.
- [98] VOLOGODSKII, A., “Energy transformation in biological molecular motors,” *Phys. Life Rev.*, vol. 3, pp. 119–132, 2006.
- [99] WADE, R. H. and KOZIELSKI, F., “Structural links to kinesin directionality and movement,” *Nat. Struct. Biol.*, vol. 7, no. 6, pp. 456–460, 2000.
- [100] WANG, H. and OSTER, G., “Ratchets, power strokes, and molecular motors,” *App. Phys. A*, vol. 75, pp. 315–323, Aug. 2002.
- [101] WARSHAW, D. M., KENNEDY, G. G., WORK, S. S., KREMENTSOVA, E. B., BECK, S., and TRYBUS, K. M., “Differential labeling of myosin V heads with quantum dots allows direct visualization of hand-over-hand processivity,” *Biophys. J.*, vol. 88, pp. L30–L32, May 2005.
- [102] XING, J., BAI, F., BERRY, R., and OSTER, G., “Torque-speed relationship of the bacterial flagellar motor,” *Proc. Natl. Acad. Sci. U.S.A.*, vol. 103, pp. 1260–1265, 2006.
- [103] YILDIZ, A., TOMISHIGE, M., VALE, R. D., and SELVIN, P. R., “Kinesin walks hand-over-hand,” *Science*, vol. 303, no. 5658, pp. 676–678, 2004.
- [104] ZHOU, H. X., “How do biomolecular systems speed up and regulate rates?,” *Phys. Biol.*, vol. 2, no. 3, pp. R1–R25, 2005.